

Design of a Rocket- Based Combined Cycle Engine

A project present to
The Faculty of the Department of Aerospace Engineering
San Jose State University

in partial fulfillment of the requirements for the degree
Master of Science in Aerospace Engineering

By

Andrew Munoz

May 2011

approved by

Dr. Periklis Papadopoulos
Faculty Advisor



© 2011
Andrew Munoz
ALL RIGHTS RESERVED

SAN JOSÉ STATE UNIVERSITY

The Designated Masters Project Committee Approves the Thesis Titled

DESIGN OF A ROCKET-BASED COMBINED CYCLE ENGINE

By

Andrew Munoz

APPROVED FOR THE DEPARTMENT OF AEROSPACE ENGINEERING

SAN JOSÉ STATE UNIVERSITY

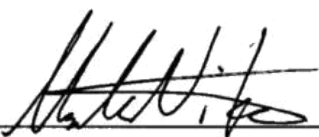
May 2011



Dr. Periklis Papadopoulos
Committee Chair
Department of Mechanical and Aerospace Engineering

5 / 16 / 11

Date



Dr. Nikos Mourtos
Committee Member
Department of Mechanical and Aerospace Engineering

5-18-11

Date



Professor Nikola Djordjevic
Committee Member
Department of Mechanical and Aerospace Engineering

5-18-11

Date

DESIGN OF A ROCKET-BASED COMBINED CYCLE ENGINE

by

Andrew Munoz

ABSTRACT

Current expendable space launch vehicles using conventional all-rocket propulsion systems have virtually reached their performance limits with respect to payload capacity. A promising approach to increase payload capacity and to provide reusability is to utilize airbreathing propulsion systems for a portion of the flight to reduce oxidizer weight and potentially increase payload and structural capacity. A Rocket-Based Combined Cycle (RBCC) engine would be capable of providing transatmospheric flight while increasing propulsion performance by utilizing a rocket integrated airbreathing propulsion system.

An analytical model of a Rocket-Based Combined Cycle (RBCC) engine was developed using the stream thrust method as a solution to the governing equations of aerothermodynamics. This analytical model provided the means for calculating the propulsion performance of an ideal RBCC engine over the airbreathing flight regime (Mach 0 to 12) as well as a means of comparison with conventional rocket propulsion systems. The model was developed by choosing the highest performance propulsion cycles for a given flight regime and then integrating them into a single engine which would utilize the same components (inlet, rocket, combustor, and nozzle) throughout the entire airbreathing flight regime. In order to narrow the scope of this project, a single configuration was chosen for the analytical model. A more exhaustive study could have been performed with a greater number of permutations in the subsystem and geometry parameters. Within the constraints of existing technologies and materials, it was determined that the best performing combination of propulsion cycles is an ejector-ramjet, ramjet/scramjet (dual mode), and an all-rocket propulsion system. The performance metric calculations demonstrated that an ideal RBCC engine (neglecting the effects of drag and gravity) would greatly outperform a conventional ideal all-rocket propulsion system throughout the airbreathing flight regime. An average I_{sp} of 2065 s was calculated over the airbreathing flight regime while an I_{sp} of 1293 s over the entire flight regime (Mach 0 to 25).

ACKNOWLEDGEMENT

I would like to thank my parents, first and foremost, for their endless support and tremendous encouragement throughout my continued educational endeavors. Without them, I would not be here today. I would also like to thank the entire faculty of the Mechanical and Aerospace Engineering department for supporting me in my education and for continuously emphasizing the importance of understanding fundamentals. Also, I would like to thank my committee for providing support and feedback on my project throughout the last year and for making it possible to continue my education.

In addition, I would like to thank those people who provided moral support and kept me sane throughout this whole project. I must thank two of my fellow classmates and friends Paul Linggi and Tommy Blackwell for continuously providing moral support, encouragement, ideas, and also a laugh or two when it was most needed. Finally, my fondest appreciation goes to my girlfriend, Emmeliah Obiri, without whom I might have never finished this project. Her support throughout this whole endeavor and unwavering belief in me were often times the only thing keeping me on track.

Table of Contents

	<u>General Acronyms</u>	9
	<u>Nomenclature: General Terms</u>	1
	<u>.....</u>	0
	<u>.....</u>	1
<u>Symbols</u>	<u>.....</u>	1
<u>Subscripts</u>	<u>.....</u>	1
	<u>.....</u>	2
<u>Superscripts</u>	<u>.....</u>	1
	<u>.....</u>	2
	<u>List of Figures</u>	1
	<u>.....</u>	3
	<u>List of Tables</u>	1
	<u>.....</u>	6
	<u>1. Introduction</u>	1
	<u>.....</u>	7
	<u>Background and Purpose of the</u>	1
1.1	<u>Project</u>	7
	<u>Current Space Launch Vehicles and Launch</u>	2
1.2	<u>Costs</u>	1
	<u>Limitations of All-Rocket Propulsion Systems in SSTO Vehicles</u>	2
1.3	<u>.....</u>	4
	<u>A Combined-Cycle Approach to SSTO Launch Vehicles</u>	2
1.4	<u>.....</u>	7
	<u>2. Background on Combined-Cycle Propulsion Systems</u>	2
	<u>.....</u>	9
	<u>Introduction to Combined-Cycle Propulsion Systems</u>	2
2.1	<u>.....</u>	9
	<u>Subsystems of Combined-Cycle Propulsion Systems</u>	3
2.2	<u>.....</u>	1
	<u>Turbofans and</u>	3
	<u>Turbojets</u>	3
2.2.1	<u>.....</u>	1
	<u>Ramjet</u>	3
2.2.2	<u>.....</u>	2
	<u>Scramjet</u>	3
2.2.3	<u>.....</u>	2
	<u>Rocket</u>	3
2.2.4	<u>.....</u>	3
	<u>Types of Combined-Cycle Propulsion Systems</u>	3
2.3	<u>.....</u>	3
	<u>.....</u>	3
2.3.1	<u>Turbine-Based Combined Cycle (TBCC) Propulsion Systems</u>	3

	<u>2.3.2 Rocket-Based Combined Cycle (RBCC) Propulsion Systems</u>	<u>3</u>
	<u>4</u>
	<u>History of Combined-Cycle Propulsion Systems</u>	<u>3</u>
<u>2.4</u>	<u>5</u>
	<u>3. Combined Cycle Propulsion System Design</u>	<u>3</u>
	<u>Considerations.....</u>	<u>8</u>
	<u>Weight Considerations</u>	
	<u>3</u>
<u>3.1</u>	<u>8</u>
	<u>Fuel</u>	
	<u>Considerations.....</u>	<u>3</u>
<u>3.2</u>	<u>8</u>
	<u>Engine Performance Based on Component Efficiencies</u>	<u>4</u>
<u>3.3</u>	<u>2</u>
	<u>Launch Configuration: Staging and Launch</u>	<u>4</u>
<u>3.4</u>	<u>Type.....</u>	<u>3</u>
	<u>Overall Vehicle Geometry Selection</u>	<u>4</u>
<u>3.5</u>	<u>6</u>
	<u>Propulsion System Integration into the Airframe</u>	<u>4</u>
<u>3.6</u>	<u>8</u>
	<u>Continuous Stability and Operation in All Flight Regimes</u>	<u>5</u>
<u>3.7</u>	<u>1</u>
	<u>4. RBCC Propulsion System</u>	<u>5</u>
	<u>Overview.....</u>	<u>3</u>

	<u>Definition of Rocket-Based Combined</u>	
4.1	<u>Cycles.....</u>	<u>54</u>
	<u>Rocket-Based Combined Cycle Literature</u>	
4.2	<u>Review.....</u>	<u>55</u>
	<u>Pre-</u>	
	<u>□¶V/LWHUDWXUH.....</u>	
4.2.1	<u>.....</u>	<u>55</u>
	<u>Current Literature</u>	
	<u>.....</u>	
4.2.2	<u>.....</u>	<u>60</u>
	<u>Rocket-Based Combined Cycle Technical Overview</u>	
4.3	<u>.....</u>	<u>67</u>
	<u>Interim Summary</u>	
	<u>.....</u>	
4.4	<u>.....</u>	<u>69</u>
5.	<u>Gas Dynamics: Introductory</u>	
	<u>Review.....</u>	<u>71</u>
	<u>Introduction</u>	
5.1	<u>.....</u>	<u>71</u>
	<u>A Review of Fundamentals</u>	
	<u>.....</u>	
5.2	<u>...</u>	<u>71</u>
	<u>Hypersonic Flow and Related Physical Phenomena</u>	
5.3	<u>.....</u>	<u>74</u>
	<u>Chemical Effects in Hypersonic</u>	
5.4	<u>Flows.....</u>	<u>75</u>
	<u>The Ideal Rocket and Quasi One-Dimensional Flow Theory</u>	
5.5	<u>.....</u>	<u>77</u>
6.	<u>RBCC Propulsion Performance</u>	
	<u>Metrics.....</u>	<u>82</u>
	<u>Specific</u>	
	<u>Thrust.....</u>	
6.1	<u>.....</u>	<u>82</u>
	<u>Specific Fuel</u>	
	<u>Consumption.....</u>	
6.2	<u>.....</u>	<u>82</u>
	<u>Specific</u>	
	<u>Impulse.....</u>	
6.3	<u>.....</u>	<u>83</u>
	<u>Fuel/Air Ratio</u>	
	<u>.....</u>	
6.4	<u>.....</u>	<u>84</u>
	<u>Airbreathing Engine Overall Efficiency</u>	
6.5	<u>.....</u>	<u>85</u>
	<u>Engine Performance</u>	
	<u>Analysis.....</u>	
7.	<u>.....</u>	<u>88</u>
	<u>Introduction</u>	
7.1	<u>.....</u>	<u>88</u>

	<u>Thermodynamic Cycle Analysis</u>	
7.2	<u>.....</u>	<u>89</u>
	<u>First Law</u>	
	<u>Analysis.....</u>	
7.3	<u>.....</u>	<u>93</u>
	<u>Stream Thrust</u>	
	<u>Analysis.....</u>	
7.4	<u>.....</u>	<u>94</u>
	<u>AERSPC Mode Analysis Inputs</u>	
7.5	<u>.....</u>	<u>98</u>
	<u>The Standard Atmosphere Model and Flight Trajectories</u>	<u>10</u>
7.6	<u>.....</u>	<u>0</u>
	<u>Mode I: Ejector-Ramjet Performance Calculations</u>	<u>10</u>
7.7	<u>.....</u>	<u>5</u>
	<u>7.7.1 Ejector-Ramjet</u>	
	<u>Results.....</u>	<u>10</u>
	<u>.....</u>	<u>8</u>
	<u>Mode II & III: Dual-Mode Ramjet and Scramjet Performance</u>	<u>11</u>
7.8	<u>Calculations.....</u>	<u>2</u>
	<u>Mode IV: All-Rocket Performance Calculations</u>	<u>11</u>
7.9	<u>.....</u>	<u>5</u>
8.	<u>Overall AERSPC Propulsion System Performance</u>	<u>11</u>
	<u>.....</u>	<u>6</u>
	<u>Conclusion</u>	<u>12</u>
9.	<u>.....</u>	<u>0</u>
	<u>References</u>	<u>12</u>
	<u>.....</u>	<u>1</u>
	<u>SSHQGL[5%&&¶V6WXGLHGLQ1\$6\$&RQWUDFW</u>	<u>12</u>
	<u>1\$6-377)</u>	<u>4</u>
	<u>Appendix B: U.S. Standard Atmosphere 1976 Properties</u>	<u>12</u>
	<u>.....</u>	<u>5</u>

[Appendix C: Ejector-Ramjet Mode Performance Calculation Tabulated Results](#)

.....
[127](#)

[Appendix D: Ramjet Propulsion Performance Calculations Using PARA](#)

.....
[128](#)

[Appendix E: Scramjet Mode Propulsion Performance Using Stream Thrust Analysis](#)

.....
[129](#)

General Acronyms

Acronym	Description
AERSPC	Air-augmented Ejector-Ramjet Scramjet Propulsion Cycle
CCPS	Combined-cycle propulsion system
CPS	Combination propulsion system
DAB	Diffusion and afterburning
ET	Space Shuttle external tank
GLOW	Gross lift-off weight
HThL	Horizontal take-off horizontal landing
HtVL	Horizontal take-off vertical landing
IRS	Independent ramjet stream
ISS	International Space Station
LEO	Low-Earth orbit
LH2	Liquid hydrogen
LOX	Liquid oxygen
MMAG	Martin Marietta Aerospace Group
MTBO	Mean time between overhaul
NASP	North American Space Plane
OTIS	Optimization of Trajectories by Implicit Simulation
PARA	Parametric Cycle Analysis
POST	Program to Optimize Simulated Trajectories
RBCC	Rocket based combined cycle
SMC	Simultaneous mixing and combustion
SRB	Space Shuttle Solid Rocket Booster
SSME	Space Shuttle Main Engine
SSO	Space Station orbit
SSTO	Single-stage-to-orbit
TBCC	Turbine based combined cycle
TSTO	Two-stage-to-orbit
VThL	Vertical take-off horizontal landing
VtVL	Vertical take-off vertical landing

Nomenclature: General Terms

Symbol	Description
A	Cross-sectional area
a	Speed of sound
C_f	Skin friction Coefficient
C_D	Coefficient of Drag
C_L	Coefficient of Lift
C_M	Moment coefficient
C_{p_c}	Coefficient of pressure-burner
C_{p_c}	Coefficient of pressure-compressor
C_{p_e}	Coefficient of pressure-expander
c	Velocity
e	Specific internal energy
D	Drag
E	Internal energy
F	Force; Uninstalled thrust
f	Fuel/air ratio
f_{st}	Stoichiometric fuel/air ratio
g_0	Acceleration of gravity
h	Specific enthalpy
h_{PR}	Heat of reaction
\dot{a}_{+c}^0	Heat of combustion
I^*	Equivalent effective impulse
I_{eff}	Effective specific impulse
I_t	Total Impulse
I_{sp}	Specific Impulse
k	Ratio of specific heats; Thermal conductivity
K	Kelvin

	Mass flow rate
	Average molecular mass
m_f	Fuel mass
m_o	Initial vehicle mass
m_p	Propellant mass
m_s	Structural Mass
M	Mach number
O/F	Oxidizer-to-fuel air ratio
p	Static pressure
q	Dynamic pressure
Q	Heat interaction
R	Universal gas constant
S	Universal gas constant
s	Entropy
S	Specific fuel consumption; Reference area
S	Stream thrust function
T	Thrust; Temperature
T/W	Thrust to Weight ratio
u	velocity
V	velocity; Volume
W	Work; Weight
	Rate of shaft work done to the system

Symbols

l	Bypass ratio
\hat{u}	Ratio of specific heats
ξ	Efficiency
ζ	Vehicle flight path angle
μ	Absolute viscosity
ρ	Density

ij Cycle static temperature

Subscripts

b Burner
c Compressor
e Expansion system; Exhaust
f Fuel
i Inlet
p Primary; Propulsive
s Secondary
st Stoichiometric
t Total condition
th Thermal
0 Total/Stagnation condition
 $\square\square\square\square\square$ $\square\square$ Different locations/Stations

Superscripts

* State corresponding to $M = 1$
 \circ Reference temperature for absolute enthalpy

List of Figures

- Figure 1.1: Major launch cost components according to (Foust, 2010).
- Figure 1.2: Maximum or ideal velocity achievable by a launch vehicle as a function of its mass fraction and specific impulse.
- Figure 1.3: Specific impulse as a function of the flight velocity for selected propulsion systems (Escher and Flornes 1966).
- Figure 1.4: The broken arrow-line indicates the I_{sp} vs. flight velocity that a combined cycle propulsion system could possibly obtain (Escher and Flornes 1966).
- Figure 3.1: Diagram of the pressure balance on chamber and nozzle interiors. The location of the stations of the propulsion system is the focus of this figure (Biblarz & Sutton, 2001).
- Figure 3.2: Specific impulse and exhaust velocity of an ideal rocket at optimum nozzle expansion as functions of the absolute chamber temperature T_1 and the molecular mass κ for several values of k and p_1/p_2 (Biblarz & Sutton, 2001).
- Figure 3.3: Potential capture area limits for non-axisymmetric (left) and axisymmetric vehicles (right) (Escher et al., 1989).
- Figure 3.4: Effects of flight at positive angles of attack on an axisymmetric vehicle (Escher et al., 1989).
- Figure 3.5: Example of conical shock wave (red line) at maximum air-breathing Mach number. The outer diameter of the inlet must remain within the shock wave.
- Figure 3.6: Inclination of a conical shock for an eight degree half-angle cone at a zero degree angle of attack. Ideal gas with $k=1.40$ (Escher et al., 1989).
- Figure 3.7: Rectangular vs. round engine module integration approach (Escher et al., 1989).
- Figure 4.1: Simplest form of air augmentation of a rocket propulsion system (Escher et al., 1989).
- Figure 4.2: The Rocket Engine Nozzle Ejector (RENE) Concept (Escher et al., 1989).
- Figure 4.3: Ejector ramjet with Simultaneous Mixing and Combustion (SMC) from (Escher et al., 1989).
- Figure 4.4: Ejector ramjet with Diffusion and Afterburning (DAB) from (Escher et al., 1989).
- Figure 4.5: GTX reference vehicle geometry (Woodrow et al, 2000).

Figure 4.6: Propulsion system operating modes. (a) Mode 1, lift-off and low speed (ejector-rocket). (b) Modes 2 & 3, ramjet and scramjet. (c) Mode 4, all-rocket. (d) Re-entry concept. (Trefny, 1999).

Figure 4.7: Compressible flow in converging and diverging ducts (Anderson, 2007).

Figure 4.8: The inlet is mounted on a diverter pylon in this integrated propulsion pod used for subscale testing at the Propulsion Test Complex at GASL, Inc. (Thomas et al., 2001)

Figure 4.9: Strutjet - The integration of a rocket into a ramjet combining the benefits of both (Siebenhaar, 1995).

Figure 4.10: Schematic diagram of a RBCC engine with a rocket acting as an ejector to augment the airflow into the ramjet/scramjet segment (Segal, 2004).

Figure 4.11: Operation of an ejector scramjet RBCC: a) rocket-ejector, b) ramjet, c) scramjet and, d) rocket-only (Segal, 2004).

Figure 5.1: Velocity-Amplitude map with superimposed regions of vibrational excitation, dissociation, and ionization (Anderson, 2006).

Figure 7.1a: Air-breathing engine reference station numbers and related terminology- Typical Ramjet (Heiser &Pratt, 1994).

Figure 7.1b: Air-breathing engine reference station numbers and related terminology- Typical Scramjet (Heiser &Pratt, 1994).

Figure 7.2a: T-s Diagram for a typical Brayton Cycle (Heiser &Pratt, 1994).

Figure 7.2b: T-s diagram showing engine reference stations (Heiser &Pratt, 1994).

Figure 7.3: Variation of static temperature as a function of altitude.

Figure 7.4: Variation of static pressure with altitude.

Figure 7.5: Variation of static density with altitude.

Figure 7.6: Hypersonic vehicle trajectories subject to constant dynamic loading.

Figure 7.7: Schematic diagram for ideal ejector ramjet analysis

Figure 7.8: Thrust augmentation for freestream Mach number during the ejector-ramjet operating mode.

Figure 7.5: Ejector-Ramjet specific impulse as a function of freestream Mach number.

Figure 7.6: Ejector-ramjet specific thrust as a function of freestream Mach number.

Figure 8.1: AERSPC specific impulse as a function of airbreathing flight Mach number.

Figure 8.2: AERSPC specific thrust as a function of flight Mach number.

Figure 8.3: AERSP thrust specific fuel consumption as a function of airbreathing flight Mach number.

Figure 8.4: AERSPC overall propulsive efficiency as a function of airbreathing flight Mach number.

List of Tables

Table 1.1: Launch Vehicle Capabilities to LEO from Table 20-14 of (Kirkpatrick, 1999).

Table 3.1: Properties of commonly used aerospace fuels (Heiser and Pratt, 1994).

Table 3.2: Engine component efficiencies and their effect on engine performance (Kors, 1990).

Table 3.3: Trade Study: SSTO vs. TSTO

Table 7.1: Air-breathing Engine Reference Station Locations

Table 7.2: Constants typically used for hypersonic air-breathing propulsion system analysis.
(Heiser & Pratt, 1994).

1. Introduction

1.1 Background and Purpose of the Project

From the very beginning of the space age, launch vehicle propulsion systems have utilized exclusively all-rocket chemical propulsion systems integrated into multiple stage vehicles to place any payload into Earth orbit. Ever since the inception of the very first propulsion system, there simply have not been any viable alternatives to the relative simplicity, reliability, and high thrust-to-weight ratio that rocket engines provide in the role of space launch vehicles. However, conventional all-rocket engine technology has nearly reached its performance plateau with currently available and near-future fuels and materials.

Furthermore, the total operating cost of current multi-stage rocket launch vehicles to low-Earth orbit (LEO) or space-station orbit (SSO) remains prohibitively high at approximately \$10,000/lb into orbit according to recent estimates (Woodrow et al, 2000). These prohibitive costs are the result of expendable multi-stage launch vehicles, high total operating costs, and expensive research and development costs. For many aerospace engineers over the last few decades, the dream of affordable launch costs has constantly been on the horizon. From time to time, the promise and allure of revolutionary new reusable launch vehicle concepts have reignited that hope. However, over the years, promising programs aiming to increase reusability and thus reduce launch costs have often met tremendous technical difficulties and more often than not also drastic lack of financing after repeated loss of schedule integrity. Nevertheless, the relentless pursuit of more affordable access to space continues to be a major driver of new research in the aerospace industry and it will only be realized when launch vehicle operations

,QRUGHUWRDFKLHYHDQ³DLUOLQH-OLNH

´PRGHRIWUDQVSRUWDWLRQWR(DUWKRUELW many technological obstacles must first be overcome. Airline-like operations are only achievable with an entirely reusable launch vehicle with advanced Combined-Cycle Propulsion Systems CCPs and a Single-Stage-To-Orbit (SSTO) configuration. Currently, all-rocket propulsion space launch vehicles including the Atlas V, Delta IV, and the Space Shuttle need to carry all of their oxidizer (in the form of liquid oxygen or LOX) with them as well as the fuel in the form of liquid

hydrogen or LH₂. The Space Shuttle, for example, carries 610,000 kg of LOX and only 100,000 kg of LH₂ (Space Shuttle, 2010). The result is an oxidizer-to-fuel ratio (O/F) of almost six-to-one. This results in an excessive amount of added structural weight to support the tremendous oxidizer weight. Utilizing an air-rocket propulsion system in an SSTO vehicle to low-Earth orbit (LEO) ZRXOGUHTXLUHWKDWSSUR[LPDWHO\RIWKHYHKLFOH\IV gross lift-off weight (GLOW) be in the form of propellant (oxidizer plus fuel).

SAN JOSE STATE UNIVERSITY

The Designated Masters Project Committee Approves the Thesis Titled

DESIGN OF A ROCKET-BASED COMBINED CYCLE ENGINE

According to the equation shown below (Sutton et al, 2001), assuming a constant thrust (T), the total impulse (I_t) imparted upon a launch vehicle is proportional to the specific impulse (I_{sp}). The specific impulse is defined as the total impulse per unit weight of propellant and the total effective propellant mass is symbolized by m_p .

By
Andrew Munoz

APPROVED FOR THE DEPARTMENT OF AEROSPACE ENGINEERING

SAN JOSÉ STATE UNIVERSITY

☪

May 2011

At the most fundamental level, a launch vehicle requires a set amount of I_t in order to get from its initial position on the ground at zero velocity to its final position in orbit at orbital velocity. As the achievable I_{sp} increases, then m_p can be decreased to achieve the same I_t required for orbit resulting in a lower m_p and thus a higher structural mass (m_s). Therefore, a propulsion system with a higher I_{sp} can accommodate a lower m_p . This is reiterated in the equation shown below. For an initial vehicle mass (m_0), as m_p decreases then m_s can increase for the given m_0 .

Dr. Periklis Papadopoulos

Date

Department of Mechanical and Aerospace Engineering



☪

5-18-11

Dr. Nikos Mourtos
Committee Member

Date

One of the keys to having a fully reusable launch vehicle is to increase the structural mass fraction available in order to build a more robust vehicle. The most promising approach to increasing the achievable I_{sp} of a launch vehicle is to utilize an air-breathing engine with a significantly greater I_{sp} in some aspect of the launch. Successful test flights of air-breathing hypersonic vehicles such as the X-43 and, more recently, the X-51 have proven the technical feasibility of high Mach number air-breathing propulsion systems. However, high Mach number air-breathing propulsion systems such as the ramjet and scramjet engine cannot function in vacuum or produce static thrust; both of which are required for trans-atmospheric flight.

Dr. Nikos Mourtos
Committee Member

Date

Department of Mechanical and Aerospace Engineering

Throughout the last several decades, numerous attempts have been made to combine the benefits of air-breathing propulsion systems with the benefits of rocket propulsion systems. These types of propulsion systems are known as CCPSs (CCPS). The benefits of CCPS stem from the combination of multiple propulsion systems to take utilize the benefits of each propulsion system in different flight regimes. One subset of CCPS is the rocket-based combined cycle (RBCC) propulsion system. An RBCC propulsion system utilizes a high I_{sp} air-breathing engine cycle or multiple air-breathing cycles, and possibly a rocket for the trans-atmospheric portion of the flight. Though the theory of RBCC propulsion systems has been known for some time [WKHUHDUHQ¶WPDQ\DQDO\WLFDOPRGHOVDYDLODEOHLQWKHOLWH UDWXUH]. The goal of this project is to develop an analytical model of an RBCC propulsion system which will accomplish the following:

1. Analytically provide evidence of the benefits in propulsion performance awarded by implementing an RBCC propulsion system in a SSTO vehicle over a conventional all-rocket SSTO vehicle.
2. Verify the analytical model developed herein by comparing the propulsion performance results against other implementations of RBCC propulsion systems available in the literature. Typical propulsion performance metrics to be compared are specific impulse, overall efficiency, air mass capture ratio, thrust specific fuel consumption, and total inlet pressure recovery.

The analytical model developed as the result of this project utilizes the stream thrust functions for solving the governing aerothermodynamics equations. In order to solve for the propulsion performance across the entire flight regime, a constant dynamic pressure trajectory was used and the atmospheric properties at discrete points in the trajectory were evaluated using the U.S. Standard Atmosphere 1976 values. A spreadsheet, with iterative solving capabilities, was developed to solve the one dimensional compressible flow equations for each mode of operation separately and called the Air-augmented Ejector-Ramjet Scramjet Propulsion Cycle or (AERSPC) for short.

AERSPC utilizes one-dimensional compressible flow equations to solve for the flow properties of each mode of operation based on a finite control volume approach wherein each component of the propulsion system is treated as a control volume and the flow properties at the inlet and exit of each component are calculated using the appropriate relations. Modeling of individual subsystems closely follows the work performed by (Heiser and Pratt, 1994). This model is meant for first-pass design verification of vehicle dimensions and external drag, vehicle or propulsion system weight, or boundary layer effects.

1.2 Current Space Launch Vehicles and Launch Costs

6SDFHH[SORUDWLRQDQGFRORQL]DWLRQKDYHQ¶WWDNHQRIIDVPXFKDVSUHGLFW HGby aerospace engineers largely because the costs of a space launch have remained at relatively the same levels for the last few decades despite various efforts to bring down launch costs. According to Steven Buckley, a Northrop Grumman aerospace engineer who works with the Rocket Systems Launch Program (RSLP), the reason for fairly constantly high launch costs of around \$20 million is because of what he calls the rocket cost equation, which splits the flyaway cost of a launch into five major components (Foust, 2010). The five major launch cost components are shown below in Figure 1.1.

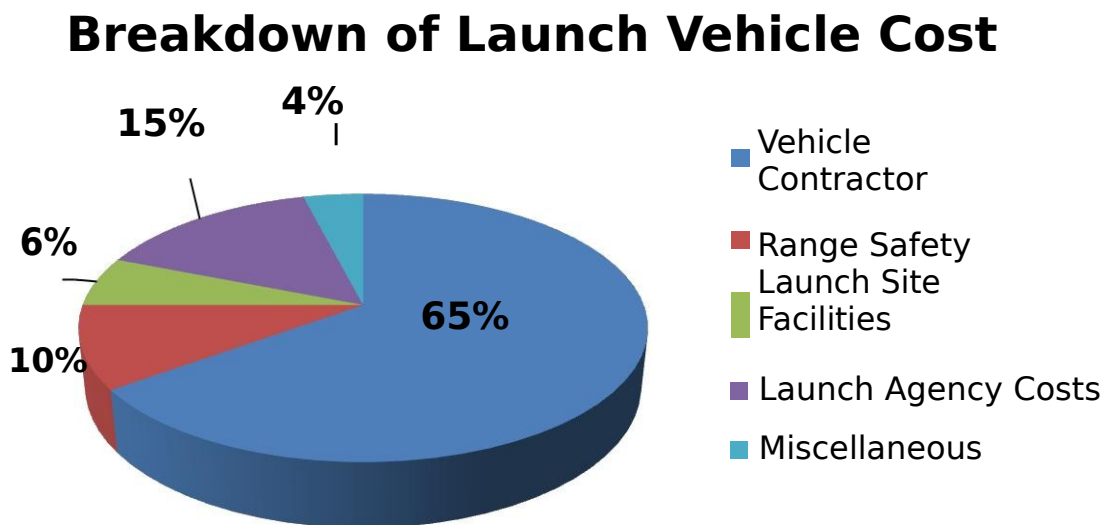


Figure 1.1: Major launch cost components according to (Foust, 2010).

The vehicle contractor costs, which includes the cost of the development, launch vehicle hardware, and the cost of any required enhancement and analysis, accounts for a total of 65% of the cost. Traditionally, this is the main cost that launch vehicle and propulsion system designers aim to reduce. Range safety costs include the direct range cost of the launch as well as the range safety approval process. Launch site facility costs cover the payload and launch vehicle processing. Launch agency costs cover equipment provided by the agency, personnel costs, and mission assurance activities. Finally, the miscellaneous costs include any additional studies, payload adapters, or any other costs that do not fall into any of the above categories.

An entire 35% of the costs associated with a launch are not affected by the type of launch vehicle at all. On average, a team of 50 people are required for a launch team which incurs a fixed cost of around \$7.5 million per year regardless of the number of launches due to fully-burdened launch teams (Foust, 2010). Without a revolutionary new propulsion technology that causes a complete paradigm shift in our approach to reaching space, the best approach to reducing the cost per space launch is to increase the number of launches per year. There is certainly demand for more launch capacity, but with current launch vehicle technology it is very difficult to meet demand.

&XUUHQWO\ WKHPDLQUHDVQRWQKDWKWHUHDUHQ\WPRUHODXQFKHVSHU\HDULVGXHWRWKHOD
XQFK

vehicle architectures employed. To this day, there are no fully reusable launch vehicles in existence. The case may be made that the Space Shuttle is a reusable launch vehicle, and while this is true of the shuttle itself, it still requires the use of the shuttle solid rocket boosters (SRB)

DQGWKH6SDFH6KXWWOH([WHUQDO7DQN
(7

:KLOHWKH65%¶VDUHUHXXVDEOH ¶ LW¶VRQO\DIWHUDQ

expensive and time consuming ocean recovery and months-long repair process. Meanwhile, the (7¶VDUHFRPSOHWHO\QRQ-reusable since they burn up during reentry into the atmosphere (Lockheed, 2007). Therefore, even with a large number of different launch vehicles from different manufacturers such as Boeing, Lockheed Martin, Orbital Sciences, International Launch Services, Space X, Arianespace, and RSC Energia, the number of launches per year is still limited by how often each can be used. Since all of the vehicles are expendable, they must build new launch vehicles for every new launch which greatly restricts launch availability.

Though it is arduous to compare launch costs from vehicle to vehicle or even from mission to mission, launch costs can generally be summed up as approximately \$4-5,000/lb for Western heavy launch vehicles and approximately \$2,000/lb for Russian and Chinese heavy launch vehicles. **Table 1.1**, below, lists the launch capabilities of many launch vehicles to LEO and the associated cost in fiscal year 2000 dollars per kg of payload. These prices have changed little in the eleven years since this table was made.

Table 1.1: Launch Vehicle Capabilities to LEO from Table 20-14 of (Kirkpatrick, 1999).

Launch Vehicles	Payload to L E O (kg)	Cost Per Kg (F Y00\$ K /kg)
Atlas II	6,580	12.2-13.7
Atlas II A	7,280	11.7-13.0
Atlas II AS	8,640	11.6-12.7
Athena 1	800	22.5
Athena 2	1,950	13.3
Athena 3	3,650	8.5
Delta II (7920, 7925)	5,089	9.8-10.8
Pegasus XL	460	28.3
Saturn V	127,000	6.5
Shuttle (IUS or TOS)	24,400	16.4
Titan II	1,905	19.4
Titan IV	21,640	9.9
Taurus	1,400	14.3-15.7
Ariane 4 (AR40)	4,900	10.2-13.3
Ariane 4 (AR42P)	6,100	10.7-13.1
Ariane 4 (AR44L)	9,600	9.9-12.5
Ariane 5 (550 km)	18,000	7.2
Long March C23B	13,600	5.5
Proton SL-13	20,900	2.6-3.6
Kosmos C-1	1,400	7.9
Soyuz	7,000	1.9-3.9
Tsyklon	3,600	3.1-4.4
Zenit 2	13,740	2.8-3.6
H-2	10,500	15.2-19.5
J-1	900	61.1-68.7

Completely reusable SSTO launch vehicles are thus the key to increasing launch availability, increasing the number of launches per year, and ultimately reducing the cost per launch by a significant degree. However, it is not trivial to design an SSTO vehicle based on a rocket propulsion system as shall be explained in the proceeding section.

1.3 Limitations of All-Rocket Propulsion Systems in SST O V ehicles

All launch vehicles today use all-rocket propulsion systems which use either solid, liquid, or hybrid propellants systems. Conventional all-rocket propulsion systems require both an oxidizer and a fuel as propellants with a much larger proportion of the propellant as oxidizer than fuel, with a typical O/F of around 6. As an example, the Space Shuttle ET which provides propellant to the Space Shuttle Main Engine (SSME) carries over 610,000 kg of LOX and only around 100,000 kg of LH2 (Space Shuttle, 2010). This is due to the relatively poor performance of rocket engines in respect to their I_{sp} . Rewriting the equation for I_t in terms of I_{sp} and expanding on the equation for m_p , makes it clear what causes a low I_{sp} for rocket propulsion systems. The requirement of to carry all of the required oxidizer mass ($m_{oxidizer}$) from lift-off to orbital insertion greatly increases m_p and reduces the I_{sp} achievable for rocket propulsion systems.

$$\frac{m_{oxidizer}}{m_{fuel}} = \frac{I_{sp}}{I_{sp} - g_0 t}$$

Another way to see the impact that a low I_{sp} plays in the overall configuration of a launch vehicle is to examine the maximum velocity achievable by a launch vehicle given ideal conditions. Examining the maximum velocity or ideal velocity ($\dot{a}g_{ideal}$) equation below, it is apparent that the achievable $\dot{a}g_{ideal}$ for a propulsion system is directly proportional to the I_{sp} .

$$\dot{a}g_{ideal} = I_{sp} \ln \left(\frac{m_{initial}}{m_{final}} \right)$$

The results of the $\dot{a}g_{ideal}$ are plotted below, in Figure 1.2, for a range of I_{sp} values from $I_{sp} = 200$ s to $I_{sp} = 1000$ s. Included in this graph is a straight line at $\dot{a}g = 7784$ m/s that represents the $\dot{a}g$ required to achieve insertion into low-Earth orbit (LEO). As can be seen in the graph, I_{sp} has a significant impact on the propellant mass fraction required of a launch vehicle to achieve insertion into LEO. For the a high-SHUIRUPDQFH³VWDWH-of-the-DUW'URFNHWZLWKDQ I_{sp} of 350s, it can be estimated from the graph that approximately 90% of the YHKLFOH¶VPDVV is required to be

propellant mass. Only 10% of the remaining weight can be dedicated to structure, payload, and any other non-propellant weight.

, WPXVWDOVREHQRWHGWKDWKLVGLGHDOYHORFLW\HTXDWLRQGRHVQ¶W take into

account any parasitic forces due to drag in the atmosphere or other aerodynamic and propulsive losses, so the m_p for

a real launch would need to be higher than 90%.

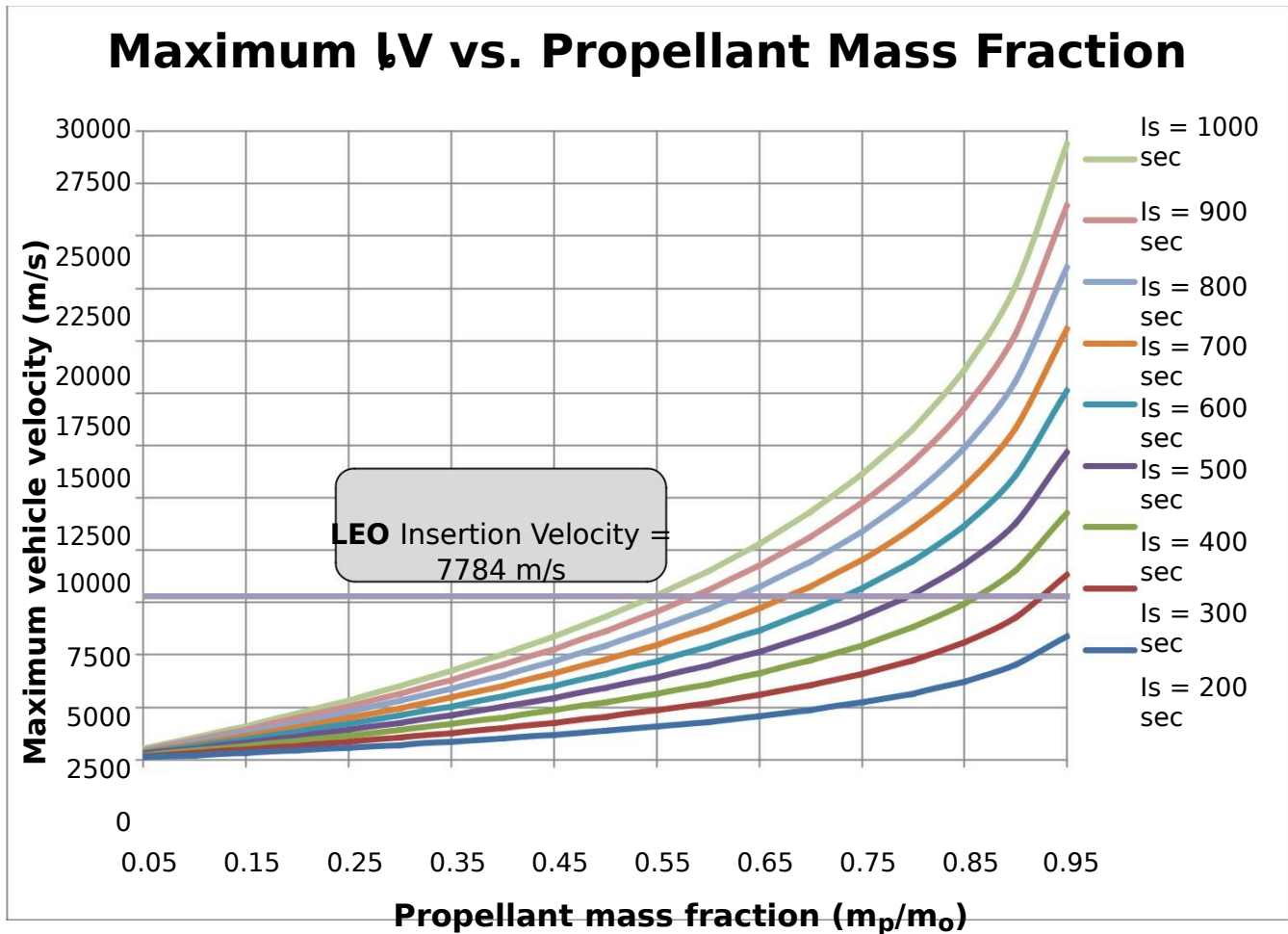


Figure 1.2: Maximum or ideal velocity achievable by a launch vehicle as a function of its mass fraction and specific impulse.

Furthermore, no launch vehicle currently in existence utilizes an SSTO launch approach. SSTO approaches are not used because the excessive amount of oxidizer that must be carried by an all-rocket propulsion launch vehicle means that the propellant tanks would have to scale to accommodate all of this weight and also stay attached to the spacecraft throughout its ascent. Without the ability to jettison the 'dead' structural weight of the tanks during some point in the

ascension (as we currently do through the implementation of multiple stages), it would be nearly impossible to place a payload into the desired orbit without a significant advance in rocket propulsion performance in terms of increased efficiency. However, the need to have multi-stage vehicles has also limited reusability since most rockets jettison their first stage boosters or additional tanks at high altitudes which can cause damage upon reentry or make recovery and repair expensive.

Additionally, for economical reasons, the payload weight must be maximized. As a consequence, launch vehicle designers need to reduce the necessary structural weight as much as possible, while staying within safety margins, in order to allow this. Compounded with the issue of non-reusable launch vehicles that would be expendable simply due to their lack of robustness. An SSTO launch vehicle with only a rocket propulsion system is therefore impractical with current structural materials and propulsion systems. In order to use a rocket-only SSTO vehicle, the engine must have an *isp* on the order of 400-500 s to remain feasible with current aerospace structural materials and manufacturing methods.

It seems that the best way to increase the reusability of a launch vehicle is to increase the robustness by increasing structural mass fraction as well as using a SSTO approach. By increasing the vehicle robustness, the mean time between overhaul (MTBO) can be reduced. Currently, the MTBO is just one flight as no launch vehicle can be fully reused. In order to achieve reusable operation, the MTBO must be increased to anywhere from 10 to 100 (Siebenhaar, 1995). The most promising approach to achieving both requirements of having a higher structural fraction and utilizing an SSTO vehicle is to greatly reduce the required oxidizer mass. These two requirements are most readily accomplished by extracting the oxygen in the atmosphere by using a combined cycle propulsion system such as a RBCC.

1.4 A Combined-Cycle Approach to SST O Launch Vehicles

Air-breathing engines have a significantly greater effective specific impulse (I_{eff}) in atmospheric flight regimes than even the most advanced rocket engines with the most efficient fuels as shown in Figure 1.3 below. This was discussed in the previous section and is a result of the method of operation of air-breathing engines. They extract oxygen from the atmosphere and thus do not need to carry an oxidizer (which will normally be used at a ratio of 6:1 or more to fuel) during flight. Some air-breathing propulsion systems such as turbofan engines can even have specific impulses upwards of 5,000 s as shown below in Figure 1.3.

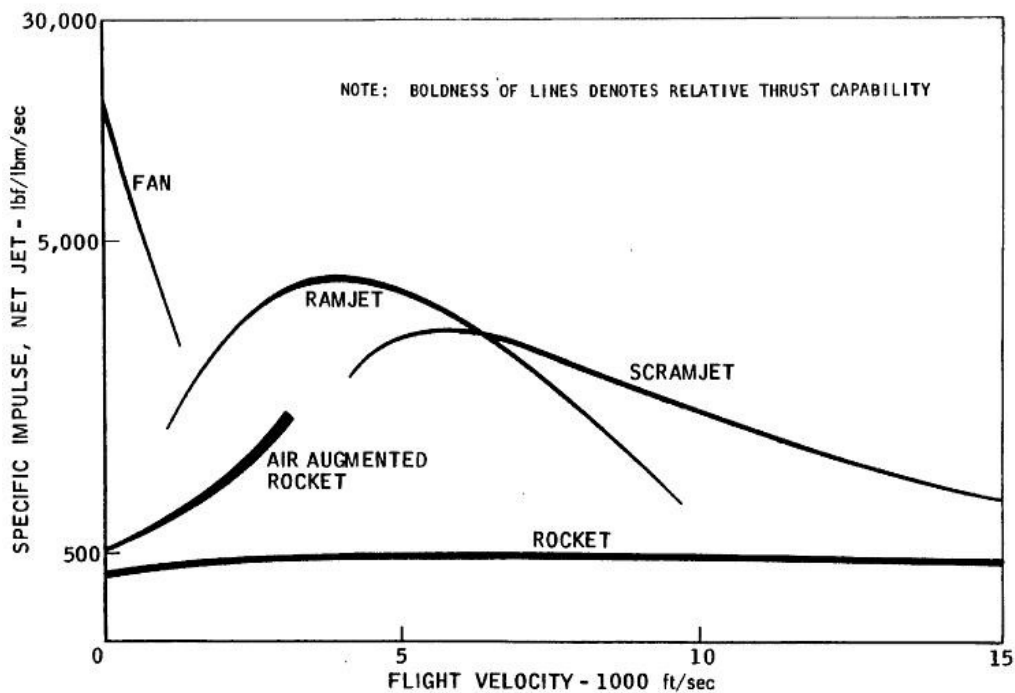


Figure 1.3: Specific impulse as a function of the flight velocity for selected propulsion systems (Escher and Flornes 1966).

Theoretically, by combining compatible propulsion systems in some form, the benefits of each propulsion system within its designed flight regime can be gained as depicted by the arrows in Figure 1.4 below. For example, turbojet engines are the most efficient in the flight regime from Mach 0 to around 3. If the only goal of a vehicle design is to absolutely maximize the efficiency, a turbofan engine can be integrated into a CCPS where it operates in the low-speed flight regime. Once it enters a higher flight regime, ramjet engines become more efficient and

thus the propulsion system switches away from the turbojet engine and to an integrated ramjet and so forth until the vehicle is finally in the upper atmosphere where air-breathing propulsion is no longer possible or efficient and thus a rocket-propulsion system becomes the only option.

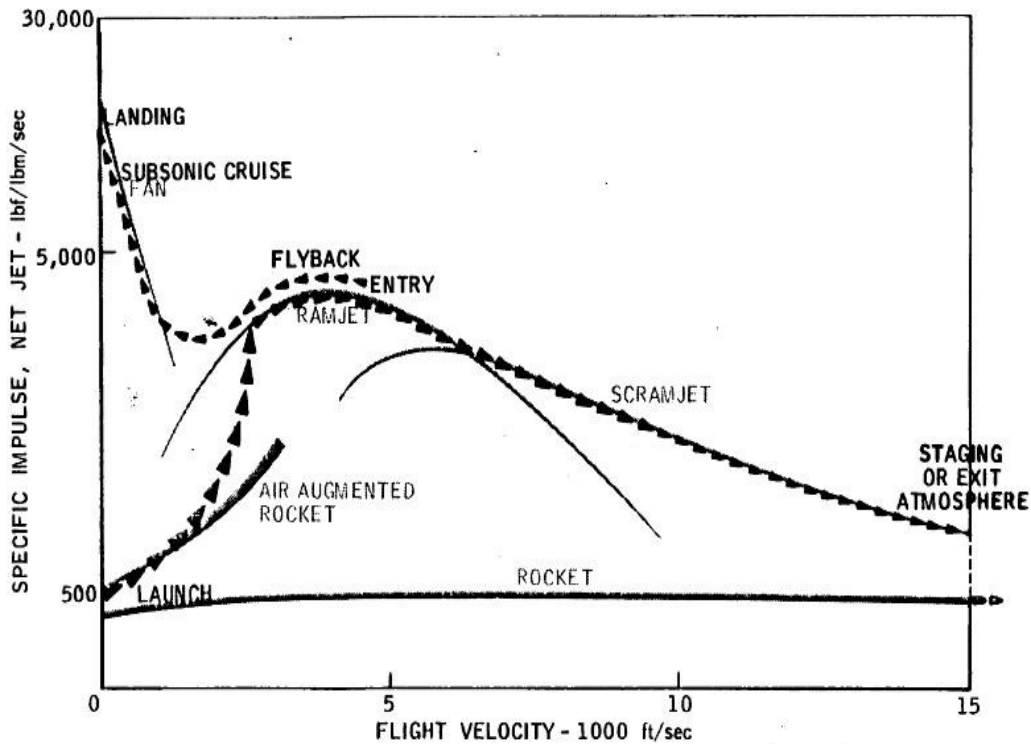


Figure 1.4: The broken arrow-line indicates the Isp vs. flight velocity that a combined cycle propulsion system could possibly obtain (Escher and Flornes 1966).

This combination of propulsion system cycles greatly increases the equivalent effective specific impulse (I^*) of the launch vehicle. I^* will be defined and expanded on more thoroughly in a later section. Though the prospect of combining multiple propulsion cycles is extremely daunting due to the difference in flow path requirements and fuel injection schemes for each cycle, a successful design holds tremendous promise in further increasing accessibility to space. It is because of this promising possibility that the study of CCPSs for future space launch

2. Background on Combined-Cycle Propulsion Systems

In the introduction, the case was made that the best approach to reducing the cost of access to space is to employ the use of launch vehicles with CCPSs. With this approach, the argument is that you can reduce the $\frac{YHKLFOHV}{2}$: by reducing the amount of oxidizer required for trans-atmospheric flight by using the oxygen in the atmosphere. In addition to using a CCPS, it was argued that an SSTO launch vehicle would be the best suited configuration to increasing reusability and ultimately reducing launch costs. Though, CCPS concepts have been around for almost 50 years or more (Heiser and Pratt, 1994), the definition of what exactly constitutes a combined-cycle engine is debated. The following sections will attempt to define what exactly is meant by a combined-cycle engine in the context of this project and also attempt to eliminate the number of concepts to be considered for applications in an SSTO launch vehicle.

2.1 Introduction to Combined-Cycle Propulsion Systems

What exactly is meant by a CCPS? The exact definition and terminology vary from paper to paper, but an attempt will be made to establish some commonality between the various definitions. Some papers categorize a propulsion system as being a CCPS only if all of the propulsion subsystems are in use at all times during the flight. By this definition, an engine such as the turbo-ramjet would not qualify as a CCPS. During low Mach number flights, the upstream $WXUERMHWSRUWLRQRIWKHHQJLQHZLOOEHXWLOLJHGDQGWKHORQJDIWHUEXUQLQJGXFWRZQ\WSURYLGHDQ\$ propulsion assistance. At higher Mach numbers, the afterburner will act as a ramjet and provide all the propulsion performance while the turbojet will essentially remain as dead weight. Therefore, under the first definition of a CCPS, a turbo-ramjet would not be considered a CCPS.

However, this definition of a CCPS is not the predominant definition because it excludes a wide range of propulsion systems that are by all other means combined-cycle in nature. A better definition of a CCPS was given by (Escher and Flornes, 1966) in their volume of papers $WLWOHG \text{ }^3\text{A Study of Composite } 3URS\text{XOVL}RQ6\backslash\text{VWHPVIRU}\$GYDQFHG/DXQFK9HKLFOH\$SSOLFDWLRQV'$ They differentiate between a combination propulsion system (CPS) and a combined-cycle

propulsion system (CCPS). According to them, a CPS is defined as a combination of completely independent propulsion systems operating on one vehicle at different flight regimes, whereas a CCPS is defined as a single propulsion system assembly operating in several modes at different points throughout the flight regime. (Curran, 1990) further elaborates this definition by stating that D&&36LV □ ³DQHJLQHV\VWHPZKRVHPDLQHOHPHQW is the ramjet engine (with subsonic and/or supersonic combustion) that is boosted to ramjet takeover speed by means of a turbo-engine (turbo-accelerator) or rocket ± based system, and that uses ramjet propulsion at the higher VSHHGV´

These explanations on the difference between a CPS and a CCPS are used to shape the definition used in this project. For this project, a CCPS is defined as a single propulsion system assembly that has multiple operating modes using the same propulsion subsystems (compressor, combustor, and nozzle) interchangeably throughout the flight. Ideally, a CCPS should integrate the same subsystems between rocket, ramjet, and scramjet in order to reduce dead weight and optimize propulsion performance through a wide range of flight speeds and operating altitudes. A CCPS would closely integrate subsystems from many different cycles such as turbo-machinery from turbojets, gas generators or ejector rocket engines, compression inlets from air-breathing systems, and combustors from turbojets, ramjets, and scramjets. The integration of all of these systems with the intent of coupling each system across different operating modes forms the basis for CCPS design.

For the majority of designs, CCPS are intended for two modes of operation; air-breathing and rocket. As previously mentioned, the goal of a CCPS is to utilize each operating mode in the flight regime where it is most efficient as defined by its *isp*. Typically, the first mode of operation is low speed subsystem from Mach 0 to 3, supersonic subsystem from Mach 3 to 5, hypersonic subsystem from Mach 5 to 10, and finally the rocket subsystem from Mach 10 to orbital velocity.

2.2 Subsystems of Combined-Cycle Propulsion Systems

The driving factor for designing a CCPS is that no one propulsion system is efficient across the full range of flight Mach numbers that a launch vehicle will travel through. A CCPS will utilize at least two or more subsystems, air-breathing and rocket (if the intention is to use the CCPS on a launch vehicle). Before proceeding into a comprehensive discussion on a full CCPS design, each subsystem will be defined and briefly described in a high-level fashion. This section is just meant to provide a brief first-pass overview to introduce concepts. More detail on specific subsystems and how they interact throughout the range of flight regimes will be given in the RBCC overview in a later chapter.

2.2.1 Turbofans and Turbojets

Turbo-machinery subsystems consist of turbojets and turbofans. Both of these propulsion subsystems are among the most efficient propulsion systems, as shown above in Figure 1.1, with high isp in the low Mach number flight regime. They utilize high compression and bypass ratios to make use of the air in the atmosphere as the principle working fluid and oxidizer. The temperatures at which they can operate are limited by their mode of operation, however. As a result of deceleration from high speeds to low speeds, the extremely high stagnation temperatures and pressures present on the fan blades of turbofans and the turbine would cause damage and likely failure. Until materials are designed that can withstand these extreme temperatures, turbofans and turbojets are confined to operate at low Mach numbers. If they were to be used in a CCPS they would have to be stowed away and out of the flight path during high speed flight. This would require complex and heavy structures which might reduce the propulsion performance beyond the efficiency gains made by having a turbofan or turbojet subsystem in the first place.

2.2.2 Ramjet

Ramjet propulsion systems operate with no moving parts and are possibly the simplest form of propulsion system devised. Within the high supersonic flight regime, ramjets outperform any other type of propulsion system including turbofans, turbojets, and rockets in terms of *Isp*. They operate on the principle of compression due to oblique shockwaves forming based on the inlet geometry and the supersonic flight velocity. These shockwaves undergo a series of impingement and reflections upon walls inside the inlet duct and inlet wedge. This results in compression of the flow up to a certain point suitable for combustion. When fuel is added into this highly compressed, high temperature air, it combusts and then travels through a convergent-divergent supersonic nozzle creating thrust. While ramjets are highly efficient between the Mach numbers of around 2 to 6, they are limited above approximately Mach 6 due to the extreme stagnation temperatures encountered in facilitating subsonic compression at these speeds. Current materials limitations impose this upper limit on ramjet operating Mach number.

2.2.3 Scramjet

At the point where subsonic combustion in a ramjet is no longer feasible, supersonic combustion ramjet engines or scramjet engines become operable. A scramjet is a ramjet engine which is designed to also operate at Mach numbers above 6 and possibly up to Mach 10. It does so by enabling supersonic combustion through varying the inlet geometry and no longer moving the fluid through a convergent-divergent nozzle. Instead, it slows the incoming flow down to low supersonic speeds, sprays fuel and then combusts supersonically, and finally expands the working fluid through a nozzle. Scramjets are significantly more efficient than rockets in the flight regimes in which they operate and have been test flow on several experimental aircraft including the X-51. So far, these experimental aircraft have provided good test-beds for verifying scramjet system designs and prove that it is possible to operate at high Mach numbers. However, they are also subject to extreme heating limitations due to the high stagnation temperatures present at such high speeds.

2.2.4 Rocket

Of course there is the all-time most widely used space launch vehicle propulsion system, the rocket. Rockets are not confined to operating at any particular flight regime or altitude. They carry all of their working fluid and oxidizer with them at all points in the flight, so they are the most reliable, predictable, and simplest form of propulsion systems used for launch vehicles. Additionally, there is no need to ensure that a rocket powered launch vehicle follows an optimum air-breathing trajectory which will reduce overall performance by means of greatly increased drag throughout the atmosphere. In addition, rocket engines have some of the highest thrust to weight (T/W) ratios of any propulsion system. However, their extensive utility, reliability, and simplicity come at the price of efficiency. Rocket propulsion systems will play a role in space travel for a long time to come, but will likely take on drastic changes in the future such as beam-ignition rockets.

2.3 Types of Combined-Cycle Propulsion Systems

There are several different types of CCPSs, but most either fall into one of two broad categories: Turbine-Based Combined Cycle (TBCC) or Rocket-Based Combined Cycle (RBCC). The former utilizes a turbine based engine cycle for the low-regime portion of the flight while the latter uses a rocket or set of rockets for this portion of the flight as well as the end portion of the flight.

7KHWZRPDMRUFDWJHRULHVRI&&36¶VZLOOEHGHWDLOHGVRPHPRUHEHORZZLWK
DQ emphasis on applications to space launch vehicles.

2.3.1 Turbine-Based Combined Cycle (T B C C) Propulsion Systems

Not much overview will be given on TBCC propulsion systems since they are currently being developed mainly for the flight regime of Mach 0 to 4 and within the atmosphere (Bartolotta et al, 2003) whereas this project focuses specifically on a space launch vehicle application. A TBCC propulsion system would theoretically make use of the extreme efficiency of turbofans from static conditions to transonic Mach numbers and the efficiency of a turbojet

from that speed to around Mach 3. In order to do this, a rather complex propulsion system would have to be designed which would incorporate fan blades or turbine blades as well as, at least, another high Mach number air-breathing propulsion system.

A typical TBCC propulsion system would utilize a turbofan or turbojet to produce thrust and accelerate the vehicle from rest to an intermediate Mach number. A secondary airstream would bypass the main combustor of the turbojet or turbofan and go to an afterburning ram duct which provides greater thrust at higher Mach numbers. Once the vehicle is at supersonic speeds, an inlet shock cone and turbo-compressor diffuse the air into the ramjet afterburner. A great example of a TBCC propulsion system, the Pratt & Whitney J-58, is used to power the supersonic Lockheed Martin SR-71 Blackbird.

While the TBCC propulsion system would be extremely useful at relatively low Mach numbers, it is not suitable for use on an SSTO launch vehicle. In order to use a TBCC propulsion system on an SSTO vehicle, the fan and turbine components would have to be moved out of the main flight path and into stowage during high-speed flight through the atmosphere. However, they would be well suited for applications in a two-stage-to-orbit (TSTO) vehicle as the lower stage booster.

2.3.2 Rocket-Based Combined Cycle (RBCC) Propulsion Systems

In this project, an RBCC propulsion system is categorized by having a rocket engine as its main propulsion element. These propulsion systems include ejector rockets and air-breathing rockets. Ejector-rockets act as a jet by forcing air into the inlet by means of a lower pressure gradient caused by the rocket flow in the duct. Entrained air reacts with fuel-rich exhaust and combusts while the rocket exhaust itself also expands through a supersonic nozzle. Engine types such as the Liquid Air Combustion Engine or (LACE). LACE engines utilize a low-temperature condenser at the inlet to liquefy incoming air and then separate the liquefied oxygen for use as oxidizer for the rocket engine. In this sense, it is RBCC propulsion systems, like TBCC propulsion systems, can be used either to enhance an existing engine or on their own for an entire mission profile. Since

the focus of this project is RBCC propulsion systems, much greater detail on the history, theory, and current literature on RBCC propulsion systems will be given in the following sections.

2.4 History of Combined-Cycle Propulsion Systems

Combined cycle propulsion systems have been around since almost the beginning of the widespread use of jet engines and have their history closely intertwined with the development of the ramjet engine. In fact, their history goes as far back as 1913, when Rene Lorin of France proposed a method of propulsion utilizing ram air pressure and heat addition to produce thrust in an engine

DQGUHFHLYHGSDWHQWIRUWKHZRUOG¶VILUVWUDPMHW

%LEODUJDQG=XFNHU □□□

. In 1915, one of Lorin's predecessors, Albert Fono of Hungary, proposed the use of a ramjet propulsion unit on long-range artillery to increase its range

□ WHUPHGD³VHUUWLDWRUSHGR´ (Gyorgy, 1977). He took his proposal to the Austro-Hungarian Army, but the proposal was rejected. Many years after WWI in 1928, Fono once again took up the problem of jet propulsion E\HODERUDWLQJRQWKH³DLU-jet engiQH´VXLWDEOHIRUKLJK-altitude supersonic aircraft and applied for a German patent. In 1932, he filed an additional patent application wherein he adapted his engine for subsonic speeds as well and was finally awarded both patents with a priority date of May 1928. 7KHVHPHQ¶V patents had tremendous ingenuity and foresight, however they came up with the theory at a time when its implementation was impractical because the sonic barrier had not yet been broken and many at the time believed that it would remain that way forever.

The French were making great strides in ramjet propulsion in the □¶VYet another Frenchman by the name of Rene, Rene Leduc, pioneered one of the first practical ramjet-powered aircraft named the Leduc 0.10. It was first successfully flown in 1949 after being released from the Languedoc aircraft since it had no ability to produce static thrust on its own and thus to accelerate to the required speeds for ramjet propulsion. During its test flights, it accomplished a significant milestone by reaching speeds of up to Mach 0.84 at a time when the sonic barrier had not yet been broken. Shortly thereafter, the French state-owned aircraft manufacturer Nord AYLDWLRQGHVLJQHGWKH*ULIIRQDLUFUDIWZKLFKIHDWXUHGWKHZRUOG¶VIL UVW turbojet-ramjet power-plant. It was capable of reaching speeds of up to Mach 2.19, but encountered difficulties with the airframe and propulsion system overheating at high speeds and

also the ramjet was hard to control at mid-speed (Biblarz and Zucker, 2002). This was the ZRUOG¶VILUVWWUXHLP SOHPHQWDWLRQRIDFRPELQHG-cycle propulsion system.

One of the premiere examples of high speed, high altitude use of combined cycle propulsion systems is seen in the SR-71 Blackbird in the ¶¶VIt was powered by two Pratt & Whitney J-58 turbojet engines. The turbojet engines were designed for operation in the subsonic and transonic flight regimes. At higher supersonic Mach numbers, the diffuser cone would translate rearward, maintaining shock on lip conditions, and would slow the incoming supersonic flow to subsonic speeds for combustion. Therefore, it can also be defined as a turbo-ramjet engine since its second operating mode uses the same principles of ramjet propulsion. It also demonstrated the practicality and promise of using variable geometry in engine design. With variable geometry, the size of an engine can be greatly reduced as the geometry is optimized for whatever the flow regime in which the vehicle is operating (Heppenheimer, 2006).

\$URXQGWKH ¶¶VWR ¶¶VUDPMHWHQJLQHXVHEHFDPHPRUHZLGHVSUHDGDVL
WZDV

adapted to many missiles such as the Navaho, X-7, Bomarc, Gorgon, and Talos. However, it became apparent that there were limitations to the operational Mach number at which ramjet engines could operate due to overheating of the engine and airframe at around Mach 5 to 6 (Heppenheimer, 2006). In order to address this issue, the ramjet engine had to be modified to allow for supersonic combustion in order to avoid the high stagnation temperatures encountered during subsonic ramjet combustion.

It was clear that there were issues due to high temperatures and pressures in the near hypersonic regime for ramjet propulsion, so researchers began focusing on scramjet propulsion. In 1957, the Russian, E.S. Schetinkov, produced experimental data on scramjet performance up to Mach 20 and proved the superiority in performance over a ramjet (Sabel'nikov and Penzin, 2001). In 1958, the analytical results of a theoretical Scramjet were introduced by DHURG\QDPLFLVWV5LFKDUG:HEHUDQG- RKQ0F.D\DW1\$&\$¶¶V/HZLV)OLJKW3URSXOVL RQ Laboratory. Also in 1958, others including R. Dunlap, R.L. Brehm, and Antonnio Ferri are attributed to development of the scramjet propulsion system (Falempin, 2001).

After the introduction of the scramjet concept, the integration of a ramjet and scramjet propulsion system into one engine using the same components for both subsystems became an LPSRUWDQWJRDO, QWKH ¶¶V ¶&XUUDQDQG6WDOOSURSRVHGDQGS DWHQWHGDWUXH GXDOPRGH propulsion system that could produce thrust at low supersonic Mach numbers via subsonic combustion and also produce thrust at hypersonic Mach numbers via the scramjet operating mode (Heiser and Pratt, 1994). The goal of their development was to relieve the high heating and compression technical issues of near-hypersonic ramjet combustion.

However, the practicality of ramjet and scramjet engines still remained low because of their inability to produce static thrust. This inconvenience led to the development of the ejector ramjet concept in tKH ¶¶VDQG¶¶V. The idea of an ejector was not new, however, since it was used by Horatio Phillips, a late 19th century aeronautics experimentalist, in his attempts to design wind tunnels using pressurized streams of airflow in ducts (Heppenheimer, 2006). It was actually in 1947 that Jack Charshafian, an engineer at Curtiss-Wright, filed a patent for an ejector ramjet. His patent was enticing because it combined a rocket with the dual-mode combustion systems of ramjets and scramjets. This could potentially lead to the development of a propulsion system capable of producing thrust from zero velocity to orbital velocity and all in one single stage. Another significant source of extensive development into RBCC concepts was the work done by the Marquardt CoUSRUDWLRQLQWKH ¶¶V7KH\UHVHDUFKHGGR]HQVVRISRWHQWLDOFRPELQHG cycle propulsion systems and gave renewed focus on the liquid air cycle engine (LACE) and ScramLACE developed by Randolph Rae at the Garret Corporation. This paved the way for current development in the field.

3. Combined Cycle Propulsion System Design Considerations

3.1 Weight Considerations

Combined cycle propulsion systems have great potential to reduce the overall GLOW of a launch vehicle, but they are in some ways also a double-edged sword. On the one hand, they greatly reduce the mass of oxidizer required throughout the flight by extracting oxygen from the atmosphere. By using a CCPS, oxidizer would only be required for the initial rocket-ejector and final all-rocket portions of the flight. The weight reduction via fuel savings would be significant, but a typical CCPS is also more complex and heavier than a rocket-only engine. This is due to the increased length of the flow path and additional structures and subsystems required to operate at all modes of combustion. While it is widely accepted that the reduction in required oxidizer mass exceeds the mass gained from incorporating a more massive propulsion system, the additional weight of the CCPS must be taken into account when attempting to predict vehicle performance.

3.2 Fuel Considerations

One of the primary considerations for choosing what type of fuel to use for a space launch vehicle is the energy content of the fuel and more specifically its energy density. In order to maximize the payload, the mass of every other component of the launch vehicle must be as reduced as much as possible within allowable constraints. Below, in **Table 3.1**, is a comparison of fuels commonly used for aerospace applications along with their heat of combustion values ($\dot{a}+c^0$). The heat of combustion is a measure of the amount of energy that is released when an exothermic reaction occurs, i.e. energy which can perform work on accelerating the working fluid. In this table the lower heating value (LHV) of $\dot{a}+c^0$ is used under the assumption that the latent heat of vaporization of water in the fuel and reaction products is not recovered, i.e. there is no condensation and water remains in vapor form after the combustion process. This is quite typical of high temperature (over 150 °C) conditions.

Table 3.4: Properties of commonly used aerospace fuels (Heiser and Pratt, 1994).

Fuel	H eat of Combustion (kJ/ k G)	H eat of Combustion (B T U/lb _m)	Liquid Phase Density (kg/m ³)
Hydrogen (H ₂)	119,954	51,571	67.8
Methane (CH ₄)	50,010	21,502	416
Ethane (C ₂ H ₆)	47,484	20,416	546.49
Hexane (C ₆ H ₁₄)	45,100	19,391	654.83
Octane (C ₈ H ₁₈)	44,786	19,256	917.86

Hydrogen, (molecular formula H₂), clearly is the desirable choice of fuel over the hydrocarbons typically used because its $\dot{a}+c^0$ is over greater than that of the hydrocarbon fuels listed by a factor of two. Furthermore, H₂ is the lightest molecule and when combusted with oxygen the H₂O produced will be at much higher exhaust velocities than a hydrocarbon fuel can achieve. Hydrogen-oxygen combustion systems typically run fuel-rich as well, which will lower the average density of the exhaust further increasing the exhaust velocity. As shown in the simplified thrust equation below, a higher exhaust velocity or effective exhaust velocity, c , directly contributes to a higher engine thrust. Here, \dot{m} is the mass flow rate and T is the thrust.



A more detailed way to examine the effect that the fuel selection has on the T and efficiency of a propulsion system is to look at a typical all-rocket propulsion system as an example, which still has applicability in this project. Shown below, in Figure 3.1, is a simplified free body diagram of a control volume encompassing an extremely simplified, typical rocket propulsion system. The main focus of this diagram is to highlight the relative magnitude of the pressure distribution within the engine. The location of different stations of the propulsion system such as the thrust chamber (station 1), the nozzle throat (station t), the nozzle exit (station 2), and also the atmosphere (section 3).

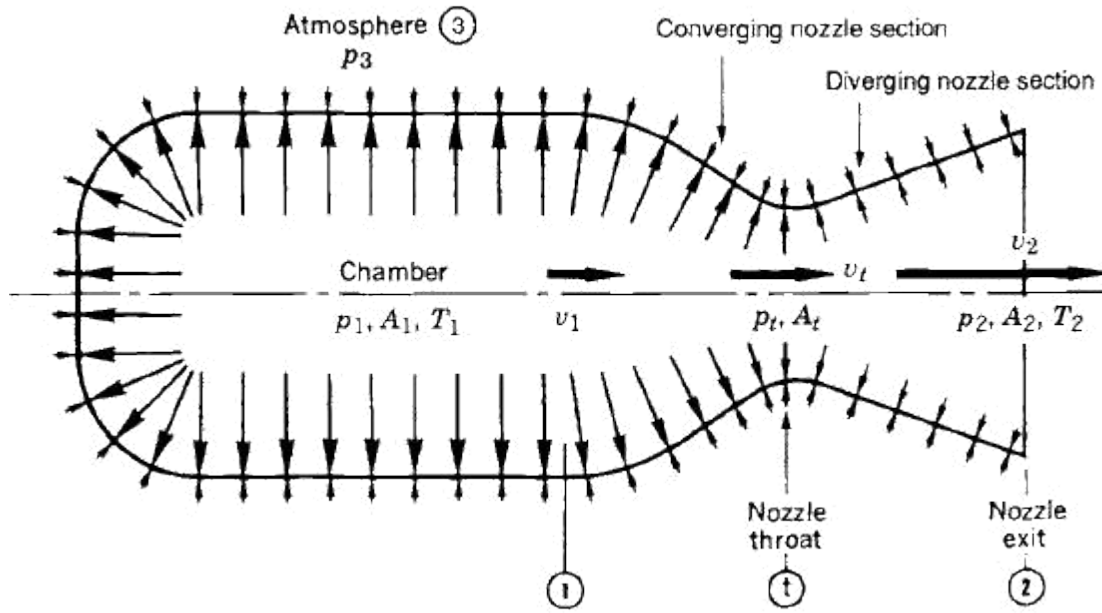


Figure 3.7: Diagram of the pressure balance on chamber and nozzle interiors. The location of the stations of the propulsion system is the focus of this figure (Biblarz & Sutton, 2001).

Using these station definitions, the thrust equation is expanded, as shown in the equation below.

$$F = \dot{m} v_2 + (p_2 - p_3) A_2$$

Where,

v_2 = nozzle exit velocity (equal to c)

p_2 = pressure at the nozzle exit

p_3 = pressure of the atmosphere

A_2 = area of the nozzle exit

A better description of the effective exhaust velocity is now derived (assuming isentropic flow through the nozzle). This is a fairly good assumption for a converging-diverging nozzle where a large fraction of the thermal energy of the gases is converted into kinetic energy in a reversible process.

$$c = \sqrt{\frac{2 \gamma}{\gamma - 1} \frac{p_t}{\rho_t}}$$

Where,

k = the ratio of specific heats

R = universal gas constant

T_1 = stagnation temperature of the chamber or nozzle

M = average molecular mass of the fuel

p_1 = chamber pressure

p_2 = pressure at the nozzle exit

The influence of the molecular mass of the fuel can be seen below, in Figure 3.2, by

plotting the ideal specific impulse against the ratio of the inlet temperature at the nozzle to the average molecular mass of the

fuel.

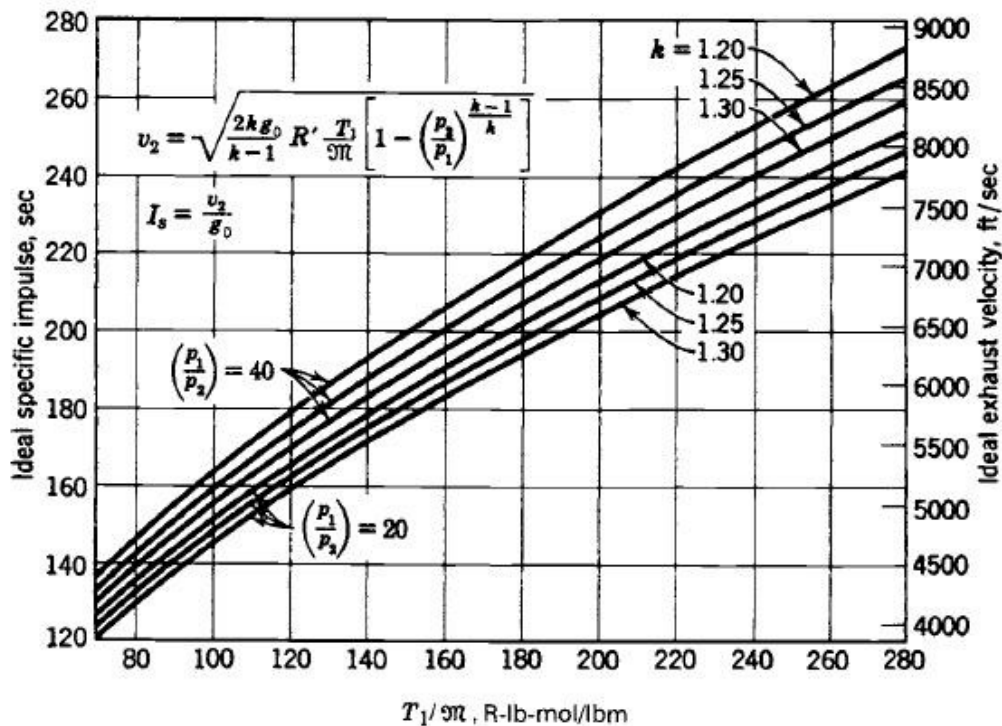


Figure 3.8: Specific impulse and exhaust velocity of an ideal rocket at optimum nozzle expansion as functions of the absolute chamber temperature T_1 and the molecular mass M for several values of k and p_1/p_2 (Biblarz & Sutton, 2001).

As depicted in Figure 3.2, the ideal specific impulse, I_{sp} , is directly proportional to the effective exhaust velocity, v_2 , which is inversely proportional to the average molecular mass of the working fluid (fuel + oxidizer mixture). Therefore, using hydrogen as the fuel source,

instead of a hydrocarbon fuel, results in the highest possible propulsive efficiency. However, it must also be noted that hydrogen also has the lowest density and therefore also requires fuel tanks occupying the largest volume. Larger fuel tanks result in a larger vehicle and that extra required volume will result in an increase to the cross-sectional area of the vehicle, resulting in increased base drag on the vehicle throughout its flight through the atmosphere.

One method to reduce the density of hydrogen is to super cool it to its freezing temperature. This results in a mixture of liquid hydrogen and small suspended frozen particles of frozen hydrogen, which is denser than liquid (Biblarz & Sutton, 2001). Experiments have been SHUIRUPHGRQWKLV³VOXVK
'KIGURJHQDQGLWKDVEHHQIRXQGWREHGLILFXOWWRSURGXFHQDQGPDLQWDLQ a uniform mixture. To this date, slush hydrogen has not been used on a flight vehicle. Nevertheless, the benefits of hydrogen fuel outweigh the disadvantages due its high energy content, but using it also comes with design compromises and increase in complexity.

3.3 Engine Performance Based on Component Efficiencies

A combined-cycle propulsion system is only as effective a propulsion system as the combination of efficiencies of its subsystems. In order to have a high over all engine efficiency, each subsystem of the engine (inlet, burner, and nozzle) must stay within a range of acceptable efficiencies. The overall performance of the propulsion system is extremely sensitive to any drop in propulsion performance of any of these subsystems. The highest sensitivity to these changes in efficiency is in the hypersonic flight range (Kors, 1990).

Below, in Table 3.2, the nominal, theoretical, and underachieved efficiencies are listed for the three main engine components. Along with their efficiencies, the table lists what affect in efficiency each component has on the overall engine performance.

Table 3.5: Engine component efficiencies and their effect on engine performance (Kors, 1990).

Component	Efficiency	Efficiency Relation	Relative Efficiency		
			Ideal	Nominal	Underachieved
Inlet	KE	Kinetic efficiency	1	0.975	0.95
Burner	b	$\frac{C_p T_3}{C_p T_2}$ $\frac{C_p T_3}{C_p T_2}$	1	0.90	0.80
Nozzle	c	$\frac{C_p T_3}{C_p T_2}$ $\frac{C_p T_3}{C_p T_2}$	1	0.975	0.95

From this table, it can be seen that the efficiencies of the inlet and nozzle must be kept at the highest possible values (above 95%) in order to not drastically reduce the propulsion system performance at hypersonic velocities. While the burner

desired to maintain a high efficiency here to extract the most energy out of the fuel as possible. In order to achieve these high efficiencies, each of these subsystems must be capable of operating efficiently in each operating mode at varying Mach numbers. This is no small feat as it is already difficult to maintain component efficiency for a single operating mode. Variable geometry must be utilized for both the inlet and nozzle in order to maintain the required high level of efficiency.

3.4 Launch Configuration: Staging and Launch Type

Another important consideration that was briefly discussed in the first chapter is whether to use vehicle staging to utilize SSTO approach. Now a basic preliminary trade study will be performed to determine the advantages and disadvantages between an SSTO and a TSTO vehicle approach. The seven criteria for selecting one approach over another are operating cost, safety, reliability, operations complexity, reusability, design complexity, and payload performance. Some of these evaluation criteria will be explored in later proceeding sections of this report.

The expectation is that by using a robust reusable SSTO vehicle, the operating costs and complexity will be significantly lower since the MTBO will most likely increase to approach a number much closer to airliner-type values or at least allow several flights before a complete repair. In the long term, this will lead to lower operating and maintenance costs as opposed to a TSTO where the lower stage will most likely have to be heavily repaired after being jettisoned at a high altitude.

Safety and reliability are improved by using an SSTO approach because there are no separation events and thus no chance for separation failure. However, by using a single stage, there is a potentially very significant risk if the vehicle were to take any form of damage early on in the flight. For example, the lower stage of a multi-stage vehicle may take mild damage from debris during launch, but if it makes it to the separation altitude it can jettison the damaged lower stage and still successfully complete the mission with the in-tact upper stage. If an SSTO vehicle were to take mild damage during an early portion of the launch, it would have to ascend completely and also descend with the increased likelihood of the earlier damage possibly HVFDODWLQJWRVRPHWKLQJFDSDEOHRIGHVWUR\LQJWKHYHKLFOH7KHUHKDYHQ¶WEHHQPDQ\LQVW DQFHVRI this type of rare event occurring, so the overall risk is low when compared to the risk for a faulty stage separation.

However, the TSTO approach does have significant advantages in two criteria that have been extremely important to both launch vehicle designers and launch customers: design complexity and payload performance. These two criteria have been the dominant reasons for the use of multi-stage vehicles. With current all-rocket propulsion systems, it has just been too difficult to design a vehicle that can obtain orbit with just a single stage, let alone while hauling a considerable payload that can provide the opportunity for profit. However, using an RBCC propulsion system in an SSTO creates leeway to design more robust structures while carrying heavier payloads, so the TSTO advantage is slightly diminished.

Overall, the SSTO approach wins in the important criteria of operating cost, safety, reliability, operations complexity, and reusability, while giving the slight edge to TSTOs in design complexity and payload performance. To get a more comprehensive trade study, one

approach would be to compare the payload performance per flight and then flights possible per year for two fully derived SSTO and TSTO designs to calculate the total payload performance per year and thus per cost. The results of the preliminary trade study are shown below in Table 3.3.

Table 3.6: Trade Study: SSTO vs. TSTO

Category	SST O	TST O
Operating Cost	█	
Safety	█	
Reliability	█	
Operations Complexity	█	
Reusability	█	
Design Complexity		█
Payload Performance		█
Winner	█	

In addition to the considerations for vehicle staging, the launch and landing method play a role in determining how the vehicle is designed. There are four general categories of takeoff and landing configurations:

1. Vertical Takeoff, Vertical Landing (VTVL)
2. Vertical Takeoff, Horizontal Landing (VTHL)
3. Horizontal Takeoff, Vertical Landing (HTVL)
4. Horizontal Takeoff, Horizontal Landing (HTHL)

Currently, every single all-rocket launch vehicle uses a vertical takeoff approach since the high T/W ratio of all-rocket engines enables the use of a ballistic trajectory as opposed to a lifting trajectory that would typically be used by a winged vehicle. A horizontal takeoff would

require that the launch vehicle be capable of aerodynamic lift via wings. This would of course require that the launch vehicle spend a great deal of time in the atmosphere and at high velocities resulting in significant aerodynamic heating and drag. However, less fuel would be required by utilizing some lift provided by the wings for at least some portion of the flight. A tradeoff must be made for implementation in a CCPS wherein a portion of the trajectory is vertical, then horizontal, and finally vertical again. Using this method would negate the need for heavy landing

JH DUVLQFHWKH*/2:ZRXOGQ¶WQHGGWREHVXSSRUWHGRQWKHUXQZD¶ EXWZRXOGD OVRrequire that the T/W ratio of the beginning rocket portion of the flight be sufficiently high enough for vertical takeoff.

Choosing the method of landing is fairly simple since it would be impractical to have a vertical landing, so the only option left is a horizontal landing. Lift generating wings would be required for the reentry portion of the trajectory as well as landing gear, but it could be designed for minimal weight since it would only be supporting the vehicle dry weight. Benefits for choosing a horizontal landing are the ability to have a controlled descent, less vehicle heating than a ballistic landing, and thus also more reusability. Noting the benefits of a vertical takeoff and horizontal landing (VTHL) scheme, this method is chosen for this project.

3.5 Overall Vehicle Geometry Selection

Before delving into the details on what considerations are made in integrating the propulsion system and airframe, the considerations that are used to select the overall vehicle geometry must first be detailed. A great deal of the information in this section and the proceeding sections

FDQEHDWWULEXWHGWRDVWXG\WLWOHG³\$LU\$XJPHQWHG5RFNHW3URSXOVLRQ &RQFHSWV 'SHUIRUPHGE\WKH\$VWURQDXWLFV&RUSRUDWLRQRI\$PHULFDIRUWKH\$LU)RUFH\$VWURQDXWLFV

Laboratory in 1989. There are numerous methods in which the launch vehicle can be designed and arranged ¶ EXWWKHWZRPRVWFRPPRQO\XVHGPHWKRGVIRU&&36¶VDUHDZHGJH-like shape with the propulsion system(s) integrated into the underside of the airframe or an axisymmetric vehicle with discrete propulsion pods at equal angles along the vehicOH¶Vlongitudinal axis.

,W¶VGHVLUHGWR be able to launch the vehicle vertically as mentioned in the previous section, so the former wedge-like geometry would not be ideal since it relies on low angles of attack in order to

operate. A wedge-shaped vehicle with a CCPS would make an ideal second stage vehicle where it could fly at lower angles of attack and not have to launch vertically. An axisymmetric design will be examined for the remainder of this project.

Axisymmetric vehicles enable the maximum utilization of the vehicle geometry to impart work on the flow. The vehicle forebody provides the first step in flow compression and also allows for maximum flow capture if the engines are integrated at multiple points along the length of the vehicle as discussed in the preceding sections providing maximum volumetric efficiency over any other configuration as shown below in Figure 3.3. An axisymmetric design also allows for a vertical takeoff if all of the engines are spaced at equal angles and distances from the longitudinal axis.

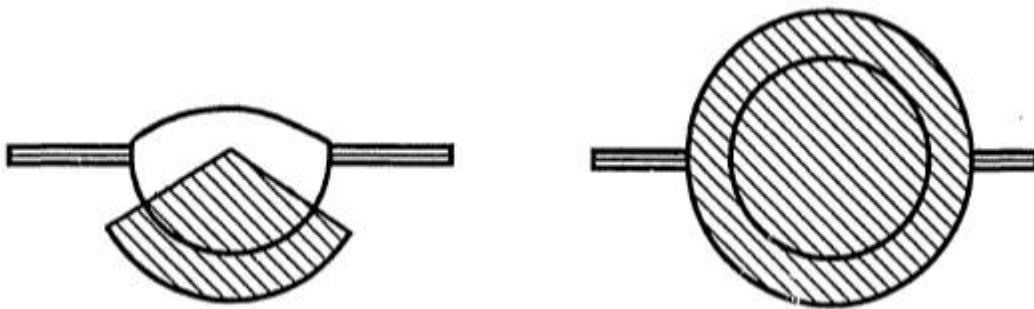


Figure 3.9: Potential capture area limits for non-axisymmetric (left) and axisymmetric vehicles (right) (Escher et al., 1989).

However, several undesirable flow effects manifest themselves on axisymmetric bodies at higher angles of attack such as reduced forebody compression on the upper portion of the vehicle due to a decrease in the effective cone angle with respect to the freestream flow as depicted below in Figure 3.4. This is accompanied by an increase in the thickness of the boundary layer which has the potential to distort the flow going into the inlet and causing unstart conditions. Furthermore, local vorticity may develop and contribute to nonuniform flow entering the engine system. Additionally, there is also the problem of conical cross flow around the vehicle forebody at sustained angles of attack (Escher et al., 1989).

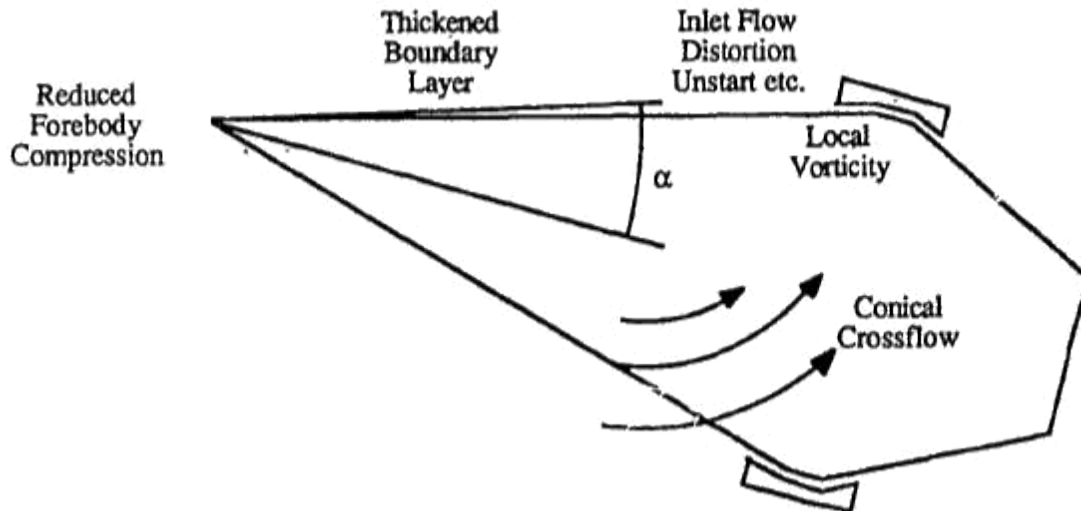


Figure 3.10: Effects of flight at positive angles of attack on an axisymmetric vehicle (Escher et al., 1989).

Despite the possible issues with axisymmetric vehicle geometry, it has more advantages in terms of volumetric efficiency, ease of launch, reduced complexity, and weight potential. From this point on, the only vehicle geometry that will be considered and referenced is axisymmetric vehicle geometry.

3.6 Propulsion System Integration into the Airframe

One of the main factors to consider when designing a CCPS is integration within the airframe. High-speed air-breathing propulsion systems and vehicle geometry/integration are highly coupled in their development due to the need to utilize the vehicle body upstream of the propulsion system for pre-compression and diffusion. This section will elaborate on some of the possible configurations for propulsion system/vehicle integration and what factors must be taken into consideration when choosing a specific configuration.

When integrating a CCPS into a vehicle structure, one of the first considerations is the vehicle forebody conical shock geometry as a function of flight speed (Escher et al., 1989). Ideally the maximum outer diameter of the inlet should be kept within the thin shock layer formed by the conical shock wave at the apex of the conical forebody at the maximum air-breathing flight speed as shown in an example in Figure 3.5, below.

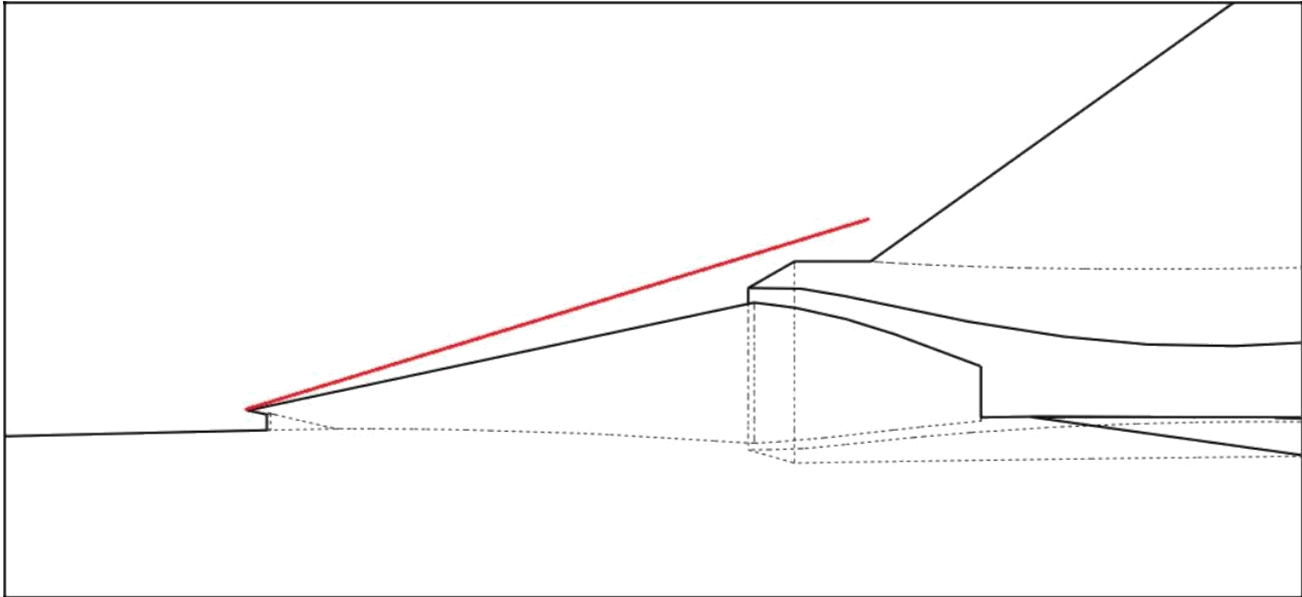


Figure 3.5: Example of conical shock wave (red line) at maximum air-breathing Mach number. The outer diameter of the inlet must remain within the shock wave.

One method that could be used to determine if this condition is satisfied for a given inlet cone geometry is to use CFD to examine the conical shockwave angle at multiple angles of attack and at various flight regimes (altitude and velocity). A full 3D CFD analysis would take into account the 3D relief effects not accounted for in a 2D oblique shock wave analytical solution. Shown below in Figure 3.6, is the variation in conical shock angles as a function of flight Mach number for an eight degree half angle slender cone at zero degree angle of attack.

For axisymmetric vehicles at hypersonic Mach numbers, Figure 3.6 and others like it, for various cone angles, are useful for determining where within the thin shock layer a cowl surface has to be fitted. A common method to ensure that the cowl surface is always within the thin shock layer is the utilization of variable geometry by means of centerbody translation. Typically, the cone centerbody will be mounted on a diverter pylon with a linear actuator driven by a computer which determines the translation required in order to satisfy proper shock location based on internal and external flow conditions.

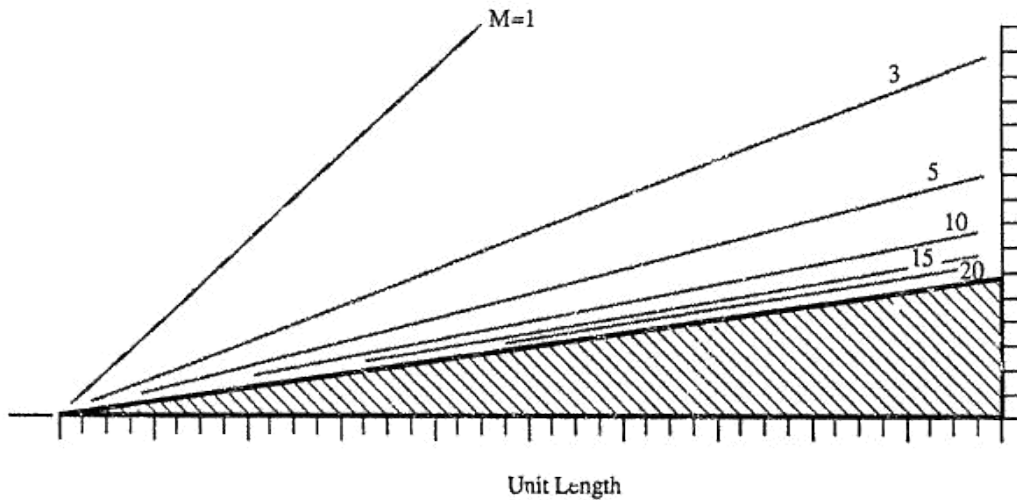


Figure 3.6: Inclination of a conical shock for an eight degree half-angle cone at a zero degree angle of attack. Ideal gas with $k = 1.40$ (Escher et al., 1989).

In addition to the placement of the engine on the vehicle, another important propulsion system/vehicle integration consideration is the determination of the number of engines and in effect also the size of each engine. Essentially, there are two extremes when it comes to the integration of the propulsion system/vehicle; multiple discrete engines or one continuous annular engine. Either rectangular or circular cross section engines can be used for each engine in the discrete and annular engine approach. Using a greater number of engines reduces the size of each one and also the thrust, but it also increases the total mass capture possible. It does also increase the drag and complexity of the vehicle, so for this project, fewer engines will be chosen.

Another important consideration when integrating the propulsion system onto the airframe is the interaction between the boundary layer from the inlet and the propulsion system. As the flight Mach number increases, the boundary layer gets thicker, so an effort must be made to keep the propulsion system out of the boundary layer. Rectangular, circular, or some other deviation of propulsion system cross-sections can be used for the propulsion pod. Rectangular cross-sectional engines have higher structural weight and also direct interaction with boundary layer if they are placed directly on the vehicle as shown below in Figure 3.7. Circular cross section engines are preferred because they can be mounted on diverter pylons which serve to keep them from interacting with the boundary layer. According to early researchers from NASA Langley, the boundary layer should not be ingested at subsonic and low supersonic Mach

numbers and should probably be ingested at higher supersonic and hypersonic velocities (Escher et al., 1989).

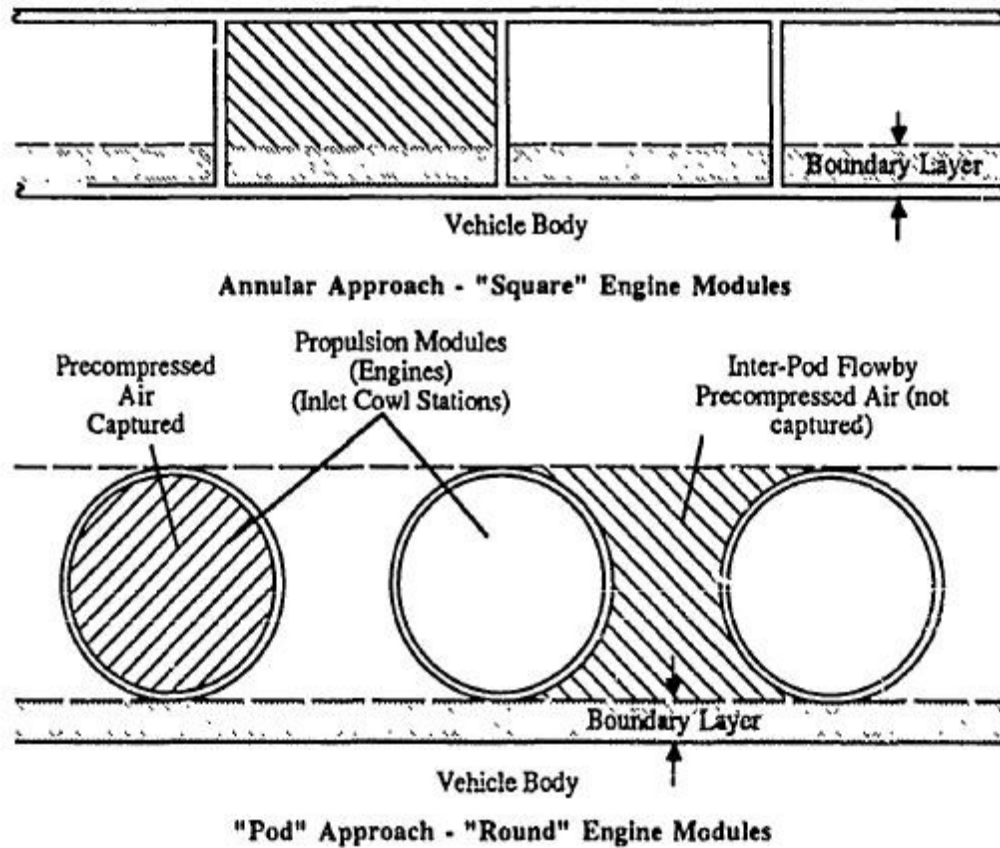


Figure 3.7: Rectangular vs. round engine module integration approach (Escher et al., 1989).

3.7 Continuous Stability and Operation in All Flight Regimes

The single greatest challenge, nay the whole goal, in designing a CCPS is to ensure that the propulsion system operates continuously throughout the flight regime from static thrust to orbital velocity. To add to the challenge, it must also do this while maintaining a high enough level of efficiency as to offset the performance losses inherent in a heavier engine flying through the atmosphere for a longer portion of the trajectory. Ever since the earliest studies into the application of H_2/O_2 for trans-atmospheric flight were carried out by the Marquardt Corporation in the 1960s it has been known that in order to maintain overall system optimization, each subsystem needs to operate at maximum efficiency in its flight regime.

2IDOORIWKHVXE\ VWHPV □ LW¶VPRVWLPSRUWDQWWKDWKHLQOHWEHSURSHUO\GHVLJQHGVLFQ
HLWLV

the only subsystem that will be operating throughout the entire air-breathing flight regime of Mach 0 to around Mach 15.

,W¶VSDUWLFXODUO\GLIILFXOWWRDFKLHYHPD[LXPPLQOHWFDSWXUHDUHDDQG high inlet efficiency over the varying geometrical requirements of the inlet system as a function of speed. For a RBCC vehicle, the propulsion system is typically on the order of 40-50% of the inert vehicle weight, with the inlet comprising approximately 50% of that inert weight. A primary concern in inlet development is the interaction between the boundary layer and inlet. According to early researchers from NASA Langley, the boundary layer should not be ingested at subsonic and low supersonic Mach numbers and should probably be ingested at higher supersonic and hypersonic velocities (Escher et al., 1989).

In order to ensure propulsion stability throughout the flight regime, the inlet must be GHVLJQHGLQVXFKDZD\DVWRHQVXUHWKDWLWFDQSURSHUO\PDLQWDLQ³VWDUWHG
´FRQGLWLRQVDWDOOWLPHV ³WDUWHG´FRQGLWLRQVUHIHUWRsupersonic flow upstream of the inlet throat, also referred to as ³VXSHUFULWLFDO´FRQGLWLRQVAdditionally, the combustion must remain ³stable □
WKHFRQGLWLRQ where the supersonic flow, upstream of the inlet throat, does not cross the throat or remains at the throat). This is an important design consideration for the operation of the ramjet which requires the choke to be downstream of the inlet in order to accelerate the flow from subsonic to supersonic.

Throughout the flight, the burner or combustor will experience extreme pressure increases and potentially some flow blockage whLKFRRXOGSRWHQWLDQO\³OHDN´RXWRIWKH combustor and back toward the inlet opening and out of the engine cowl. When this spillage occurs, it heavily degrades engine performance and is referred to as DQ³XQVWDUW´FRQGLWLRQ. In
RUGHUWRSUHYHQWDQ³XQVWDUW´ condition, typically an isolator (constant area duct) is used to isolate the inlet flow from the backflow from the combustor. An isolator adds a small amount of weight,

EXWPRUHWKQDQFRPSHQVDWHVIRUWKDWDGGHGZHLJKWE\SUHYHQWLQJ³XQVWDUW
´FRQGLWLRQV

4. RBCC Propulsion System Overview

Rocket-Based Combined Cycle (RBCC) propulsion systems are a subset of the broader class of RBCC. Basic elements comprising the RBCC such as the ramjet have been around since the advent of the very first ramjet in 1913 as mentioned in the CCPS history in a previous section. The concept of an RBCC propulsion system arose with the development of air-breathing engines.

There exists an extensive, exhaustive, even daunting collection of literature on the conceptual analysis of a multitude of RBCC propulsion system/vehicle configurations. This section makes an attempt to narrow down the overwhelming number of concepts to a more manageable few which best emphasize the basic concepts that will be relevant for this project.

First, an attempt is made to establish a definition of an RBCC propulsion system which is both inclusive of all relevant propulsion systems and that can also filter out a great deal of alternative systems. Next, the literature used throughout this project will be reviewed in detail and its applicability to this project will be outlined. Finally, a top-level technical overview of the RBCC propulsion system in terms of its overall integration will be used to develop a standard model encompassing a broad range of possible configurations. Due to the technical nature of the content, there will be a lot of overlap between the concepts described in the literature review and the technical overview. However, the literature review will only briefly outline the technical aspects of each system discussed with the majority of the detail in the technical overview and also the theory section that follows.

It must be noted that this is by no means an exhaustive overview of RBCC propulsion systems. Any attempt to document and discuss every single RBCC system at a level of any value would be futile since the number of system variations is tremendous and continuously growing. As a sort of general rule, RBCC propulsion systems which have some level of subscale model experimental testing were chosen as prime candidates for review since they represent the most fully developed concepts available in the public domain.

4.1 Definition of Rocket-Based Combined Cycles

Rocket-Based combined Cycle (RBCC) propulsion systems differ in their configurations

DQGLPSOHPHQWDWLRQVVRZLGHO\WKDWLWLVYHU\GLIILFXOWWRFDWHJRUL]HDOO&&36¶VZLWKUR
FNHW

HOHPHQWVDVEHLQJ5%&&¶V In fact, an infinite number of RBCC configurations could theoretically exist in which there are modifications to the flow path, variable geometry, different configurations of subsystems, multiple implementations of rocket engines, and a multitude of countless other variables that can be altered. For this project, an RBCC is defined as any propulsion system which utilizes a rocket element as its primary propulsion element in achieving static thrust and ultimately trans-atmospheric insertion, while simultaneously using any number of complimentary propulsion system cycles to augment the performance throughout its mission profile.

Nomenclature used to describe basic combinations of subsystems varies greatly throughout the literature and can often lead to confusion. An attempt will be made to standardize and thus reduce some of the nomenclature while still highlighting any nuances between slightly

GLIIHUHQWV\VWHPV ¶ WKRXLKLOHYLWDEO\³HMHFWRUURFNHW´DQG³URFNHWHMHFWRU
´ZLOOEHXVHG

interchangeably a number of times. Different authors refer to the basic combination of a rocket into a duct with an inlet pre-compressor and expansion nozzle as an ³HMHFWRUURFNHW´, ³HMHFWRU UDPMHW

´RU³HMHFWRUUVFUDPMHW´. For the majority of cases, the three nomenclatures are describing the same propulsion system, with the exception that there may in fact be a differentiation

EHWZHHQDQ³HMHFWRUUDPMHW´DQG³HMHFWRUUVFUDPMHW´LQWHUPVRIWKH intended maximum operating mode. If this differentiation does exist in some of the literature referenced, it is referred to just as

DQ³HMHFWRUURFNHW´LQWKLVSURMHFW

Another common misnomer is the labeling of air-augmented rockets as RBCC propulsion systems. While it is often times used to describe the ejector ramjet which is a true air-augmented rocket and also RBCC propulsion system, not all air-augmented engines are RBCC propulsion systems. For example, a simple rocket in a constant area duct, which operates on the concept of DLUHQWUDLQPHQWDQGFPEXVWLRQRIWKHPL[HGIORZ ¶ LVWUXO\DQ³DLU-
DXJPHQWHG´URcket. However,

it incorporates only one cycle (rocket ejector) throughout its flight, so cannot be defined as an RBCC propulsion system.

4.2 Rocket-Based Combined Cycle Literature Review

In an age where archived information is stored for decades and readily available to anyone with an internet connection and friends at NASA, the amount of information available on any one technical topic at a given moment can be both a blessing and a curse. Sifting through dozens or hundreds of documents looking for relevant literature is a tedious, yet rewarding process as the complex interwoven tapestry that is our current literature begins to unravel into the individual strings connecting one work to another. No technological development occurs in a vacuum and every work is built on pieces of prior work.

An attempt will be made to highlight the connections between the individual works reviewed herein and how they build upon one another. It is important to see how a concept evolves over time in order to determine its trajectory and to see where that particular technology is headed. In addition to highlighting how the literature ties together, the literature will also be divided based on its relative age. Generally, technology evolves so quickly that a literature search performed one year will be obsolete within the next 12 months. However, technology within the field of propulsion does not undergo nearly the same rapid evolution as technology in other fields. On the other hand, it must be noted that the most cutting edge developments in propulsion

DUHJHQHUDOO\WLJKWO\KHOGJRYHUQPHQWVHFUHWVDQGGRQ\WXVXDOO\JHWSXEOLVKHGLQ
SHHU UHYLHZHGMRXUQDOVXQWLO\HDUVDIWHUWKH\YHEHFRPHREVROHWH.

4.2.1 Pre-1950 Literature

The history of RBCC propulsion systems began with experiments carried out in attempts to improve the performance of all-rocket systems. The Langley Research Center (LRC) Group (MMAG) carried out investigations on air-augmented rockets with the intention of improving the thrust-to-weight ratio of a conventional rocket engine (Escher et al., 1989). Their first investigation was to determine the effect of placing a rocket engine in a constant area duct in an ejector rocket configuration where the entrained air would ignite with the fuel-rich rocket

exhaust, as shown below in Figure 4.1. During experiments carried out on this configuration by NASA Langley Research Center in 1959, they were able to augment the takeoff thrust of the rocket by 14%.

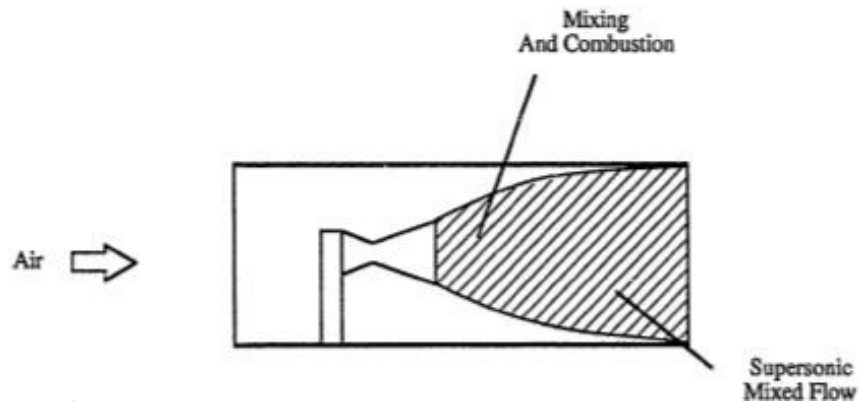


Figure 4.1: Simplest form of air augmentation of a rocket propulsion system (Escher et al., 1989).

They later devised another concept called the Rocket Engine Nozzle Ejector (RENE), which utilized a divergent mixing chamber and a lower air to rocket mass ratio (1 to 4) as shown below in Figure 4.2. Valid theoretical solutions were available for constant pressure mixing, but in order to secure constant pressure mixing over a wide range of Mach numbers, variable inlet or exit geometry was required due to the difference between ambient pressure and pressure after mixing. Experimentally, this design was able to achieve thrust and *Isp* augmentation levels of up to 55%.

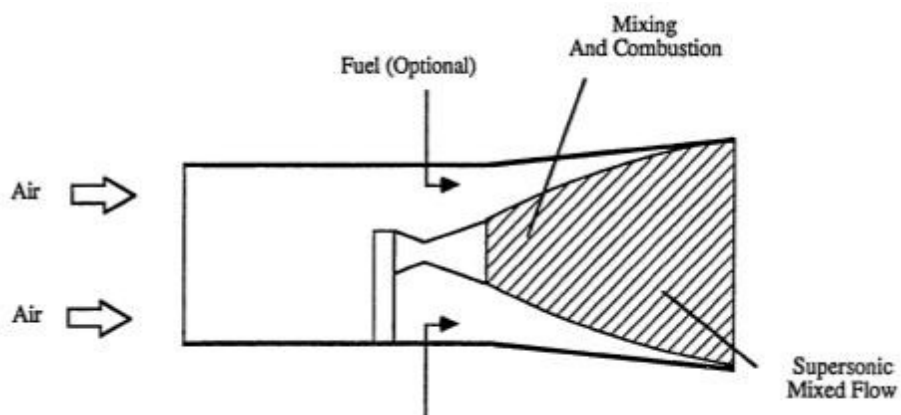


Figure 4.2: The Rocket Engine Nozzle Ejector (RENE) Concept (Escher et al., 1989).

While these investigations did not technically delve into RBCC propulsion systems, they should still be noted for their advancement of knowledge on the effect of combining rocket propulsion systems with additional flow streams. Furthermore, the RENE concept demonstrated the significant performance gains to be had while using a shroud of relatively small diameter (due to the low air to fuel ratio of between 1 and 4).

The knowledge of these proven performance gains quickly diffused throughout the aerospace industry and soon larger scale projects were funded to determine the technological feasibility of developing a system based on the concept of air-augmented rockets and the possible combination of this system with other existing propulsion systems such as the ramjet and also scramjet.

Soon thereafter, the concept of the air-augmented rocket evolved into an RBCC through the development of two different mixing and combustion schemes which incorporated a ramjet propulsion system with an air-augmented rocket. Across the literature, no credit is given to the individual or group that invented these two propulsion systems, but nevertheless they are noted here as having g. The first of these two schemes is the ejector ramjet with simultaneous mixing and combustion (SMC) as shown below in Figure 4.3. This configuration utilizes a centerbody compression cone to compress the incoming secondary flow and a converging-diverging nozzle downstream of the rocket element. In the mixing duct, the secondary air stream simultaneously mixes and combusts with the fuel rich rocket exhaust. The resulting mixed, subsonic flow is accelerated to supersonic velocity through a converging-diverging nozzle.

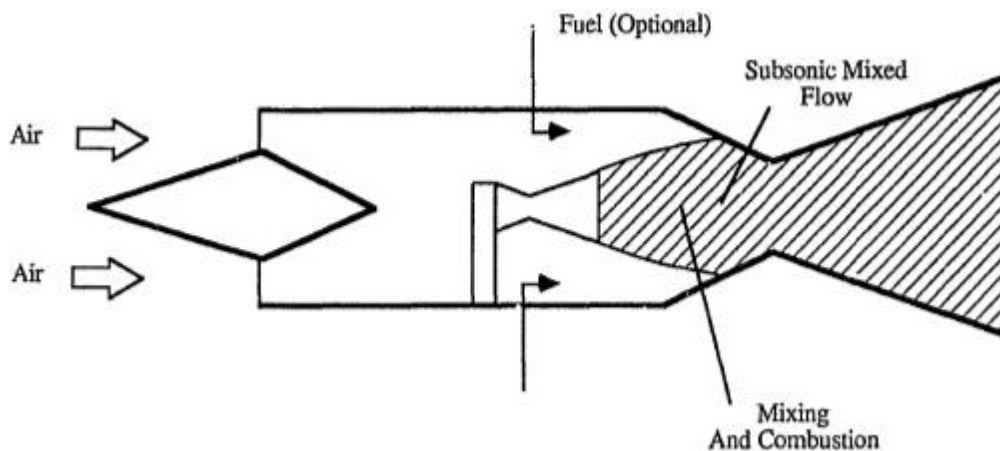


Figure 4.3: Ejector ramjet with Simultaneous Mixing and Combustion (SMC) from (Escher et al., 1989).

A similar, but modified version of this propulsion system is designed to keep the combustion and mixing separate and is aptly named the Diffusion and Afterburning (DAB) cycle, shown below in Figure 4.4.

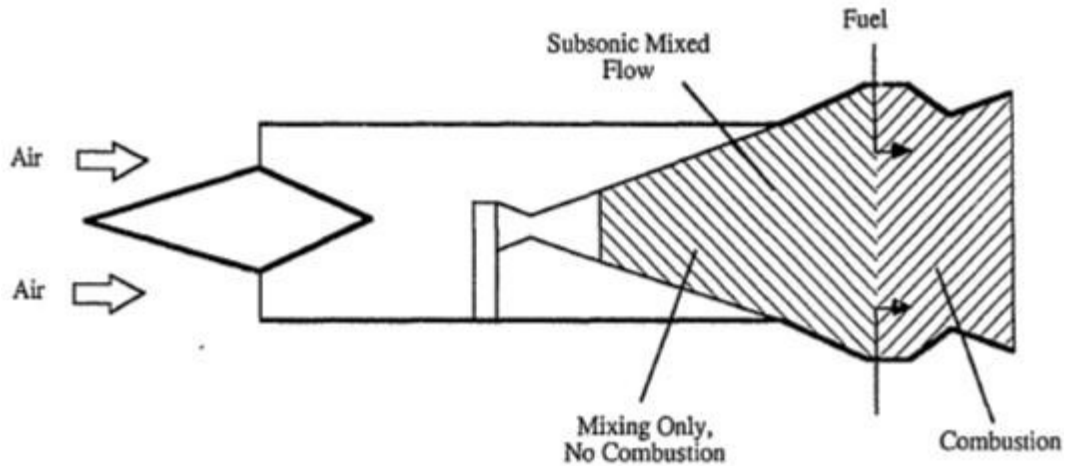


Figure 4.4: Ejector ramjet with Diffusion and Afterburning (DAB) from (Escher et al., 1989).

Generally, by separating the mixing and combustion process, a longer duct is required which slightly lowers the achievable T/W ratios compared to an SMC cycle. Here, the primary rocket stream is not

Instead, the mixture of subsonic secondary stream entrained through the inlet and the supersonic rocket exhaust expands subsonically in the diverging section upstream of the fuel injection location, increasing the static pressure. At this point, fuel is injected and the flow then expands through a converging-diverging nozzle where it exits at supersonic velocity.

Following the introduction of these basic, promising new propulsion system concepts, a veritable explosion

In an effort to process the multitude of different concepts and provide grounds for comparative analysis of the relative advantages and disadvantages of each system, NASA issued a contract (NAS7-377)

to a consortium of aerospace corporations including the Marquardt Corporation (prime contractor), Lockheed (pre-merger with Martin Marietta), and Rocketdyne. Their approach was to analyze a combination of 36 different candidate combined-cycle

Two promising RBCC propulsion systems were the ejector ramjet or supercharged ejector ramjet (engines 10 and 11 in Appendix A) and the ScramLACE (engine 22 in Appendix A).

A conclusion drawn from the study is that the most promising configurations arise from adding additional subsystems to the base rocket-ejector engine such as a turbofan to augment the low-speed specific impulse and to supercharge the rocket-ejector flow; or to use an air liquefaction subsystem that can extract oxidizer from the ambient air during atmospheric travel and use it for the all rocket mode of operation.

In 1989, DVWXG\WLWOHG³\$LU\$XJPHQWHG5RFNHW3URSXOVLQR&RQFHSWV
'ZDVSHUIRUPHGE\ the Astronautics Corporation of America under contract for the Air Force Astronautics
Laboratory, (Escher et al., 1989). A majority of the background information and literature

images found in this project are derived from this study. It picks up where the Marquardt & RUSRU DWLRQ VVWXG\OHIW-off, taking 5 of the 12 engines identified in the 3&ODVV GHVLgn phase and expanding on their development and integration into a launch vehicle. A primary focus of this study was to analyze the technology requirements unique to axisymmetric RBCC designs. An additional focus of this study was on the application of the ejector scramjet since it is defined as one of the prime candidates for a SSTO launch vehicle. This whole study is a rich resource as it delves quite a bit into specific issues with propulsion system/vehicle integration and engine cycle selection.

4.2.2 Current Literature

The main focus of the contemporary literature research was on two specific derivations of WKH5%&HQJLQH7KHILUVWLWVKHGHULYDWLRQXVHGLQ1\$6\$V*7;SURMHFWDQGWKHVHFRQG LVRQ \$HURMHWV6WUXWMHWHQJLQHThey each represent distinctly alternate approaches in propulsion system configuration and vehicle integration; with the GTX representing the most current development on axisymmetric launch vehicles with semi-axisymmetric propulsion pods and the Strutjet representinJWKHPRVWFXUUHQWGHYHORSRPHQRQ3UHFWDQJXODU' PRGXODUSURSXOVLQRQV\WHPV with variable geometry and waverider-like vehicles. In addition to the alternate propulsion system/vehicle configurations, each design also uses different propulsion cycles. 1\$6\$V GTX project focuses on a slight departure from the typical ejector-VFUDPMHWHQJLQHW\SHDVLWGRHVQVW XWLOL]HIORZPL[LQJ\$HURMHWV6WUXWMHWRHVXWLOL]HIORZPL[LQJDQGLVDKJ\GHIY HORSHG propulsion system with a lot of promise and verification testing already performed. Both concepts will be briefly discussed.

Recent RBCC development has been carried out by NASA with the GTX program (Woodrow et al, 2000). The GTX program has the objective of demonstrating the feasibility of an RBCC propulsion system implemented on a subscale SSTO vehicle with a 300 lb payload. 7KH*7;RU37UDLOEOD]HU' 7UHIQ\

UHIHUFHFKLFOHXRQXWLOL]HDQ5%&&SURSXOVLQR

system in the form of three propulsion pods placed at 120° angles to each other as shown below in Figure 4.5. The decision to make the placement of the YHKLFOH¶VSURSXOVLQRQSRGV axisymmetric is for increased structural efficiency and simplicity.

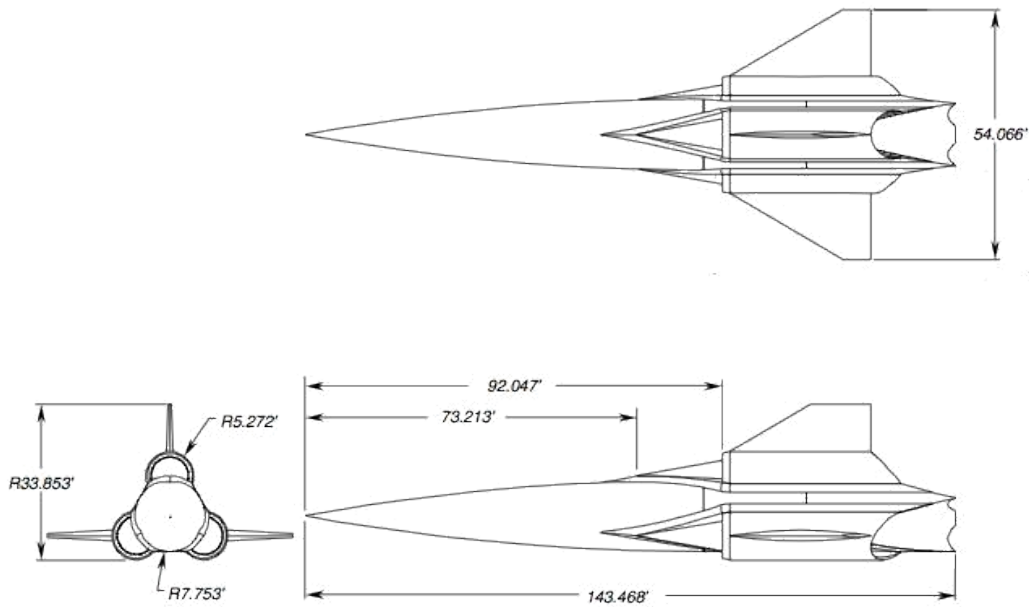


Figure 4.5: GTX reference vehicle geometry (Woodrow et al, 2000).

The operating modes of the GTX reference vehicle are very similar to those of a typical ejector-ramjet/scramjet and shown below in Figure 4.6. They are identified as ejector-rocket (operating from Mach 0 to around Mach 2.5), ramjet (operating from Mach 2.5 to around 5), scramjet (Mach 6 to Mach 10-12), and all-rocket (Mach 12 to 25). This is very similar to the ejector scramjet except that the low speed ejector rocket mode is modified slightly. Here, an Independent Ramjet Stream (IRS) cycle is used as opposed to the typical SMC or DAB cycles used by other RBCC engines (Segal, 2004).

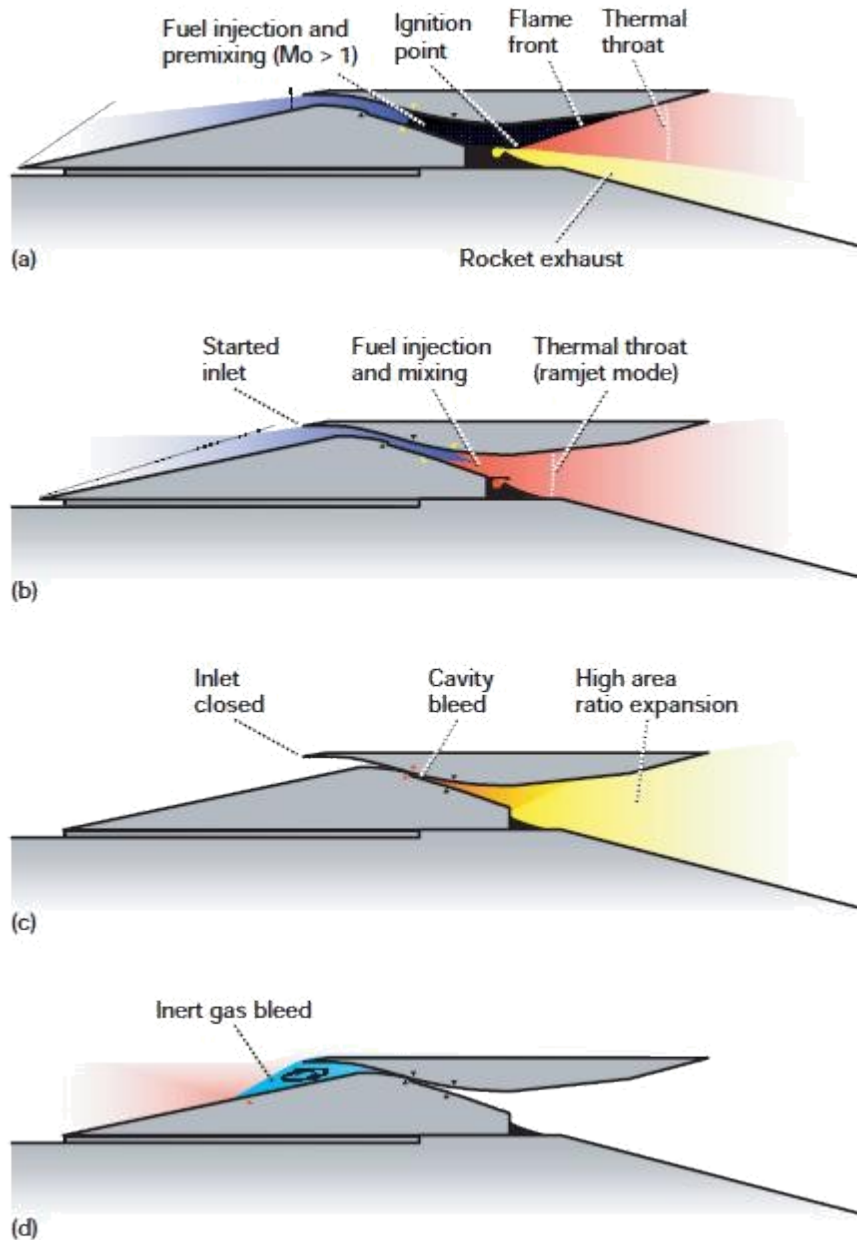


Figure 4.6: Propulsion system operating modes. (a) Mode 1, lift-off and low speed (ejector-rocket). (b) Modes 2 & 3, ramjet and scramjet. (c) Mode 4, all-rocket. (d) Re-entry concept. (Trefny, 1999).

In an IRS cycle, the rocket (primary stream) and entrained air stream (secondary stream) are separate, not intended to mix, and interact along a matched-pressure boundary (Trefny, 1999). Typically, rocket-ejector cycles with SMC have higher thermodynamic performance than an IRS cycle, but would require mixing enhancement devices or multiple rockets to shorten the duct length required for mixing. Therefore, the benefit of an IRS cycle is that it reduces

complexity by negating the need for mixing enhancers and also requiring a shorter flow-path length.

,QDGGWLWRQ

□ WKLVGHV LJQGRHVQ ¶WUHTXLUHYDULDEOHJHRPHWU\QRUPDOO\UHTXLUHGWRSSHUWH the ramjet cycle and provide a converging/diverging nozzle. Instead, it employs D³WKHUPDO WKURDW

‘ZKLFKDFWVDVDPHFKDQLFDOWKURDWE\DFFOHUDWLQJWKHIORZWRVXSHUVRQLFVSHHG7KH

radial distribution of fuel, based on measured inlet pressure, would be used to control the location of the thermal throat. Once the vehicle transitions to scramjet mode, the thermal throat is no longer required.

Before proceeding further, a brief background on the need for a thermal throat will be given. In order for an engine to operate in either ramjet or scramjet mode, it must have means of accelerating the flow to a supersonic speed at the exit plane. While an engine is operating in scramjet mode, all of the flow within the control volume of the propulsion system is moving at supersonic speed. If any of this flow encounters a converging section, the flow will slow down, as shown in Figure 4.7, and the immense kinetic energy of the flow will convert to an increase in the stagnation temperature resulting in overheating of the propulsion system.

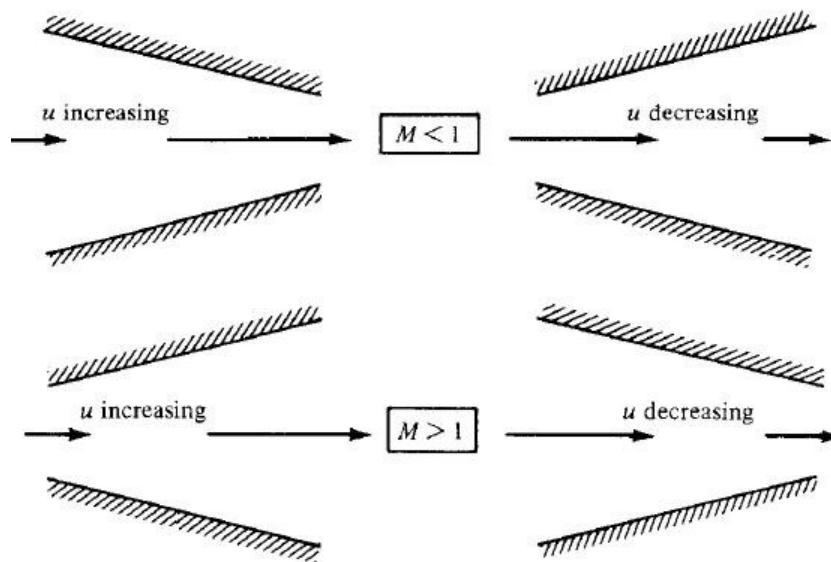


Figure 4.7: Compressible flow in converging and diverging ducts (Anderson, 2007).

However, a ramjet propulsion system operates at subsonic flow velocities within the control volume, so it must have a converging-diverging nozzle in order to expand the flow and thus accelerate it to a supersonic exit velocity. Typically, this problem in ramjet/scramjet propulsion systems is countered by employing variable nozzle geometry. This adds extra machinery to the propulsion system resulting in increased weight and complexity which is already at an extreme due to the incorporation of all of the different propulsion cycles in RBCC propulsion systems. Another approach is to use the concept of thermal choking at a thermal throat. A thermal throat is used to accelerate a subsonic flow to supersonic velocity in a divergent nozzle through the addition of heat by using flame holders and fuel injectors at a given station in the flow. Combustion occurs at this point in the flow and creates a sonic throat condition which causes the flow downstream of the thermal throat to accelerate to supersonic velocity in the divergent nozzle.

One of the key features of this design is the inlet which is a conical translating centerbody as shown below in Figure 4.8. Its primary function is to provide airflow mass capture and compression over the entire range of air-breathing Mach numbers (DeBonis et al., 1999).

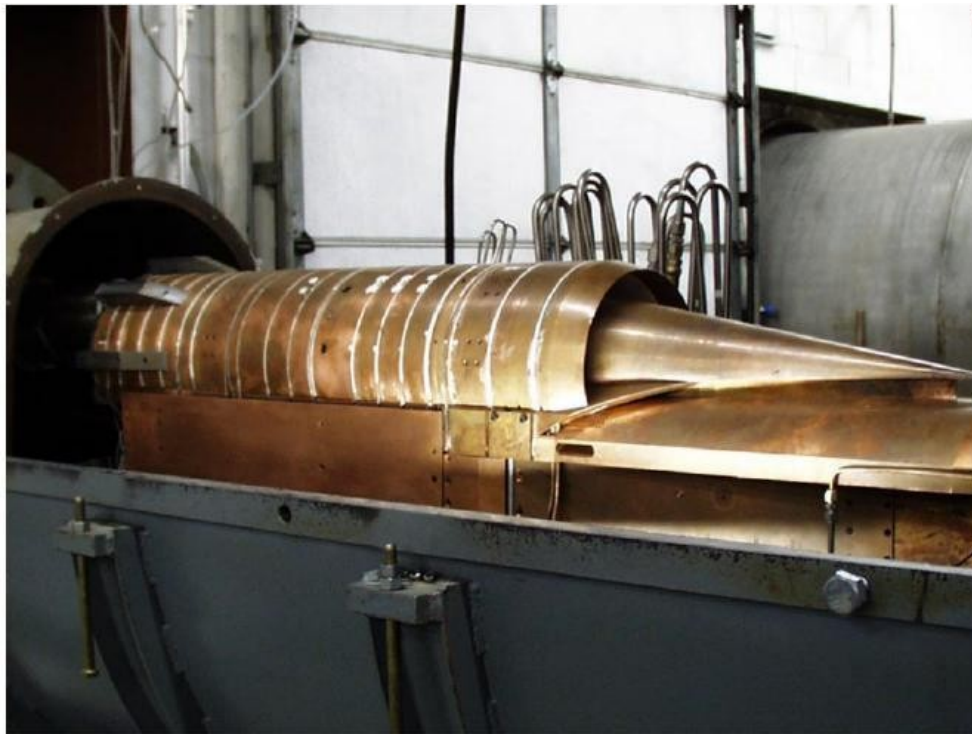


Figure 4.8: The inlet is mounted on a diverter pylon in this integrated propulsion pod used for subscale testing at the Propulsion Test Complex at GASL, Inc. (Thomas et al., 2001)

Vehicle forebody pre-compression is thus not required using this type of inlet. Additionally, it is used to change the inlet contraction ratio to keep the engine operational at various Mach numbers as well as to completely close the inlet during rocket only operation. In order to keep the boundary layer from interacting with the propulsion system, the inlet is mounted on a diverter pylon. This also reduces the need for a boundary layer bleed system which would add additional weight and complexity.

Overall, the GTX RBCC design shows great promise as one of the most state of the art RBCC propulsion systems with its high structural efficiency, low weight, and short duct length. +RZHYHU □WKHUHLVWLOODORWRIYDOLGDWLRQWKDWQHGVVREHGRQHRWRWHVWWKHHQJLQH¶VVHS DUDWH operating modes and their integration over a wide range of Mach numbers and flight conditions.

\$HURMHW¶V6WUXWMHWLVDQRWKHUSURPLVLQJVDWH-of-the-art RBCC engine as it provides greatly increased *Isp* (up to 40%) compared to all-rocket engines while increasing design margin up to approximately 30% (Siebenhaar, 1995). As a result, structure could potentially be designed to be more robust for reusability or, in exchange, a greater payload could be delivered to orbit. The rest of the benefits are: lower engine replacement costs (since required thrust is reduced by 70-80% in comparison to an all-rocket engine), lower maintenance and operating costs due to higher structural margins and redundancy, and a single propellant combination for all operation modes (LOX/LH₂).

The basic design of the Strutjet engine is shown on the next page in Figure 4.9. Essentially, the Strutjet operates in the same modes as a typical ejector-scramjet, as previously discussed, but it has novel design features which benefit it over a traditional ejector-scramjet. Key to the propulsion system, is the strut is the as it performs the following functions: compresses the incoming air, inlet/combustor isolation, ram/scram fuel distribution and injection, and rocket thruster integration. Unlike the previously discussed GTX, here the vehicle forebody precompresses the incoming air while the struts provide further compression resulting in a smooth increase in captured air mass and pressure recovery. The most significant benefit derived from the strut is geometric contraction and isolation in a shorter length than conventional inlets.

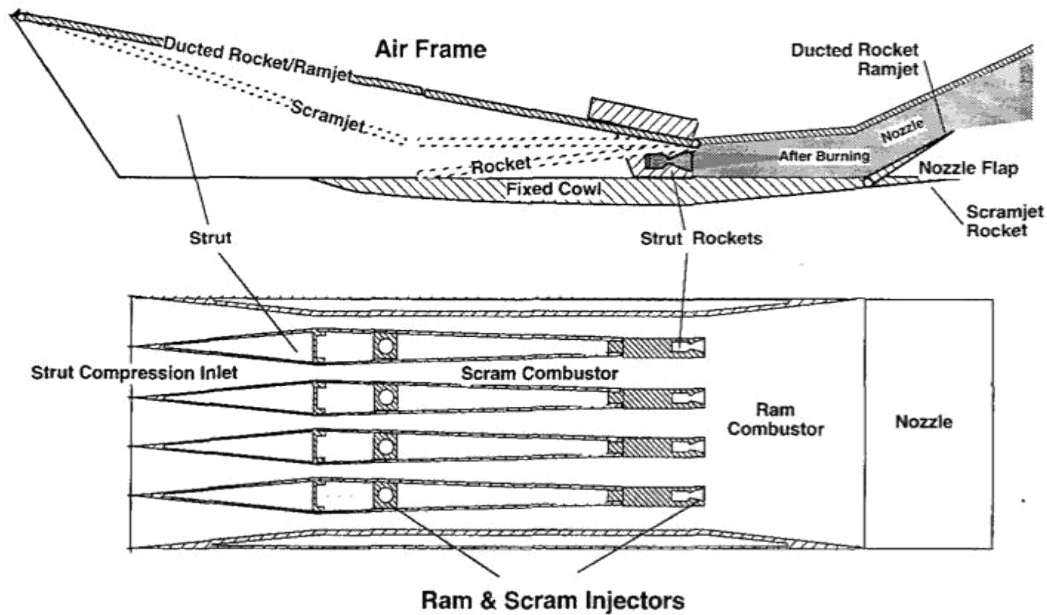


Figure 4.9: Strutjet - The integration of a rocket into a ramjet combining the benefits of both (Siebenhaar, 1995).

Due to this shorter inlet length, the overall propulsion system can be significantly lighter, easier to integrate into the vehicle, encounter less drag, and absorb less heat. Additionally, due to the geometric design of the Strutjet, it can be made modular and several modules can be incorporated into a single vehicle. All of these benefits in the geometrical efficiencies of incorporating the strut into the inlet and modularity make the Strutjet a very promising RBCC design due to the cost savings encountered from all of its innovations.

Both the GTX program RBCC engine and the Strutjet are very promising for future application and require further research to fully develop. The intent is to incorporate elements of both propulsion systems into the propulsion system being designed in this project. After reviewing the literature on RBCC propulsion systems, it is quite evident that the design of an RBCC propulsion system is truly a combination of fundamental principles as well as ingenuity in the selection and arrangement of the operating cycles and subsystems.

4.3 Rocket-Based Combined Cycle Technical Overview

A great deal of the technical aspects of RBCC propulsion systems has been intermixed within the previous sections, so this section will be a brief technical overview. One broad WHFKQLFDORYHUYLHZFDQ¶WGHVFULEHDOOV\WHPVDWDQ\OHYHORIYDOXHZLWKRX Wgoing into specifics about a single configuration (as in the literature review), so this section will serve as a top-level technical overview of the type of RBCC propulsion system which will be used for this project. In order to truly delve into the technical description at the level of first-principle physics equations, an overview of the physics of high speed flows will be given in section five of this report.

As previously discussed, the RBCC has several variations, but all RBCC propulsion systems have the capability of operating in the following modes: ejector-rocket, ramjet, scramjet, and all-rocket (Woodrow et al, 2000). Within the wide spectrum of RBCC propulsion systems, variations come about in the selection of propulsion system-vehicle integration, fuel-injection schemes, inlet design, and non-propulsion subsystems. The basic operating modes of the general ejector-scramjet, shown below in Figure 4.10, will be detailed.

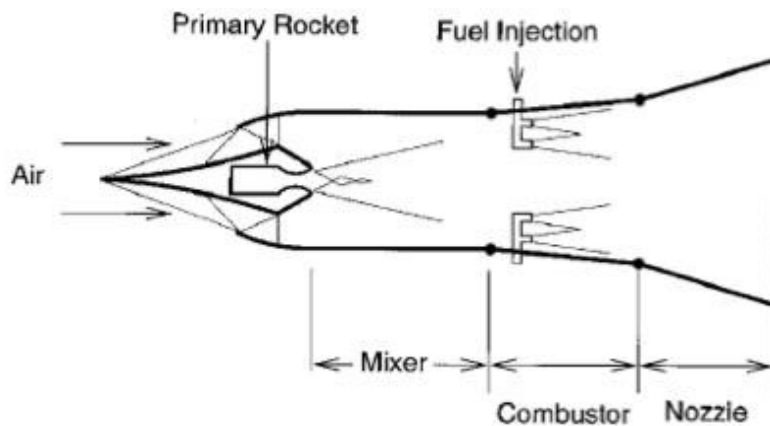


Figure 4.10: Schematic diagram of a RBCC engine with a rocket acting as an ejector to augment the airflow into the ramjet/scramjet segment (Segal, 2004).

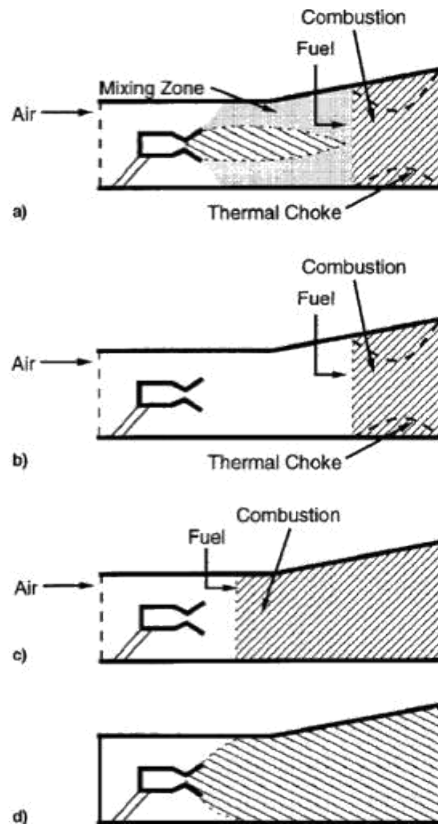


Figure 4.11: Operation of an ejector scramjet RBCC: a) rocket-ejector, b) ramjet, c) scramjet and, d) rocket-only (Segal, 2004).

The four modes of operation for a general ejector-scramjet are shown above in Figure 4.11. At takeoff, Figure 4.11(a), the primary rocket is used to provide the initial thrust and mass flow into the ramjet/scramjet segment of the engine. There are different schemes that utilize annular rockets or axial rockets (Trefny, 1999), depending on the type of flow mixing required. This rocket exhaust helps initiate the ramjet engine at airspeeds much lower than would normally be required for ramjet operation by the process of air entrainment. Furthermore, the air entering the inlet as the engine accelerates helps augment the rocket thrust by afterburning fuel with the entrained air in the duct downstream of the rocket (Dykstra et al, 1997). Fuel can be injected into the flowpath either upstream or downstream of the rocket engine or the incoming air from the inlet can be allowed to mix with the fuel-rich rocket exhaust (Woodrow et al, 2000). This mode of operation is used up until around Mach 3, where the ramjet mode becomes fully operational and the transition from ejector-rocket to ramjet occurs.

In the ramjet mode, Figure 4.11(b), the rocket can be either shut off or used as a fuel injector and mixing enhancer (Segal, 2004). Ramjet mode provides a greatly increased I_{sp} up to 3800 seconds (Siebenhaar, 1995) for some engine configurations such as the Strutjet. Ramjet mode continues up until approximately Mach 6, where the engine transitions to a scramjet mode, Figure 4.11(c), which has a higher I_{sp} than the ramjet mode. Operation continues in scramjet mode up until Mach 8 to 10, at which point the air density becomes too low for efficient scramjet operation. At this point, the inlet is closed, and the engine transitions to an all-rocket mode, Figure 4.11(d), for the transatmospheric acceleration to orbit.

4.4 Interim Summary

A brief summary of everything that has been presented thus far is given in order to outline how the work will proceed from here. Starting at the beginning, the purpose for studying RBCC propulsion systems is to be able to apply the knowledge learned to eventually design a propulsion system/vehicle combination capable of reducing launch costs through reusability, quick turn-around times, and high payload capabilities.

The goal of this project is to develop an analytical model of an RBCC propulsion system to meet a specified mission profile and to verify that the RBCC propulsion system is indeed more efficient than an all-rocket propulsion system for the same mission profile.

This goal is a precursor to a much greater design effort that would be required to carry out a detailed design of an actual propulsion system/vehicle combination. A closed design taking into consideration every factor that would weigh in to creating a flight model suitable for testing is far beyond the scope of this project and would require the efforts of a multi-disciplinary group of engineers with high-fidelity numerical modeling capability, hundreds (if not thousands) of man hours, and large amounts of funding.

In order to achieve this goal, the background introduced the concepts that will be discussed in the analytical model. In addition, the factors that must be taken into consideration when designing an RBCC propulsion system were discussed in some detail. To proceed from here and to arrive at an analytical model, the

theory governing high speed flow and combustion must first be detailed and then tailored to a specific RBCC propulsion system. In order to properly tailor these governing equations, many appropriate assumptions regarding the physics of the flow and geometry of the engine and vehicle must be made, considering their effect on the accuracy of the model.

Finally, the propulsion performance metrics by which the analytical model will be comparatively analyzed with an ideal rocket will be introduced in the next chapter.

7KH³PHDW' of the project is in the application of the stream thrust functions as solutions to the governing aerothermodynamic equations for the simplifying case of a one-dimensional flow through fine control volumes representing individual propulsion system components. If time permits, a validation attempt will be made to model the propulsion system using CAD and then CFD to analyze the flow for the various propulsion cycles.

5. Gas Dynamics: Introductory Review

5.1 Introduction

Prior to applying analytical methods in calculation of air-breathing and rocket engine performance, a review of gas dynamics is important. The operation of these engines is governed by the laws of fluid dynamics and thermodynamics, thus a review of the foundational principles is imperative. This section closely follows the writings of (Anderson, 2006), (Mattingly, 2006) and (Biblarz & Sutton, 2001) which are good references for anyone who wants to probe further into the study of gas dynamics and rocket propulsion.

This chapter commences with a brief note on real versus ideal gases, then goes on to discuss the Continuity Equation, the Momentum Equation, and the First and Second Laws of Thermodynamics. The equations listed in this section can be found in many thermodynamics or fluid dynamics texts, and the reader is referred to references such as those mentioned above for further study, including detailed derivations. The second portion of this chapter looks at hypersonic flow and characteristics that are unique to it. Physical phenomena encountered during hypersonic flow are briefly described, leading into a discussion of high-temperature flow. To conclude the chapter, the concept of the ideal rocket is introduced, as well as one-dimensional flow theory. Once again, it is stressed that the theory and equations provided herein are of an introductory nature, and the reader is directed to respective references mentioned in this study for detailed discussions.

5.2 A Review of Fundamentals

This section goes into the basics of thermodynamic and fluid dynamics relations, as these relations go on to form the building blocks for equations that are used to model component processes such as those of a nozzle and chamber. They provide tools that are used to calculate several performance parameters, which then assist designers and analysts in making key decisions. For example, knowing the conservation of energy principle and the fact that a nozzle can be modeled as a steady-

IORZDGLDEDWLF GHYLFH □ RQHFDQFD OFXODWHWKHQR]]OH¶VH[LWYHORFLty

given the initial conditions such as the operating environment and inlet properties. Likewise,

NQRZLQJ1HZWRQ¶V6HFRQG/DZ

FRQVHUYDWLRQRIPRPHQWXP

□ RQHFDQGHULYHDQGFDOFXODWHWKH uninstalled jet engine thrust.

Simply defined by (Anderson, 2006), a real gas is a gas where intermolecular forces are important and must be accounted for, whereas a perfect/ideal gas is one where intermolecular forces are negligible. Real gases are encountered at very high pressures ($p \gtrsim 1000 \text{ atm}$) and/or low temperatures ($T \lesssim 30\text{K}$), while perfect gases are encountered at lower pressures ($p \lesssim 10\text{atm}$) and higher temperatures ($T \gtrsim 300\text{K}$). Under real gas conditions, the molecules in the system are closely packed and move slowly, resulting in intermolecular forces acting on the molecules at any given instant. However, at lower pressures and higher temperatures, the molecules are widely spaced; hence intermolecular forces have little impact on the molecules in the system. While the reader might be aware of this, the difference is noted nevertheless, as a reminder that the fundamental equations that follow come bearing assumptions, and that the reader should make a note of these prior to using any of these equations.

Prior to defining the principle of conservation of mass, a steady state will be defined. Given a control volume, if the fluid properties in this control volume do not vary with time at any given point, then the flow is considered steady. It is then given as a principle that, since mass can neither be created nor destroyed, the rate at which mass enters a system is equal to the rate at which mass leaves the system (Anderson, 2007). This principle is noted below in integral form, Equation 5.1, and partial differential form, Equation 5.2, and is known as the continuity equation. The partial differential form relates the flow variables at a point, whereas the integral form relates the flow variables in a fixed space. The integral equation clearly shows that the net mass flow into a control volume must equal the rate of increase of mass inside the control volume. It applies to all flows, compressible or incompressible, viscous or inviscid.

$$\frac{d}{dt} \int_{cv} \rho U dV - \int_s \rho U V \cdot dS = 0 \quad (5.1)$$

$$\frac{d\rho}{dt} + \nabla \cdot (\rho U) = 0 \quad (5.2)$$

7KHFRQVHUYDWLRQRIPRPHQWXPLV1HZWRQ¶V6HFRQG/DZRI0RWLRQ,WVVDWHVW
 KDWWKH

force applied on a body is equal to the rate of change of momentum. In integral form, it is given as Equation 5.3, (Anderson, 2007), showing that the time rate of change of momentum of a fluid that is flowing through a control volume at any instant is equal to the net force exerted on the fluid inside the control volume (Anderson, 2004).

$$\frac{W}{wt} \int_{CV} \rho U dV = \int_S (\rho U \times dS) \cdot V + \int_S p dS + \int_{CV} \rho f dV + F_{viscous} \quad (5.3)$$

The First Law of Thermodynamics relates the internal energy of a system and the energy of the molecules within the system. The internal energy E of the system is equal to the sum of the molecular energy of all the molecules in the system, and can only be changed if heat Q is added to the system, or work W is done on the system. Simply shown as Equation 5.4, this is the conservation of energy principle, also known as the First Law of Thermodynamics (Anderson, 2006):

$$GQ = GW + GE \quad (5.4)$$

In integral form, it is written as Equation 5.5 (Anderson, 2007)

$$\int_{CV} \rho q dV + \int_{CV} \rho U dV + \int_S \rho U \cdot dS = \int_S p dS + \int_{CV} \rho f dV + \int_{CV} \rho U \cdot dS + \int_{CV} \rho U \cdot dS \quad (5.5)$$

The Second Law of Thermodynamics relates to the entropy of a system. Two classical statements of the Second Law of Thermodynamics were made by Kelvin-Planck and Clausius, while describing the operation of heat engines and refrigerators, respectively (Cengel, 2008).

Kelvin-30DQFNVDLG ¶ *It is impossible for any device that operates on a cycle to receive heat from*

a single reservoir and produce a net amount of work ,QKLVVWDWHPHQW ¶&ODXVLXVVDLG

¶ *It is impossible to construct a device that operates in a cycle and produces no effect other than the*

transfer of heat from a lower-temperature body to a higher-temperature body. (VHQLDQO\ ERWK

statements imply that a system cannot be created in a manner that it is 100% efficient, and form the basis of the Carnot principles (Cengel, 2008):

- a) The efficiency of an irreversible heat engine is always less than the efficiency of a reversible one operating between the same two reservoirs
- b) The efficiencies of all reversible heat engines operating between the same two reservoirs are the same

The Carnot principles lead us to the term entropy S , which is defined as:

$$dS = \frac{\delta Q}{T} \quad (5.6)$$

Equation 5.6 shows how entropy relates heat transfer to temperature, and also shows that losing heat is the only way the entropy of a system can be decreased. In the case where entropy is zero (isentropic), the process is reversible, and does not involve the dissipative effects of viscosity, thermal conduction, or mass diffusion. While irreversible and isentropic processes do not exist in reality, this knowledge allows design and analysis teams to know what to strive for.

5.3 Hypersonic Flow and Related Physical Phenomena

The inspiration behind this section is not only to provide the reader a background of the nature of the operating regime of hypersonic vehicles, but to illustrate the importance of knowing the equations (especially those noted in the former portion of this section). Gases in this regime begin to behave in a non-ideal manner, hence the ideal gas equations need to be corrected prior to application, so as to properly include any chemically reacting effects demonstrated by flows in this regime.

A rule of thumb exists where hypersonic flow is defined as that where the Mach number is above $M=5$, however it is best defined as the regime where certain physical phenomena

become progressively more important as the Mach number is increased (Anderson, 2006). Some of these phenomena are noted below, including some of their effects on the overall flow surrounding the vehicle.

- a) Thin shock layers- Characteristic of hypersonic flows, shock waves lie close to the body and the shock layer is thin. While this phenomena is useful at high Reynolds numbers for thin shock-layer theory (Anderson, 2006), at low Reynolds numbers shock waves close to the body can merge with, a thick viscous boundary layer already growing from the body surface, causing adverse effects.
- b) Increased entropy and vorticity interaction due to present shock waves
- c) Increased viscous interaction- As high speed flow interacts with viscous effects within a boundary layer, the flow is slowed down, resulting in the loss of kinetic energy; a portion of which is converted to internal energy of the gas. This increase in internal energy causes the temperature within the boundary layer to increase, which in turn causes the boundary layer to become thicker. As the shape of the body appears much thicker than the body really is, causing a change in the outer inviscid flow (Anderson, 2006). Consequently, the lift, drag and stability of the vehicle will be affected, to name a few.
- d) Increased temperatures-As mentioned above, the temperature in hypersonic flows increases with increasing Mach number, and not just in the boundary layer. For example, for the Apollo entry at Mach 36, the temperature in the nose region reached upwards of 11,000K (Anderson, 2006). Because aerodynamic heating dominates the design of hypersonic vehicles, a brief discussion of the nature of high-temperature flows is made below, including resulting chemical effects in respective temperature regimes.

5.4 Chemical Effects in Hypersonic Flows

As the Mach number and temperature increase, chemically reacting effects become more

SURPLQHQP, QWKL VUHJLPH QRWRQO\LVWKHJDVFRQVWDQW YDULDEOH

EXWWKHWHKUHPRG\QDPLF

H K S 7 HWF

DQGWUDQVSRUW

—DQGN

properties are different compared to the ideal cases. Non-adiabatic effects become pronounced if the gas temperature is high enough, and ionization might

even occur. Considering air at 1atm, as the temperature increases reaching about 2000K, the dissociation of O₂ begins. At about 4,000K, O₂ dissociation is complete and N₂ dissociation commences. When the temperature reaches about 9000K, most of the N₂ has dissociated, and ionization of both oxygen and nitrogen begins, above which, the air consists of partially ionized plasma consisting mainly of O, O⁺, N, N⁺, and electrons (Anderson, 2006). Below in Figure 5.1, a velocity-amplitude map is given, illustrating the regions of vibrational excitation, dissociation and ionization discussed above. It clearly shows how a majority of any given flight path falls in these regions.

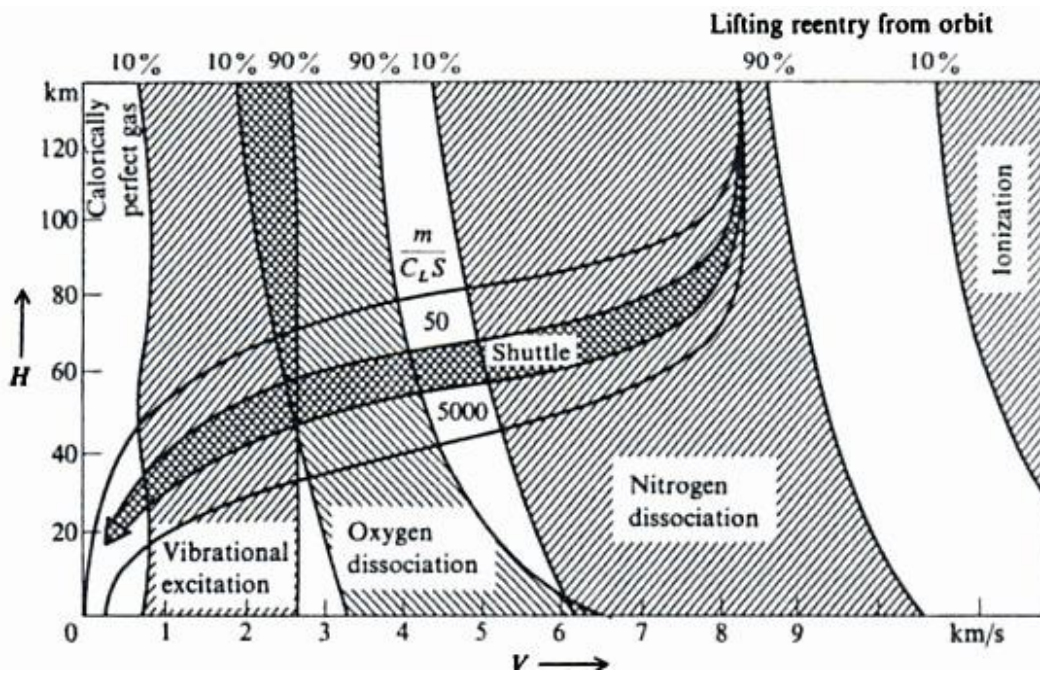


Figure 5.1: Velocity-Amplitude map with superimposed regions of vibrational excitation, dissociation, and ionization (Anderson, 2006).

At this point, this concludes the discussion of hypersonic flows and related physical high-temperature effects, viscous interaction, vorticity interaction, and chemical effects, to name a few. The next section will introduce the ideal rocket, related equations and assumptions often made in the design of propulsion systems such as that considered in this project.

5.5 The Ideal Rocket and Quasi One-Dimensional Flow Theory

The ideal rocket is an idealization and simplification of the real rocket, which often involves several two- to three-dimensional equations. In preliminary design and analysis, the ideal rocket offers a starting point where quasi one-dimensional relations can be applied, and has been shown useful in predicting system performance parameters. For example, it has been shown that measured actual performance is only 6% below the calculated ideal value for chemical rocket propulsion (Biblarz & Sutton, 2001). The discussion that follows first reintroduces the governing flow equations in their one dimensional form, then covers assumptions that are used when applying the ideal rocket model, and then goes on to discuss one-dimensional flow theory as it applies to the ideal rocket equation. Under one-dimensional flow theory, the cases covered are those that involve isentropic flow, flow with heat addition, and flow with friction.

Before listing the equations necessary for the calculation of flow parameters in an ideal rocket, the continuity (Equation 5.1), momentum (Equation 5.3), and energy equations (Equation 5.5) will be reintroduced in a one-dimensional form. Assuming the one-dimensional flow case allows designers to perform calculations using a control volume approach that greatly simplifies the full three dimensional equations while still giving fairly accurate results for simplified geometries.

Continuity:

$$\rho_1 A_1 V_1 = \rho_2 A_2 V_2 \quad (5.7)$$

Momentum:

$$\rho_1 A_1 V_1^2 + p_1 A_1 = \rho_2 A_2 V_2^2 + p_2 A_2 \quad (5.8)$$

Energy:

$$\frac{V_1^2}{2} + \frac{p_1}{\rho_1} = \frac{V_2^2}{2} + \frac{p_2}{\rho_2} \quad (5.9)$$

The ideal rocket assumptions mentioned below are taken from (Sutton & Biblarz, 2006), and the reader is directed to this reference for a detailed discussion on these assumptions, as well as nozzle theory. The assumptions are as follows:

- a) The working gas obeys the perfect gas law
- b) The working substance (or chemical reaction products) is homogeneous
- c) All the species of the working fluid are gaseous; any condensed phases (liquid or solid) add a negligible amount to the total mass
- d) The flow is adiabatic; there is no heat transfer across the rocket walls
- e) There is no appreciable friction and all boundary layer effects are neglected
- f) There are no shock waves or discontinuities in the nozzle flow
- g) The propellant flow is steady and constant; the expansion of the working fluid is uniform and steady, without vibration; transient effects are of very short duration and may be neglected
- h) All exhaust gases leaving the rocket have an axially directed velocity
- i) The gas velocity, pressure, temperature, and density are all uniform across any section normal to the nozzle axis
- j) Chemical equilibrium is established within the rocket chamber and the gas composition does not change in the nozzle (frozen flow)
- k) Stored propellants are at room temperature. Cryogenic propellants are at their boiling points

While these assumptions might seem overreaching for the real case, with current advancements in technology, most components can approach these conditions closely. For instance, for a liquid propellant rocket, the ideal case calls for perfect mixing of the fuel and oxidizer. Today, good rocket injectors can perform near this level.

Prior to commencing one-dimensional theory, a few parameters will be defined:

$$M = \text{Mach number} = V/a$$

$$a = \text{Speed of sound} = \sqrt{J R T}, \text{ where } J = \text{ratio of specific heats, } R = \text{universal gas constant}$$

$$T = \text{Temperature}$$

$$P = \text{Pressure}$$

The subscript (0) represents stagnation or total property; case when the flow is brought to rest adiabatically (for example T_0 = stagnation or total temperature). Superscript (*) represents properties at a given point in the flow where $M = 1$ (for example a^* represents the speed of sound of the flow at a given point where the Mach number $M = 1$). It then follows from the conservation of energy principle that, for isentropic flow, the following relations are true. The reader is directed to reference (Anderson, 2003) for detailed derivations:

$$\frac{T_0}{T} = 1 + \frac{\gamma - 1}{2} M^2 \quad (5.10)$$

$$\frac{p_0}{p} = \left[1 + \frac{\gamma - 1}{2} M^2 \right]^{\frac{\gamma}{\gamma - 1}} \quad (5.11)$$

$$\frac{U_0}{U} = \left[1 + \frac{\gamma - 1}{2} M^2 \right]^{\frac{1}{\gamma - 1}} \quad (5.12)$$

These equations give the ratios of total to static temperature, pressure and density, respectively, at a point in the flow as a function of the Mach number M at that point. When heat q is added to or removed from a flow, the flow is no longer adiabatic, and the direct effect is to increase or decrease the total temperature. The thermodynamic relations between two regions in a flow where heat is added can thus be found as follows:

$$\frac{p_2}{p_1} = \frac{1 + \frac{\gamma - 1}{2} M_{1,2}^2}{1 + \frac{\gamma - 1}{2} M_{2,2}^2} \quad (5.13)$$

$$\frac{T_2}{T_1} = \frac{1 + \frac{\gamma - 1}{2} M_{1,2}^2}{1 + \frac{\gamma - 1}{2} M_{2,2}^2} \frac{M_{2,1}^2}{M_{1,1}^2} \quad (5.14)$$

$$\frac{U_2}{U_1} = \frac{1 + \frac{\gamma - 1}{2} M_{1,2}^2}{1 + \frac{\gamma - 1}{2} M_{2,2}^2} \frac{M_{2,1}}{M_{1,1}} \quad (5.15)$$

$$\frac{p_{0,2}}{p_{0,1}} = \frac{1 + \frac{\gamma - 1}{2} M_{1,2}^2}{1 + \frac{\gamma - 1}{2} M_{2,2}^2} \frac{1 + \frac{\gamma - 1}{2} M_{2,1}^2}{1 + \frac{\gamma - 1}{2} M_{1,1}^2} \quad (5.16)$$

$$\frac{T_2}{T_1} = \frac{1 + \frac{\gamma-1}{2} M_1^2}{1 + \frac{\gamma-1}{2} M_2^2} \quad (5.17)$$

When solved, these equations show the following trends (Anderson, 2003):

a) For supersonic flow in region 1, when heat is added:

- x Mach number decreases, $M_2 < M_1$
- x Pressure increases, $p_2 > p_1$
- x Temperature increases, $T_2 > T_1$
- x Total temperature increases, $T_{02} > T_{01}$
- x Total pressure decreases, $p_{02} < p_{01}$
- x Velocity decreases, $u_2 < u_1$

b) For subsonic flow in region 1, when heat is added:

- x Mach number increases, $M_2 > M_1$
- x Pressure decreases, $p_2 < p_1$
- x Temperature increases for $M_1 \hat{U}^{-1/2}$ and decreases for $M_1 \hat{U}^{-1/2}$
- x Total temperature increases, $T_{02} > T_{01}$
- x Total pressure decreases, $p_{02} < p_{01}$
- x Velocity increases, $u_2 < u_1$

The above behavior is opposite when heat is removed from the flow. When an adiabatic one-dimensional flow with friction is considered, then the equations below show the relationship between the two regions:

$$\frac{T_2}{T_1} = \frac{T_0/T_1}{T_0/T_2} = \frac{1 + \frac{\gamma-1}{2} M_1^2}{1 + \frac{\gamma-1}{2} M_2^2} \quad (5.18)$$

$$\frac{p_2}{p_1} = \frac{M_1^2 \left(\frac{1 + \frac{\gamma-1}{2} M_1^2}{1 + \frac{\gamma-1}{2} M_2^2} \right)^{\frac{\gamma}{\gamma-1}}}{M_2^2 \left(\frac{1 + \frac{\gamma-1}{2} M_2^2}{1 + \frac{\gamma-1}{2} M_1^2} \right)^{\frac{\gamma}{\gamma-1}}} \quad (5.19)$$

$$\frac{U_2}{U_1} = \frac{M_1}{M_2} \left[\frac{1 + \frac{\gamma - 1}{2} M_1^2}{1 + \frac{\gamma - 1}{2} M_2^2} \right]^{1/2} \quad (5.20)$$

$$\frac{p_{02}}{p_{01}} = \frac{M_1}{M_2} \left[\frac{1 + \frac{\gamma - 1}{2} M_1^2}{1 + \frac{\gamma - 1}{2} M_2^2} \right]^{\frac{\gamma}{\gamma - 1}} \quad (5.21)$$

Likewise, when Equations 5.15-5.18 are solved, the following physical trends are noted (Anderson, 2003):

a) For supersonic inlet flow, the effect of friction on the downstream flow is such that:

- x Mach number decreases, $M_2 < M_1$
- x Pressure increases, $p_2 > p_1$
- x Temperature increases, $T_2 > T_1$
- x Total pressure decreases, $p_{02} < p_{01}$
- x Velocity decreases, $u_2 < u_1$

b) For subsonic inlet flow, the effect of friction on the downstream flow is such that:

- x Mach number increases, $M_2 > M_1$
- x Pressure decreases, $p_2 < p_1$
- x Temperature decreases, $T_2 < T_1$
- x Total pressure decreases, $p_{02} < p_{01}$
- x Velocity increases, $u_2 > u_1$

With this review of thermodynamics and fluid dynamics complete, we now have the tools to perform engine analysis, which is the basis of Chapter 7. However, before we dive into the main body of this project, a few performance metrics for airbreathing engines and rockets will be discussed in Chapter 6. These metrics allow comparison between multiple engines designed to complete a given mission.

6. RB C C Propulsion Performance Metrics

In order to measure and compare the capabilities of any propulsion system model that will be designed as a result of this project, it is necessary to be able to quantify its performance capabilities. This section will detail the methods for determining common performance metrics used across multiple propulsion systems, thus providing the methods that will be used in the comparative analysis with other propulsion systems. The discussion of propulsion performance metrics draws heavily from the established methods listed in (Heiser & Pratt, 1994).

6.1 Specific Thrust

Specific thrust is the ratio of uninstalled thrust to the entry air mass flow rate (Heiser & Pratt, 1994), where the uninstalled engine thrust is defined as the total thrust exerted by the engine, assuming ideal external flow. Specific thrust is defined by Equation 6.1:

$$\frac{\text{Uninstalled Thrust}}{\text{Entry air mass flow rate}} = \frac{F}{m_0} \quad (6.1)$$

The specific thrust points out that, with all things being equal, the total uninstalled thrust of an Airbreathing engine is directly proportional to the mass flow rate of air entering the engine.

6.2 Specific Fuel Consumption

Also known as the thrust specific fuel consumption, the specific fuel consumption is defined as:

$$\frac{\text{Fuel mass flow rate}}{\text{Uninstalled Thrust}} = S = \frac{m_f}{F} \quad (6.2)$$

The specific fuel consumption allows us to determine what fuel flow rate must be provided by the engine in for a given uninstalled thrust value.

6.3 Specific Impulse

Specific impulse is given by Equation 6.3:

$$\frac{\text{Uninstalled Thrust}}{\text{Fuel weight flow rate}} = I_{sp} \frac{F}{g_0 m_f} \quad (6.3)$$

For rockets, the specific impulse is given by:

$$I_{sp} = \frac{F}{g_0 m_f} = \frac{m_f V_e}{g_0 m_f} = \frac{V_e}{g_0} = \frac{1}{g_0} \frac{1}{S} \quad (6.4)$$

When drag forces and weight terms collinear with specific impulse are subtracted from the value of specific impulse given by Equation 6.3 or 6.4, the result is known as effective specific impulse, and is given as:

$$I_{eff} = I_{sp} \left(1 - \frac{W \sin T}{F} - \frac{D}{F} \right) \quad (6.5)$$

Effective specific impulse is an important measure of performance for hypersonic vehicles, as shown in Figure 6.1 below. The first trend that is immediately obvious by looking at Figure 6.1 is that the payload performance is affected by the effective specific impulse only so much after a certain high value. For example, switching from a RamLACE cycle to a turbojet cycle in the range of Mach 0 to 2 gives an I_{eff} increase of 850s which is a significant propulsion performance gain, but which only translates to a small payload performance gain equivalent to an increase in I_{eff} of just 5 seconds for the rocket portion of the flight regime.

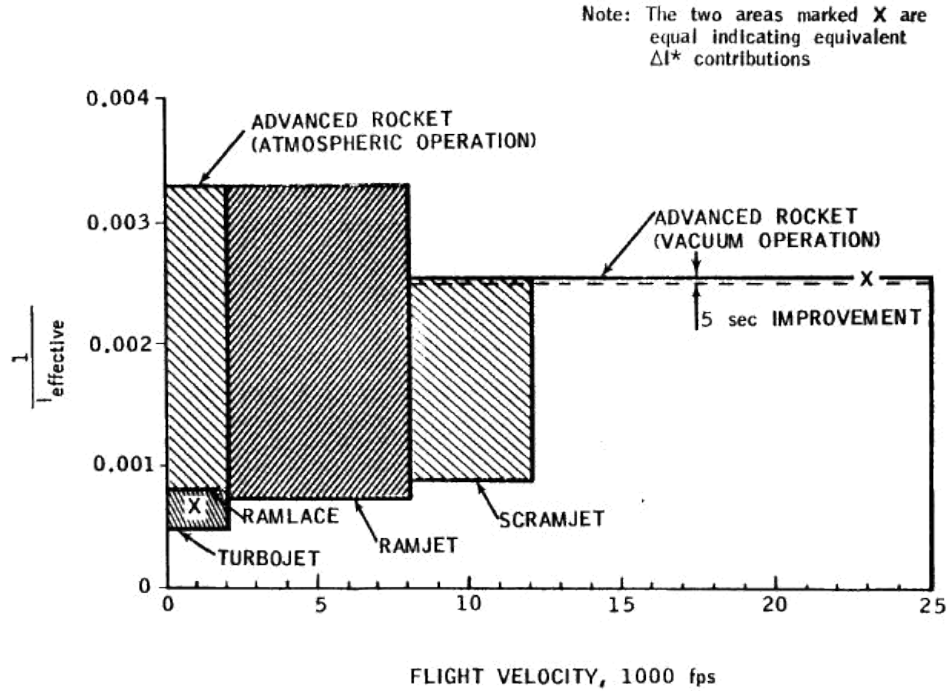


Figure 6.1: Demonstration of the significance of I_{eff} level (Escher, 1966)

This is due to both the logarithmic nature of performance increase with increasing I_{eff} and also to the relatively small portion of the flight regime over which the performance is gained. More results pertinent to the importance of specific impulse/effective specific impulse will be discussed in future chapters.

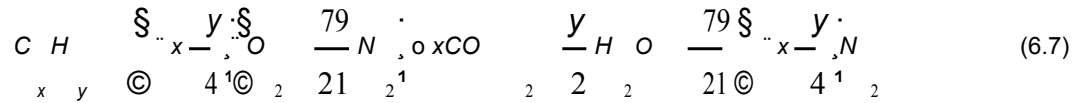
6.4 Fuel/ Air Ratio

Normally used as an indicator of the combustion conditions in the burner, the fuel/air ratio is defined as:

$$f = \frac{\text{Fuel mass flow rate}}{\text{Entry air mass flow rate}} = \frac{m_f}{m_0} \quad (6.6)$$

The ideal upper limit of the fuel/air ratio is known as the stoichiometric fuel/ratio, and it represents the point where complete combustion of oxygen and fuel takes place. The general chemical equation that ensures all carbon, hydrogen and oxygen atoms are consumed in the

reaction, leading to carbon dioxide and water being the only products, is given below (Heiser & Pratt, 1994):



Based upon the left-hand side of this equation, Heiser & Pratt (1994) show that the stoichiometric fuel/air ratio is given by:

$$f_{st} = \frac{36x + 3y}{4x + y} \quad (6.8)$$

For AERSPC, the fuel used is hydrogen, for which $x=0$ and $y=2$; this gives $f_{st} = 0.0291$, a value that was used throughout the project.

6.5 Airbreathing Engine Overall Efficiency

The overall efficiency is a direct indicator of how well the engine uses the energy originally deposited in the fuel tanks (Heiser & Pratt, 1994). Before the overall efficiency is defined, the thrust power and chemical energy will be discussed.

Thrust power indicates the rate at which the engine makes mechanical energy available to the whole aerospace system. This mechanical energy is that which is converted from chemical energy present in fuel. The thrust power is given by the following expression, which assumes that the uninstalled thrust is parallel to the direction of flight:

$$\text{Thrust power} = FV_0 \quad (6.9)$$

The rate at which the chemical reactions make energy available to the engine cycle is known as the chemical energy rate and is given by:

$$\text{Chemical energy rate} = \dot{m}_f h_{PR} \quad (6.10)$$

The overall efficiency is therefore given by:

$$K_0 = \frac{\text{Thrust power}}{\text{Chemical energy rate}} = \frac{FV_0}{\dot{m}_f h_{PR}} \quad (6.11)$$

and propulsive efficiency, the overall efficiency was also defined by Heiser & Pratt (1994) as follows:

$$K_0 = K_{th} \sim K_p$$

Where:

$$K_{th} \text{ Thermal efficiency} = \frac{\text{Engine mechanical power}}{\text{Chemical energy rate}} \quad (6.12)$$

$$K_p \text{ Propulsive efficiency} = \frac{\text{Thrust power}}{\text{Engine mechanical power}} \quad (6.13)$$

86

The Engine mechanical power is given by the following Equation 6.14:

$$\text{Engine mechanical power} = \dot{m}_0 \left[\frac{V_e^2}{2} - \frac{V_0^2}{2} \right] = \dot{m}_0 \frac{1}{2} \left[V_e^2 - V_0^2 \right]$$

This leads to the following definition of the overall efficiency:

$$K_0 = K_{th} \sim K_p = \frac{1}{\dot{m}_f h_{PR}} \frac{\dot{m}_0 \left[\frac{V_e^2}{2} - \frac{V_0^2}{2} \right]}{\dot{m}_0 \frac{1}{2} \left[V_e^2 - V_0^2 \right]} = \frac{FV_0}{\dot{m}_f h_{PR}}$$

(6.14)

(6.15)

As noted by the laws of thermodynamics, the thermal efficiency can never be greater than 1. However, when the fuel/air ratio is sufficiently large, the propulsive efficiency can slightly exceed 1. But because the fuel/air ratio is small compared to 1 even for stoichiometric combustion, the approximation commonly used to determine propulsive efficiency is often given as follows (Heiser & Pratt, 1994):

$$K_p = \frac{2}{V_e - 1} \frac{V_0}{V_e} \quad (6.16)$$

This concludes the discussion on performance metrics. As we have seen, performance metrics are essentially figures of merits that customers look at when comparing engine types. They are mostly ratios of engine properties, which make it easy to compare engines of the same type but different size. The metrics discussed were specific thrust, specific fuel consumption, specific impulse, fuel/air ratio, and the overall efficiency. Future chapters will discuss AERSPC performance using these metrics, but for now, theory on engine analysis will commence in the next chapter, providing methods that were used to analyze the performance of AERSPC.

7. Engine Performance Analysis

7.1 Introduction

In chapter 5, the fundamentals of thermodynamics and fluid dynamics were introduced, as well as equations that are normally used when performing one dimensional analysis of fluid flow. In this chapter, it is shown how these equations apply to the analysis of hypersonic Air-breathing engines. The chapter commences with a brief theory on the different performance analysis methods (Thermodynamic Cycle Analysis, First Law Analysis, and the Stream Thrust Analysis) as presented by Heiser & Pratt (1994). As will be explained, the Stream Thrust Analysis method was selected to be the main analysis tool for this project, thus this section goes into a more in-depth discussion of this method, illustrating the performance of different engine components.

From the title of the chapter, this section presents the performance of the engine during its main modes of operation:

Mode 1- Ejector Ramjet mode (from Mach 1-Mach 2.5)

Mode 2- Ramjet mode (from Mach 2.5-Mach 5.5)

Mode 3- Scramjet mode (from Mach 5.5-Mach 12)

Mode 4- Rocket mode (from Mach 12- Mach 25)

The results from the analysis in this chapter are then presented in chapter 8. Emphasis is placed on comparing the results calculated herein with existing all-rocket propulsion systems and, if possible, other analytical models of RBCC propulsion systems.

7.2 Thermodynamic Cycle Analysis

Prior to commencing any type of analysis, the Air-breathing engine reference stations were set. They were located at axial positions along the engine flowpath, at the junction of major components. They were placed in a manner that the mark represented the start of one process, and end of the other (Heiser & Pratt, 1994). The reference stations are shown in Figure 7.1a and b for a typical ramjet and scramjet, respectively, and correspond to Table 7.1 (Heiser & Pratt, 1994):

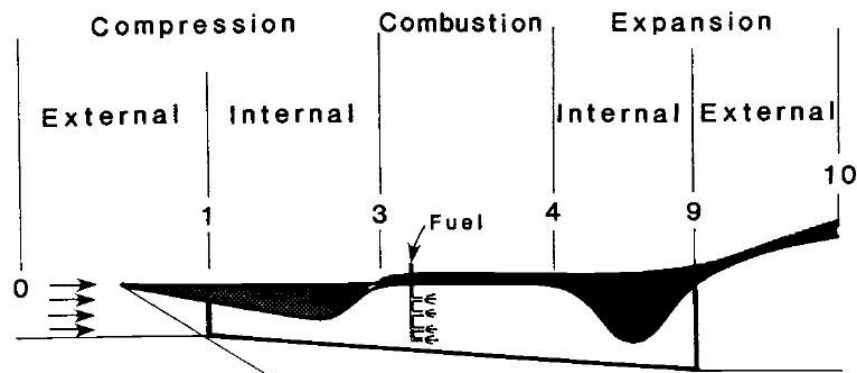


Figure 7.1a: Air-breathing engine reference station numbers and related terminology- Typical Ramjet (Heiser & Pratt, 1994).

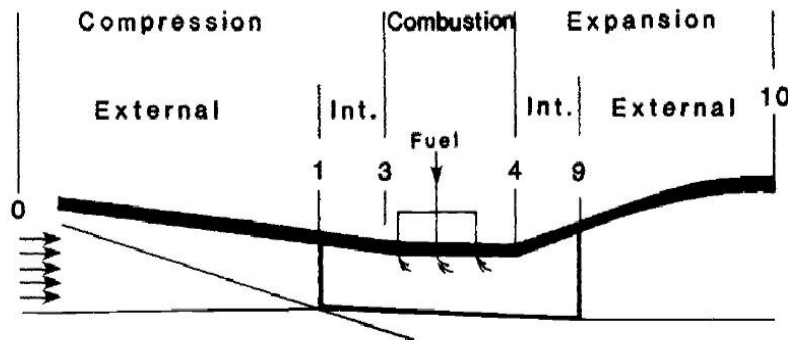


Figure 7.1b: Air-breathing engine reference station numbers and related terminology- Typical Scramjet (Heiser & Pratt, 1994).

Table 7.1: Air-breathing Engine Reference Station Locations

REFERENCE STATION	ENGINE LOCATION
0	Represents freestream conditions
	Also shows the point where External Compression <i>begins</i>
1	This marks the <i>end</i> of External Compression and The <i>beginning</i> of Internal Compression
	Also illustrates the Inlet/Diffuser <i>entry</i>
3	Shows the Inlet/Diffuser <i>exit</i> , as well as The <i>end</i> of internal Compression, and
	The <i>entry</i> of the Burner/Combustor
4	This marks the <i>exit</i> of the Burner/Combustor, The point where Internal Expansion <i>begins</i> , and
	The Nozzle <i>entry</i>
9	This marks the <i>end</i> of Internal Expansion, The Nozzle <i>exit</i> , and
	The <i>beginning</i> of External Expansion
10	External Compression <i>ends</i> here

Now, to proceed with the Thermodynamic cycle analysis, this method models the ideal heat engine, and thus, is also known as the Brayton cycle analysis. Figures 7.2 a and b show the T-s diagram of the Brayton cycle (Heiser & Pratt, 1994), where the cycle points indicate corresponding engine reference stations from Figures 7.1a and b.

Like any ideal cycle analysis, the Thermodynamic cycle analysis included the following assumptions (Heiser & Pratt, 1994):

- x Air is in its equilibrium state at all times
- x The combustion process in the engine is replaced by a constant pressure heat addition process. This process supplies energy that is equal to that released by combustion, but it does not add any mass or change the chemical constituents of the air
- x At the end of these processes, the properties of air are brought back to their original state

In looking at the T-s graphs of Figure 7.2, the four main processes are explained as follows:

Point 0 to Point 3: The process here is adiabatic compression of the air from freestream static temperature T_0 , to the burner entry static temperature T_3 . The pressure is also seen to increase from freestream static pressure p_0 , to burner static pressure p_3 . In addition, this process is not isentropic as seen by the rise in entropy from s_0 to s_3 .

Point 3 to Point 4: Here, we have heat addition that is performed at constant pressure and without friction. The temperature is raised from T_3 , to the burner exit temperature T_4 . Once again, this heat addition involves no mass addition, and entropy is noted to increase from s_3 to s_4 .

Point 4 to Point 10: The air is expanded adiabatically in this process, from burner static pressure $p_3=p_4$, to the freestream static pressure $p_{10}=p_0$. Entropy increases from s_4 to s_{10} at the end of expansion.

Point 10 to Point 0: This process ensures that the cycle is closed. Sufficient heat is rejected at constant pressure, from the exhaust air, returning it to its original temperature and entropy state.

The Thermodynamic cycle analysis essentially relies on integrating the areas under the curve in order to evaluate several physical quantities. For instance, the heat added from point 3 to point 4 is given by:

$$\text{Heat added} = \int_3^4 T ds = h_4 - h_3 \quad (7.1)$$

Whereas the heat rejected from point 10 to point 0 is given by:

$$\text{Heat rejected} = \int_0^{10} T ds = h_{10} - h_0 \quad (7.2)$$

In addition, since the compression and expansion processes are adiabatic, the cycle work can be determined by using Equation 7.3:

$$\text{Cycle work} = \text{Heat added} - \text{Heat rejected}$$

$$\frac{V_{10}^2}{2} - \frac{V_0^2}{2} = \int_3^4 T ds - \int_0^{10} T ds \quad (7.3)$$

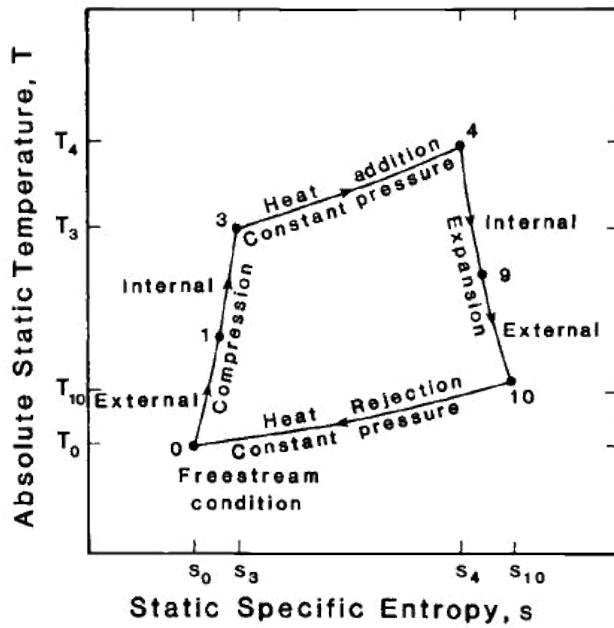


Figure 7.2a: T-s Diagram for a typical Brayton Cycle (Heiser & Pratt, 1994).

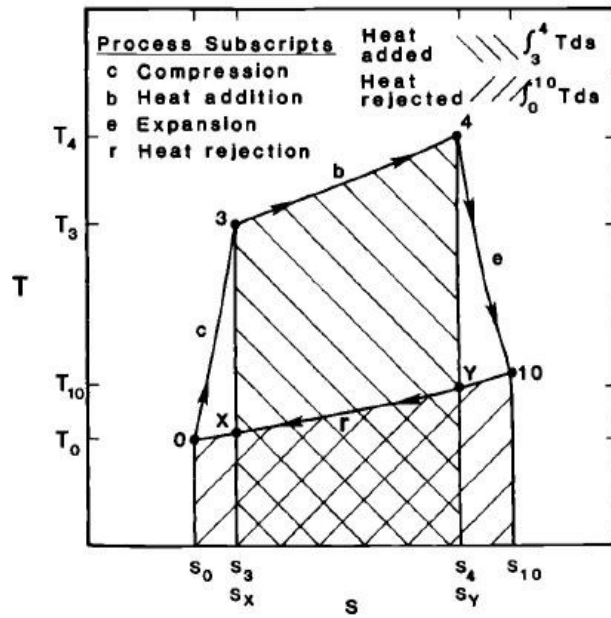


Figure 7.2b: T-s diagram showing engine reference stations (Heiser & Pratt, 1994).

K_{th} can thus be determined as:

$$K_{th} = \frac{\text{cycle work}}{\text{heat added}} = \frac{\int_1^2 T ds}{\int_1^3 T ds} \quad (7.4)$$

The reader is referred to (Heiser & Pratt, 1994) for more details on this analysis method. The First Law analysis method will now be discussed.

7.3 First Law Analysis

As explained by (Heiser & Pratt, 1994), the First Law analysis method analyzes the behavior of air across the different cycles using the static enthalpy at each of the endpoints of the thermodynamic processes. It requires the knowledge of these enthalpies as well as the h_b in order to determine the properties as shown in Equations 7.1-7.3.

The assumptions made for this analysis are (Heiser & Pratt, 1994):

- x The air is not only in its equilibrium state at all times, but it also behaves as a calorically perfect gas across all of the four thermodynamic processes
- x While the thermodynamic cycles occur at either constant pressure or adiabatically, it is

EHFRPSDUHGWRWKHLGHDOFDVHXVLQJ³FRQVWDQWHIILFLHQFLHV

‘7KLVPDNHVWKH)LUVW/DZ analysis mRUH³UHDO

‘WKDQWKH7KHUPRG\QDPLF&\FOHDQDO\VLV □ DVIROORZV

$$\text{compression process efficiency} \quad K_c = \frac{h_3 - h_x}{h_3 - h_o} \quad (7.5)$$

$$\text{expansion process efficiency} \quad K_e = \frac{h_4 - h_{10}}{h_4 - h_y} \quad (7.6)$$

This concludes the First Law analysis method. The reader is referred to the reference (Heiser & Pratt, 1994) for detailed theory, especially that pertinent to how each of the processes are analyzed using the First

Law analysis method. However, to bring the reader at ease regarding which PHWKRGLV³PRUHFRUUHFV

W¹KHDXWKRUVGRQRWHW²KDWWKHGLIIHUHQFHEHWZHHQWKH

The First Law analysis can however better determine the sensitivities and trends of air-breathing engine performance.

7.4 Stream Thrust Analysis

We have finally arrived to the analysis method of choice for the current project! The Stream Thrust analysis method is different from the aforementioned methods because it relies heavily on momentum relationships (Heiser & Pratt, 1994). For simple hypersonic air-breathing engine performance analysis, it is the preferred method since it does not, for example, ignore factors such as the mass, momentum, and kinetic energy fluxes contributed by the fuel, AND, it does not readily assume that the average static pressure at the exit plane (station 10 - Figure 7.2) is equal to freestream static pressure.

The assumptions made for this analysis are (Heiser & Pratt, 1994):

- x Because the flow is supersonic or hypersonic, the flow is undisturbed to the control volume inlet plane (station 0)
- x The flow properties at the control volume exit plane (station 10) are represented by suitable one-dimensional averages, so that the average static pressure at station 10 is not necessarily equal to the freestream value
- x The entire velocity at each engine station is aligned with the thrust or axial direction
- x The perfect gas constant R is the same at all stations (a valid approximation since the molecular weight of air does not vary significantly from station to station)

The Stream Thrust equations will now be applied to calculate the performance of each component of the propulsion system using a finite control volume approach. It must be noted that these equations are the simplified versions and that corrections are usually made to account for a more realistic behavior on a component basis. These corrections will be addressed in the ramjet/scramjet mode calculation sections.

Station 0 to Station 3: Adiabatic Compression

1. Stream Thrust Function

$$S_{a_0} = V_0 \left[\frac{\rho_0}{\rho_1} \frac{RT_0}{V_0} \right]$$

2. Burner Inlet Temperature, T_3

$$T_3 = MT_0$$

Where M = cycle static temperature ratio, and $M = \frac{T_3}{T_0} \approx 1$

3. V_3 - conservation of energy

$$V_3 = \sqrt{V_0^2 + 2C_{pc} (T_3 - T_0)}$$

4. Stream Thrust Function

$$S_{a_3} = V_3 \left[\frac{\rho_3}{\rho_1} \frac{RT_3}{V_3} \right]$$

5. Adiabatic compression process

$$\frac{p_3}{p_0} = \left(\frac{T_3}{T_0} \right)^{\frac{C_{pc}}{R}} = M^{\frac{C_{pc}}{R}}$$

6. Area ratio- conservation of mass

$$\frac{A_3}{A_0} = \frac{\rho_0 V_0}{\rho_3 V_3}$$

(7.7)

(7.8)

(7.9)

(7.10)

(7.11)

(7.12)

Station 3 to Station 4: Adiabatic Combustion

The following quantities will first be defined as they accompany the Stream Thrust analysis equations (Heiser & Pratt, 1994):

$\frac{V_{fx}}{V_3}$: this is the ratio of fuel injection axial velocity to V_3

$\frac{V_f}{V_3}$: this is the ratio of fuel injection total velocity to V_3

$C_{f \sim \frac{A}{A_3}}$ $\frac{\text{combustor drag}}{\frac{U V_3^2}{2}}$: this is the burner effective drag coefficient

$C_p T_b$: this is used to estimate the absolute static enthalpy h

1. V_4 -conservation of momentum

$$V_4 = V_3 \left(1 + C_{f \sim \frac{A}{A_3}} \frac{V_f}{V_3} \right) \quad (7.13)$$

2. Burner Exit Temperature, T_4 -conservation of energy

$$T_4 = T_b \left(1 + \frac{1}{C_p} \left[K_b f_{PR} + f_f + f C_{pb} \right] \frac{V_f^2}{V_3^2} \right) \quad (7.14)$$

3. Area ratio-conservation of mass

$$\frac{A_4}{A_3} = 1 + f \frac{T_b}{T_4} \frac{V_3}{V_4} \quad (7.15)$$

4. Stream Thrust Function

$$S_{a_4} = V_4 \frac{RT_4}{2} \quad (7.16)$$

© V₄ ¹

Station 4 to Station 10-Adiabatic Expansion

1. Exhaust exit temperature, T_{10}

$$T_{10} = T_4 \left(\frac{p_{10}}{p_4} \right)^{\frac{\gamma-1}{\gamma}}$$

2. Exit velocity, V_{10} - conservation of energy

$$V_{10} = \sqrt{2C_p(T_4 - T_{10})}$$

3. Stream Thrust Function

$$S_a = \frac{V_{10}}{V_4} \frac{RT_{10}}{V_{10}^2}$$

4. Area ratio-conservation of mass

$$\frac{A_{10}}{A_4} = \frac{p_4}{p_{10}} \frac{T_{10}}{T_4} \frac{V_4}{V_{10}}$$

(7.18)

(7.17)

(7.19)

(7.20)

The stream thrust functions apply to all modes of operation for an air-breathing cycle and are derived by modification of the governing equations of aerothermodynamics. They are modified on a component level basis or to incorporate various flow features such as thermal choking in place of a converging section. Real scramjet mode operation will modify these equations by incorporating more realistic compressor and expansion nozzle efficiencies.

7.5 A E RSPC Mode Analysis Inputs

Here is where the analysis of each individual cycles is performed using the stream thrust function listed in the previous section combined with the other one dimensional flow physics discussed. Throughout the analysis, values for propulsion system constants will be assumed based on standard or average values used in the examples mentioned by (Heiser & Pratt, 1994). These values are widely accepted as representing values of current propulsion systems, so they will be used as part of this analysis since it is a preliminary analysis. As part of a future work study, these values should be verified and/or calculated for a detailed propulsion system design.

The following inputs are constant heating values, gas properties, and the gravitational constant. Also, the h_{PR} shown below is for liquid H_2 which, as discussed in a previous section, is one of the most ideal fuels to use for a hypersonic air-breathing propulsion system. **Note:** The exact definition of each value is defined in the nomenclature and not listed here.

Table 7.2: Constants typically used for hypersonic air-breathing propulsion system analysis. (Heiser & Pratt, 1994).

INPUT	VALUE
C_{p_c}	1090 J/kgK
C_{p_b}	1510 J/kgK
C_{p_e}	1510 J/kgK
R	293 (m ² /s ²)K
h_f	0
g_0	9.81 m/s ²
h_{PR}	119,954 kJ/kg

For the sake of simplicity and due to the lack of a proper high-fidelity numerical solver with combustion and hypersonic flow modeling capabilities, the efficiencies of each of the components is based on correction factors. For current analysis, the following values taken from (Heiser & Pratt, 1994) are used:

Table 7.3: Commonly used values of propulsion component efficiencies and various propulsion system parameters. (Heiser & Pratt, 1994).

INPUT	VALUE	INPUT	VALUE
K_c	0.90	J_e	1.238
K_b	0.90	V_{f_3}	0.50
K_e	0.90	V_{f_3}	0.50
J_c	1.362	T^0	222K
J_b	1.238	$C_f \sim \frac{A_w}{A_3}$	0.10

Finally, the following inputs were either determined by the freestream conditions or were varied in order to determine other engine performance parameters:

INPUTS				
M_0	V_0	T_0	f	$\frac{T_0}{T_3}$

It should be noted that because the fuel used by AERSPC is H_2 , the resulting h_{PR} was selected as 119,954 kJ/kg, as noted in Table 3.1. To determine the fuel/air ratio f , the stoichiometric equation below was used:

$$f_{st} = \frac{36x + 3y}{1034x + y} \quad (7.21)$$

Therefore, for a system using Hydrogen as the fuel, $x=0$ and $y=2$, making $f_{st}=0.0291$.

Given these commonly used propulsion system values and component efficiencies, it is then possible to construct a preliminary analytical model of a RBCC propulsion system.

7.6 The Standard Atmosphere Model and Flight Trajectories

Before proceeding any further, a discussion on the role of the atmosphere on the air-breathing engine cycles must take place as affected by atmospheric properties. For many years, the main source of quantitative information used industry-wide is the *U.S. Standard Atmosphere, 1976* which is based on experimental data that is periodically updated by experts representing a group of U.S. experts.

JRYHUQPHQWDJHQFLHV' □
+HLVHU 3UDWW □□

The values for the static values of pressure, temperature, density, and speed of sound as a function of altitude are listed in Appendix B, directly reproduced from (Heiser & Pratt, 1994). The atmospheric property distributions are shown below in Figures 7.3 to 7.5.

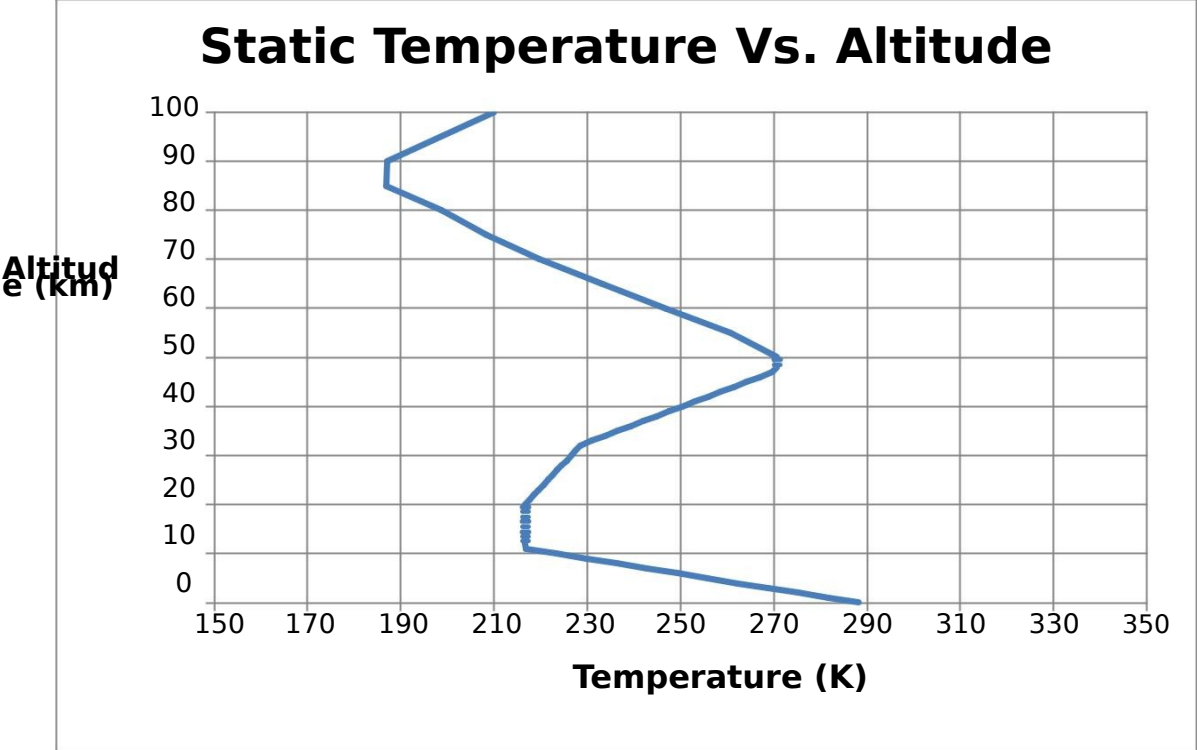


Figure 7.3: Variation of static temperature as a function of altitude.

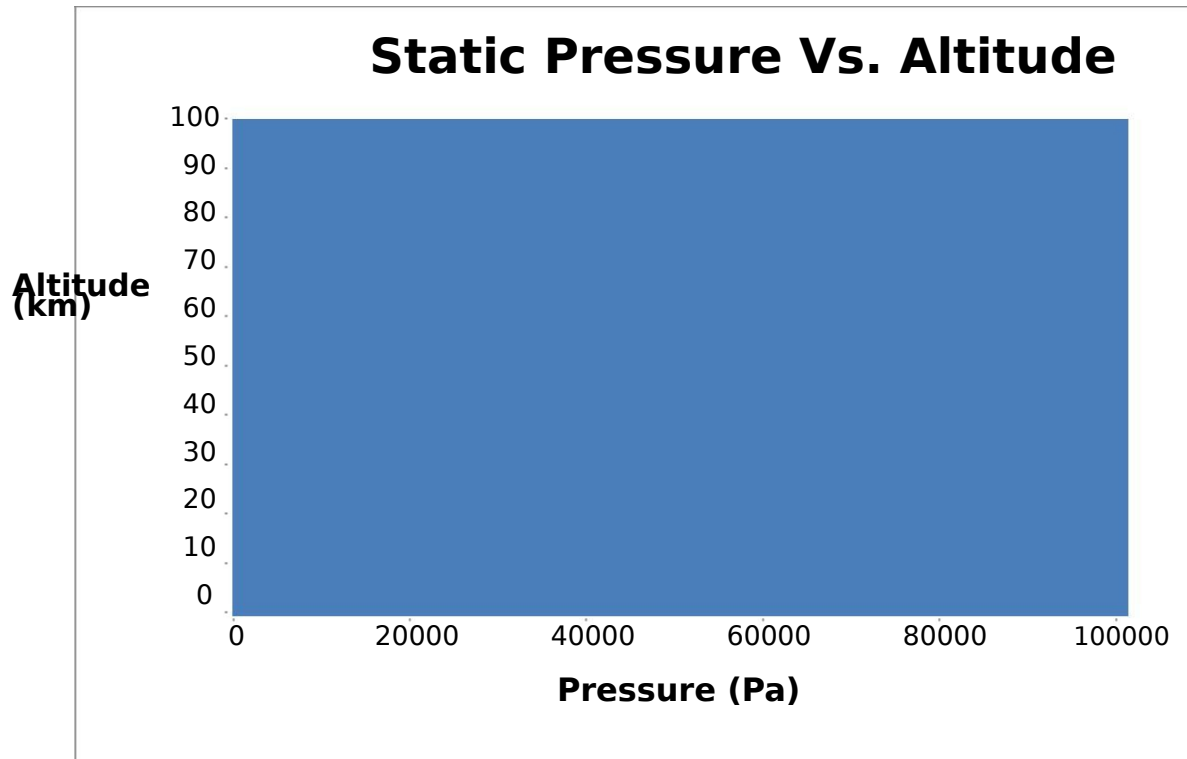


Figure 7.4: Variation of static pressure with altitude.

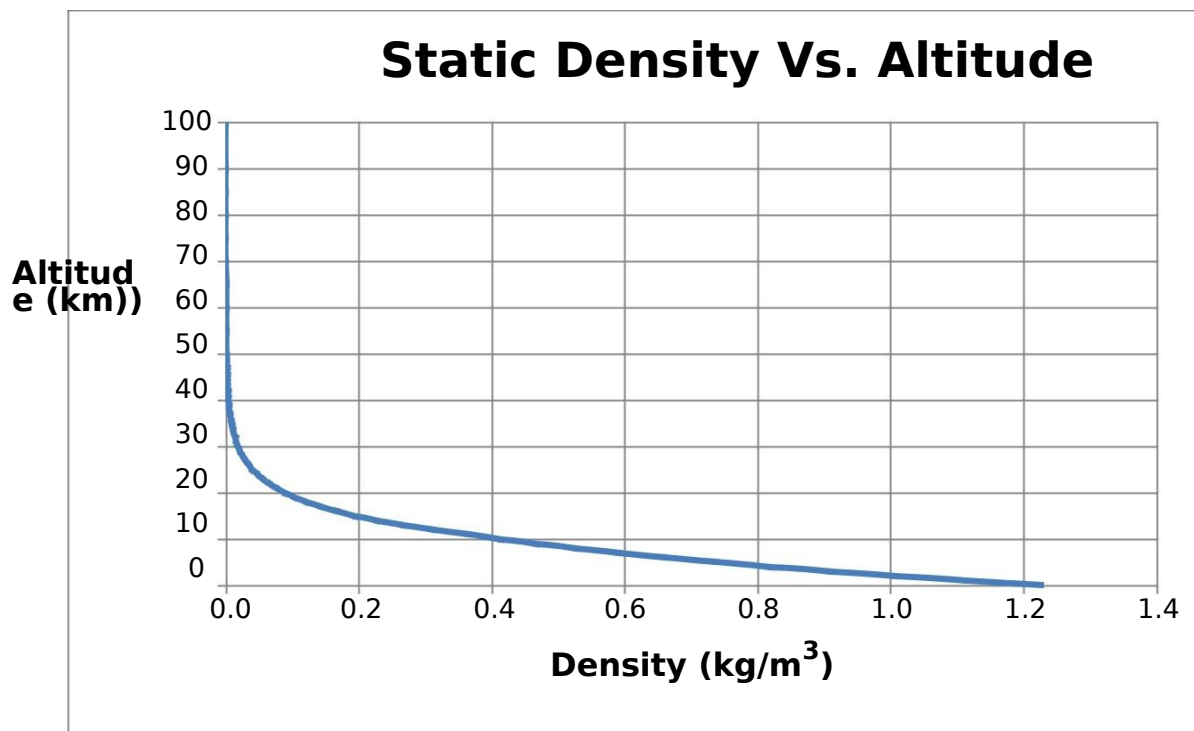


Figure 7.5: Variation of static density with altitude.

Referring to Figure 7.3, the region of the atmosphere that is of the most concern for hypersonic air-breathing propulsion design is the stratosphere, which is defined as the region between approximately 11 km and 52 km. This region consists of exactly or nearly isothermal segments. As can be seen from these figures, static temperature does not vary much throughout the atmosphere unlike the density and pressure which vary exponentially with increasing altitude.

Several important flow properties such as absolute viscosity and thermal conductivity of the air are dependent upon atmospheric variations of temperature. The absolute viscosity of air is important for hypersonic flight because of the importance of viscous effects in accurately predicting the wall skin friction and boundary layer thickness, shape, transition, and separation. Absolute viscosity of air is given by Equation 7.22 below.

$$\mu = 1.46 \times 10^{-6} \frac{T^{3/2}}{T + 111} \quad \frac{\text{Ns}}{\text{m}} \quad (7-22)$$

At hypersonic velocities, the transfer of heat to a vehicle becomes a large concern. Since the rate of heat transfer into a vehicle is governed by the thermal conductivity, it is necessary to know it is determined. The calculation for thermal conductivity is shown below in Equation 7.23.

$$k = 1.99 \times 10^{-3} \frac{T^{3/2}}{T + 112} \quad \frac{\text{J}}{\text{smK}} \quad (7-23)$$

The scaling factor of dynamic pressure on the lift and drag of a vehicle in atmospheric flight is also of great importance for hypersonic vehicle design. As seen below, in Equations 7-24 and 7-25, the lift and drag experienced by a vehicle in the atmosphere are directly proportional to the dynamic pressure.

$$L = q_0 C_L S \quad (7-24)$$

$$D = q_0 C_D S \quad (7-25)$$

With current materials, there are structural limits which restrict the maximum allowable dynamic pressure to a value of approximately 2000 lbf/ft² (95,000 N/m²). Typically, hypersonic vehicles are flown at the maximum velocity allowable by their dynamic pressure limit. A way to determine what a constant dynamic pressure trajectory looks like is by rearranging the dynamic pressure equation to solve for the free-stream Mach number as shown below in Equation 7-26.

$$M_0 = \sqrt{\frac{2q_0}{\rho_0 p_0}} \quad (7-26)$$

A trajectory can be chosen for a constant dynamic pressure by substituting values of free-stream static pressure, corresponding to a specific altitude, and then solving Equation 7-26 for the free-stream Mach number. By using the values of the Standard Atmosphere, as listed in Appendix B, and choosing a constant dynamic pressure of 1000 lbf/ft² (47,880 N/m²), a trajectory was generated as shown below in Figure 7.6. It is shown enveloped by the trajectories generated by the lower and upper limits of dynamic pressure of 500 lbf/ft² (95,000 N/m²) and 2000 lbf/ft² (95,000 N/m²), respectively.

It must be noted that for real-world applications of detailed propulsion system/vehicle designs, a trajectory optimization software tool such as OTIS (Optimization of Trajectories by Implicit Simulation) or POST (Program to Optimize Simulated Trajectories) is typically used rather than a simplified method such as the selection of a constant dynamic pressure trajectory. However, due to a lack of resources and access to the trajectory optimization software listed above, the aforementioned method of trajectory selection must be utilized.

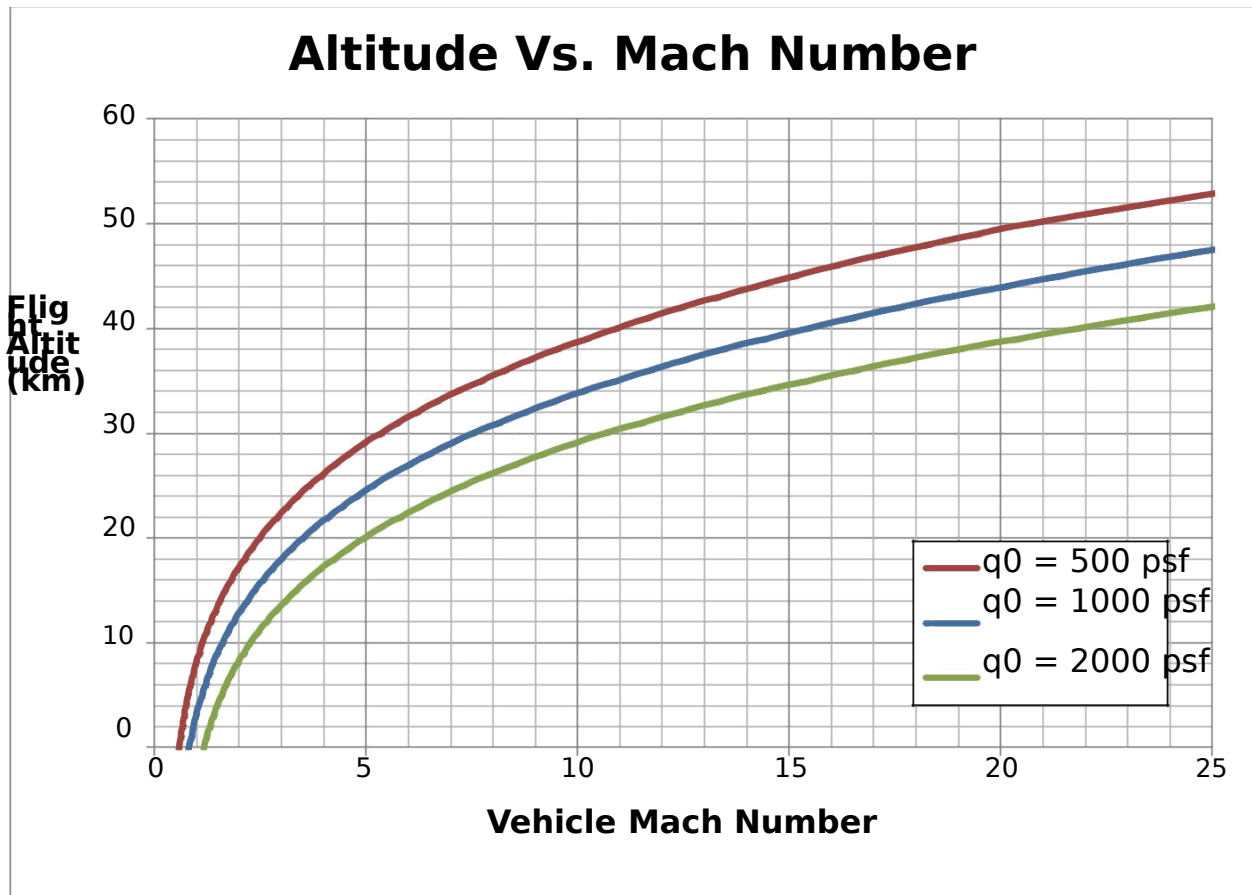


Figure 7.6: Hypersonic vehicle trajectories subject to constant dynamic loading.

This trajectory is used throughout the propulsion performance calculations for each operating mode since the free-stream properties are determined by a combination of this trajectory and the Standard Atmospheric tables in Appendix B. One method that may also have been used would involve writing a program that would interpolate values of the atmospheric region based on a piece-wise set of equations describing the variation of temperature as a function of the atmospheric altitude.

7.7 Mode I: Ejector-Ramjet Performance Calculations

Since the ejector ramjet involves primary and secondary flow, the equations used to analyze its performance parameters are slightly different, and are noted below (Heiser & Pratt, 1994). These correspond to the engine stations shown in Figure 7.7:

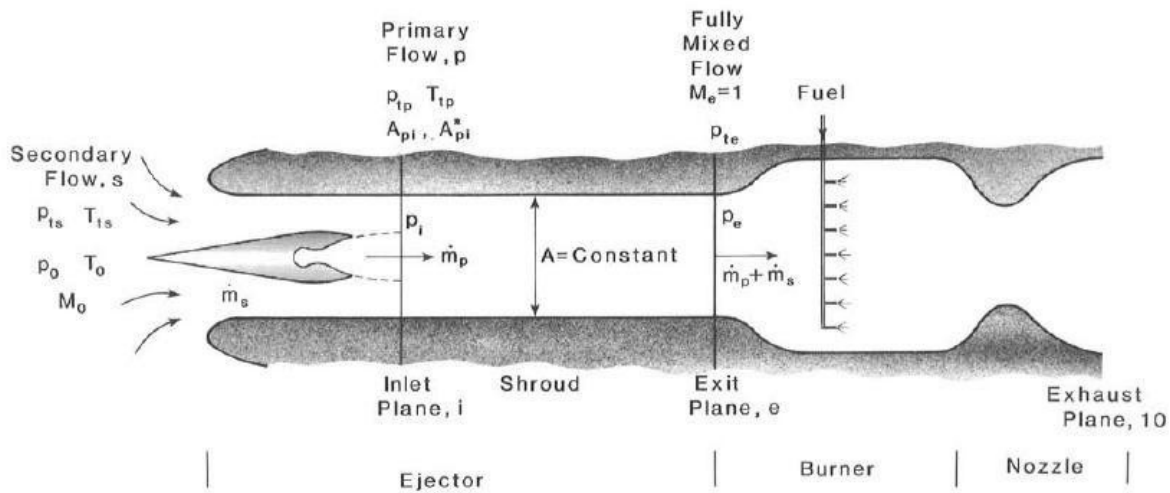


Figure 7.7: Schematic diagram for ideal ejector ramjet analysis (Heiser & Pratt, 1994).

Prior to analyzing the ejector ramjet, it was assumed that the ejector portion was of constant area and fixed geometry. In addition, the flows were treated as steady and compressible, and had the same values of calorically perfect gas constants (Heiser & Pratt, 1994). Where the inlet plane was located, the inlet primary flow was supersonic, whereas the inlet secondary flow was subsonic; at the ejector plane, flow was choked/sonic.

Inlet Plane Properties

$$M_{p_i} = \frac{a}{c} \left[\frac{2}{\gamma} \left(\frac{p_{t_p}}{p_0} \right)^{\frac{\gamma-1}{\gamma}} \frac{p_0}{p_i} \right]^{\frac{1}{2}} \quad (7.27)$$

$$\frac{A_{p_i}}{A_p^*} = \frac{1}{M_{p_i}} \left[\frac{2}{J_1} \left(\frac{J_1}{2} \right)^{\frac{1}{2}} \right] \quad (7.28)$$

$$\frac{A_{p_i}}{A} = \frac{A_{p_i}^*}{A_p^*} \frac{A_p^*}{A} \quad (7.29)$$

$$\frac{A_{s_i}}{A} = \frac{A_{p_i}}{A} \quad (7.30)$$

$$M_{s_i} = \frac{2}{J_1} \left[\frac{J_1}{2} \left(\frac{J_1}{2} \right)^{\frac{1}{2}} \right] \quad (7.31)$$

$$D \frac{m_s}{m_p} \text{ bypassratio} = \frac{p_{t_s}}{p_0} \frac{p_0}{p_{t_p}} \frac{A}{A_{p_i}} \frac{M_{p_i}}{M_{s_i}} \sqrt{\frac{T_{t_p}}{T_0}} \frac{T_0}{T_{t_s}} \frac{J_1}{2} \left[\frac{J_1}{2} \left(\frac{J_1}{2} \right)^{\frac{1}{2}} \right] \quad (7.32)$$

Exit Plane Properties

$$\frac{T_e}{T_{t_p}} = \frac{2}{J_1} \left[\frac{J_1}{2} \left(\frac{J_1}{2} \right)^{\frac{1}{2}} \right] \quad (7.33)$$

$$\frac{p_e}{p_0} = \frac{1}{A} \frac{A_p^*}{p_0} \frac{p_{t_p}}{p_0} \sqrt{\frac{T_e}{T_{t_p}}} \frac{J_1}{2} \left[\frac{J_1}{2} \left(\frac{J_1}{2} \right)^{\frac{1}{2}} \right] \quad (7.34)$$

Since the value of (p_i/p₀) is an iterated value, and was guessed at the beginning of the ejector ramjet analysis, at this point, the value will be checked using Equation 7.35 to make sure the ratio is unity for the correct solution. This is the result of the assumption that the primary and

secondary flows are at equal pressures at the inlet plane of the combustor for constant pressure combustion.

$$\frac{p_i}{p_0} = \frac{A_1}{A_2} \left(\frac{p_e}{p_0} \right)^{\frac{1}{2}} \left(\frac{J}{J_1} \right)^{\frac{1}{2}} \quad (7.35)$$

$$\frac{p_{ts}}{p_0} = \frac{p_i}{p_0} \left(\frac{p_e}{p_0} \right)^{\frac{1}{2}} \left(\frac{J}{J_1} \right)^{\frac{1}{2}} \quad (7.36)$$

The iteration can be performed by any zero-VROYHU EXWLQWKLVDVH tool was used subject to the constraint shown above in Equation 7.36. Once (p_i/p_0) is iteratively solved, the Ejector ramjet exit total pressure ratio and thrust augmentation ratio are determined as follows:

$$I_p = \frac{m_e V_{e10} + m_s V_0}{m V} = 1 + D \frac{V_{e10}}{V_0} \frac{D}{V_0}$$

where:

$$M_{p_0} = \frac{V_0}{V} = \frac{M_0}{M_0} \left(\frac{T_{t0}}{T_{t0}} \right)^{\frac{1}{2}} \left(\frac{J}{J_1} \right)^{\frac{1}{2}} \left(\frac{p_e}{p_0} \right)^{\frac{1}{2}} \left(\frac{J}{J_1} \right)^{\frac{1}{2}}$$

(7.38)

(7.37)

(7.39)

(7.40)

$$M_{10} \left(\frac{p}{p_0} \right)^{\frac{\gamma}{\gamma-1}} = \left(\frac{T}{T_0} \right)^{\frac{\gamma}{\gamma-1}} \left(\frac{J_1}{J_2} \right)^{\frac{1}{2}} \quad (7.41)$$

$$\frac{V}{V_0} = \frac{M_{10}}{M_0} \left(\frac{T_0}{T} \right)^{\frac{1}{2}} \left(\frac{J_1}{J_2} \right)^{\frac{1}{2}} \quad (7.42)$$

7.7.1 Ejector-Ramjet Results

The above equations were used to calculate the one-dimensional flow properties at the discrete volumes or components of the flow for a range of Mach numbers extending from Mach 0 (static) to Mach 2.5. In order to facilitate these calculations, the following assumptions were made about the rocket element performance parameters as well as the propulsion system exit plane parameters:

- x p_{tp}/p_0 = primary rocket stream total pressure ratio = 15
- x T_{tp}/T_0 = primary rocket stream total pressure ratio = 10
- x A/A_p^* = primary rocket stream exhaust expansion area ratio = 12
- x α ratio of specific heats at constant pressure and constant volume = 1.35
- x p_{10}/p_0 = exit pressure to freestream pressure = 1 (fully expanded flow)
- x T_{t10}/T_{tp} = exit plane exhaust total temperature to freestream total temperature = 1

These properties of the primary and exhaust flow are chosen as constant and the values chosen represent common propulsion system values (Heiser & Pratt). One caveat should be mentioned now, is that shockwaves were not modeled as part of this analytical model and instead isentropic compression relations were chosen due to their ease of implementation and to simplify the geometry. As a result, the isentropic equations from

(Anderson, 2004) were used to calculate the temperature and pressure ratios between the total secondary stream and the static freestream values.

As mentioned in the introduction section of this report, a spreadsheet with iterative solving capabilities was created to automate the calculation of these equations for a wide variety of Mach numbers. The tabulated results of these calculations are included in **Appendix C**. The tabulated results split up the equations according to the type of governing principles or assumptions that were used to facilitate the calculations. Cells are also differentiated by colors representing if the cell is an input, constant, calculated value, or iterated value. A more robust application might be developed in the future using MATLAB, if time permits.

Of great interest in calculating the propulsion performance of an ejector-ramjet is the level of thrust augmentation (ρ) that the combination of an ejector rocket and ramjet operating mode provides. Thrust augmentation is defined as the ratio of thrust produced by air augmentation to the unmodified rocket thrust. This value is greater than 1 throughout the operating flight regime of this operating mode and nearly approaches a value of 16 Mach 2.5, as shown below in **Figure 7.8**.

Thrust Augmentation Vs. Freestream Mach Number

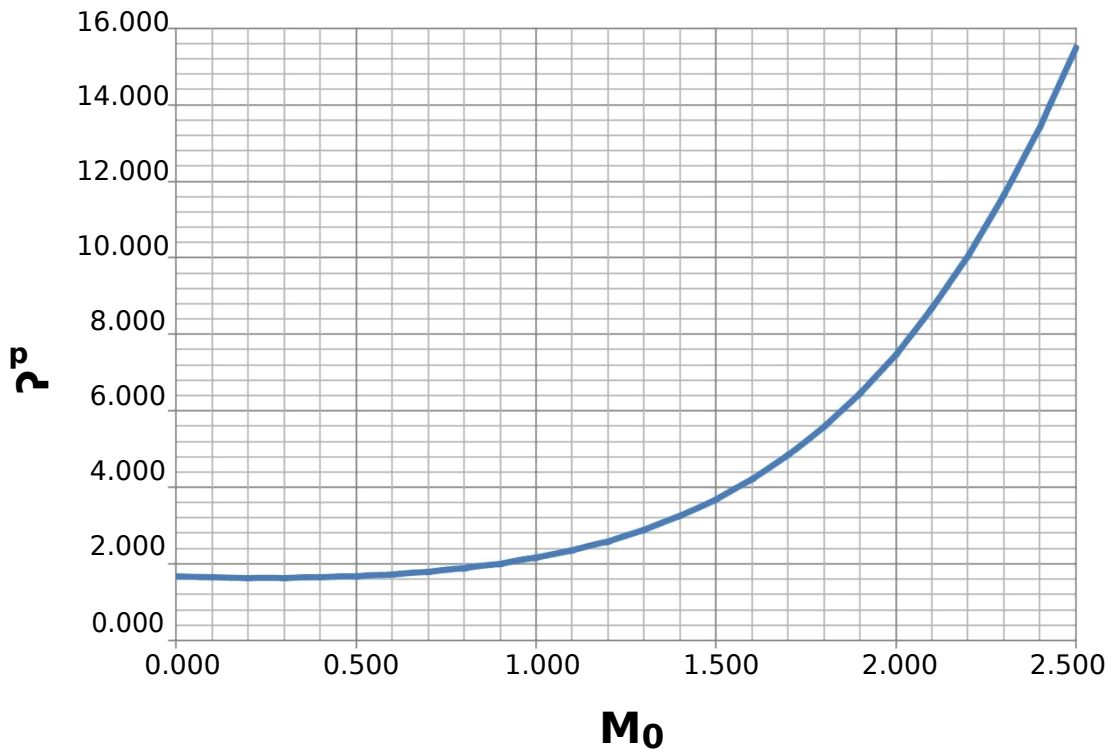


Figure 7.8: Thrust augmentation for freestream Mach number during the ejector-ramjet operating mode.

Therefore, the uninstalled thrust and thrust augmentation are useful performance metrics for comparing propulsion system to propulsion system, but the overall vehicle integration scheme must be taken into account whenever extra propulsion subsystems are being added. To truly judge the effectiveness of the ramjet-ejector, two common propulsion performance metrics (I_{sp} and F/\dot{o}) are graphed below as a function of freestream Mach number in **Figures 7.9 & 7.10**, respectively.

As expected, the I_{sp} performance of the ejector-ramjet is significantly higher than a traditional all-rocket propulsion system throughout its flight regime. This increase in performance is due to the utilization of air entrainment into the duct as a result of momentum transfer through viscous forces. Entrained air is combusted with the fuel-rich

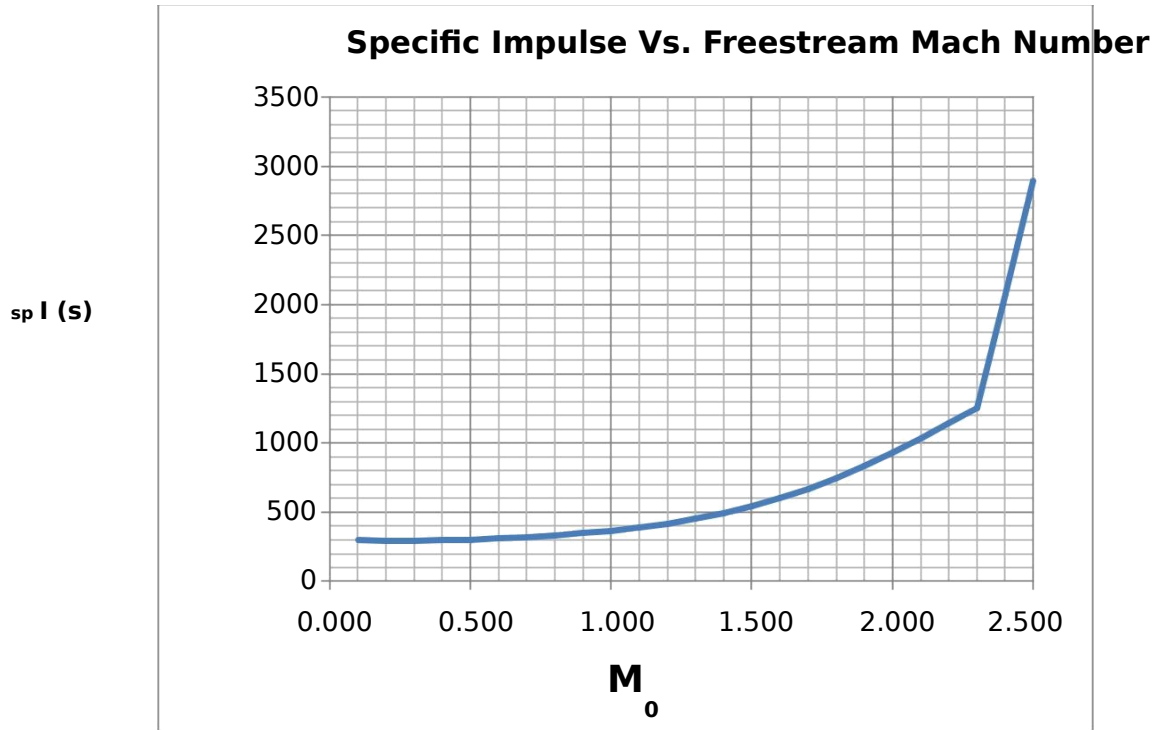


Figure 7.11: Ejector--Ramjet specific impulse as a function of freestream Mach number.

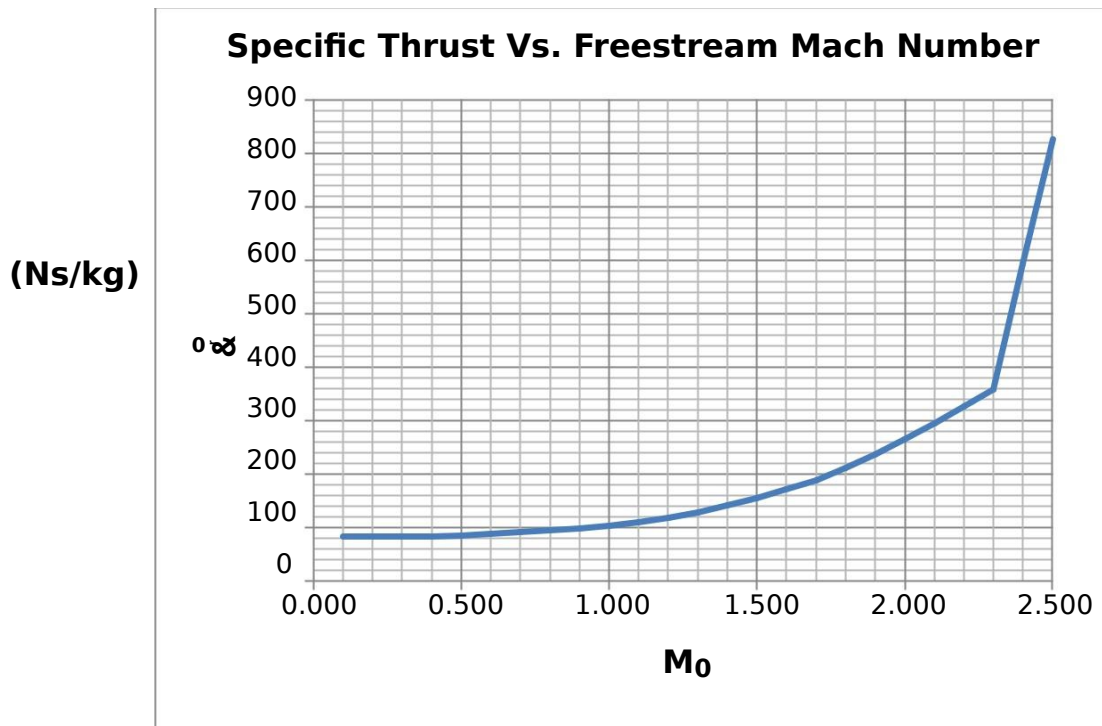


Figure 7.12: Ejector--ramjet specific thrust as a function of freestream Mach number.

rocket exhaust and then expanded using a thermal throat instead of a converging-diverging section. The reason behind the use of a thermal throat rather than a converging-diverging section was explained in a previous section, and will be discussed in more detail in the ramjet-scrumjet dual mode proceeding section

The ejector-ramjet operates only until a high enough freestream Mach number is reached so that sufficient pre-compression can be achieved and a ramjet operating mode be used instead since it becomes more efficient to operate in pure ramjet mode than ejector-ramjet mode as shown in the next section.

7.8 Mode II & III: Dual-Mode Ramjet and Scramjet Performance Calculations

Next, the ramjet/scramjet dual-mode cycle was analytically modeled using Equations 7.7 to 7.20. The propulsion system was split into components or control volumes for analysis as mentioned in the stream thrust analysis section. In order to operate in both the ramjet and scramjet modes, the propulsion system must have the means to provide for subsonic combustion in the ramjet mode while also providing supersonic expansion. Typically, two physical

FRQYHUJLQJVHFWLRQVSURYLGH³WKURDWV´DWZKLFKWKHORFDOODFKnumber is sonic.

The first choke is in the isolator (station 1 to station 3) in Figure 7.1a and 7.1b. It is used to diffuse and compress the supersonic freestream (usually aided by vehicle forebody pre-compression with oblique shockwaves) to a subsonic Mach number. In sidewall isolators, this is SHUIRUPHGWKURXJKD³VKRFN-WUDLQ´RIQRUPDOVKRFNVDWORZVXSHUVRQLF0DFKQXPEHUV DQGWKHQ WKURXJKDQREOLTXH³VKRFN-WUDLQ´DWK LJKHUVXSHUVRQLFWRK\SHUVRQLF0DFKQXPEHUVIn this sense, the isolator typically pOD\V³GRXEOHGXW\´E\SURYLGLQJDPHFKDQLVPIRUF RPSUHVVL RQDQG also inlet isolation. As a result of the normal or oblique shock-trains terminating at the end of the isolator outlet plane, station 3 (combustor inlet), high back-pressure has the potential to cause boundary layer separation and flow reversal into the inlet. When this occurs, the inlet is ³XQVWDUWHG´DQGWKHEDFN-pressure in the combustor will continue to increase, potentially resulting in the propulsion system overheating beyond design values.

Next, the flow in a ramjet propulsion system must be accelerated from the subsonic combustor velocity to supersonic velocity in the nozzle. This is typically accomplished by the second converging-diverging section. However, a dual-mode ramjet/scramjet propulsion system variable geometry mechanisms are utilized, some other means of providing these choke points must be found for the ramjet portion of the flight. At hypersonic Mach numbers, the stagnation temperature becomes too high for a converging section to be used within the combustor, so supersonic expansion is instead performed by Rayleigh heat addition at a specified station in the duct with the necessary values of $T_t(x)$ and $A(x)$ to sustain a thermal throat.

A thermal throat is modeled in the stream thrust method employed by (Heiser & Pratt, 1994) through the use of their constant area, frictionless combustion process. Instead of the constant pressure heat addition equations listed as Equations 7.13 to 7.15 here, the following constant area heat addition equations are used for the combustor section from station 3 to 4.

1. Calculating V_4 from the conservation of momentum and energy:

$$V_4 = \frac{b r \sqrt{b^2 + 4ac}}{2a} \quad (7.44)$$

Where:

$$\begin{aligned}
 a &= \frac{R}{2C_{pb}} \\
 b &= \frac{V_3}{1 - f_3} \left[\frac{RT_3}{V_3^2} - \frac{V_3}{V_3} \frac{C_{pb}}{2} \frac{A_3}{A_4} \right] \\
 c &= \frac{RT_3}{1 - f_3} \left[\frac{1}{C_{pb}} \left(K_{b,PR}^{fh} - f_{h,PR} - f_{C_{pb}}^T \right) \right] + \frac{V_2 \cdot V_2^{1/2}}{V_2} \left(\frac{V_2}{2} \right)^{3/4}
 \end{aligned}$$

2. Calculating T_4 from the conservation of momentum and energy:

$$T_4 = \frac{c}{R} - \frac{V_2^2}{2C_{pb}} \quad (7.45)$$

3. p_4/p_0 (Conservation of mass):

$$\frac{p_4}{p_0} = 1 - f \frac{p_3 T_4 V_3}{p_0 T_3 V_4} \quad (7.46)$$

There was one issue encountered while using these equations, however. It resulted when trying to use the stream thrust function in the Mach number range from 2.5 to around 5.7. At these Mach numbers, Equation 7-9 for the combustor inlet velocity V_3 gives an error since the term V_0^2 is less than $-2C_{pb}T_0(j-1)$ within the radical. This results in an imaginary number and termination of the calculations. Therefore, these equations were abandoned for flight Mach numbers in this range. Instead

DSURJUDPQDPHG³3DUDPHWULF&\FOH\$QDO\VLV
 'RU
 3\$5\$

written by David T. Pratt, co-author of *Hypersonic Airbreathing Propulsion*, was used for the ramjet mode calculations in this flight range. PARA utilizes an ideal (perfect) gas model with constant specific heats, but with the option to specify

FRPSRQHQWHIILFLHQFLHVWRVLPXODWHD³UHDO UDPMHW´

Tabulated results of the calculations performed in PARA are listed in Appendix D. The inputs were chosen in order to match the constant dynamic pressure trajectory established earlier. Also, the rest of the input parameters followed those used for the rest of the propulsion cycle calculations as closely as possible. A note must be made that PARA calculates ramjet performance with converging-diverging sections as opposed to utilizing a thermal throat, so the performance values may deviate to some extent. The rest of the assumptions previously made within this analysis apply for the model that PARA uses as well.

Stream thrust analysis equations did work for freestream Mach numbers greater than 5.8, so they were used to calculate the scramjet propulsion performance from Mach 5.8 to Mach 12. Tabulated results for these calculations are presented in Appendix E.

7.9 Mode I V : All-Rocket Performance Calculations

7KHUHVWRIWKHYHKLFOH\|VWUDMHFWRU\|URP0DFK □□ WR0DFK □ LVFDUULHGRXWLQ WKHDOO-rocket propulsion mode. To calculate the performance in this mode, it is fairly straightforward since the specific impulse does not vary as a function of altitude or any other parameter except for the rocket chamber pressure, nozzle characteristics, and propellant mass flow rates. To facilitate these calculations, the ideal rocket equations listed in Chapter 4 are used to calculate the specific impulse, thrust specific fuel consumption, specific thrust, and overall propulsion system efficiency across the flight regime in which it is operating. Not much discussion will take place in this section because the focus of this project is not in optimizing the rocket mode, though that would be carried out in real world design due to sensitivity of improving rocket performance. As discussed in an earlier section and represented by Figure 6.1, improving the rocket specific impulse by just 5 seconds is an equivalent increase in overall system performance as adding a turbojet subsystem to the low Mach number flight. This is due to the much larger velocity over which the rocket mode operates than all of the other propulsion modes.

8. Overall A E RSPC Propulsion System Performance

The whole goal of this project was to develop an analytical model combining the best propulsion systems across the entire flight regime to see the benefits over a traditional rocket-powered launch vehicle. This section addresses this potential performance improvement. Now the individual performance of each propulsion cycle can be combined across the entire airbreathing flight regime to depict the improvement in performance over a traditional all-rocket propulsion system. Depicted below in Figure 8.1, is the overall specific impulse of the uninstalled propulsion systems over the entire airbreathing Mach number range.

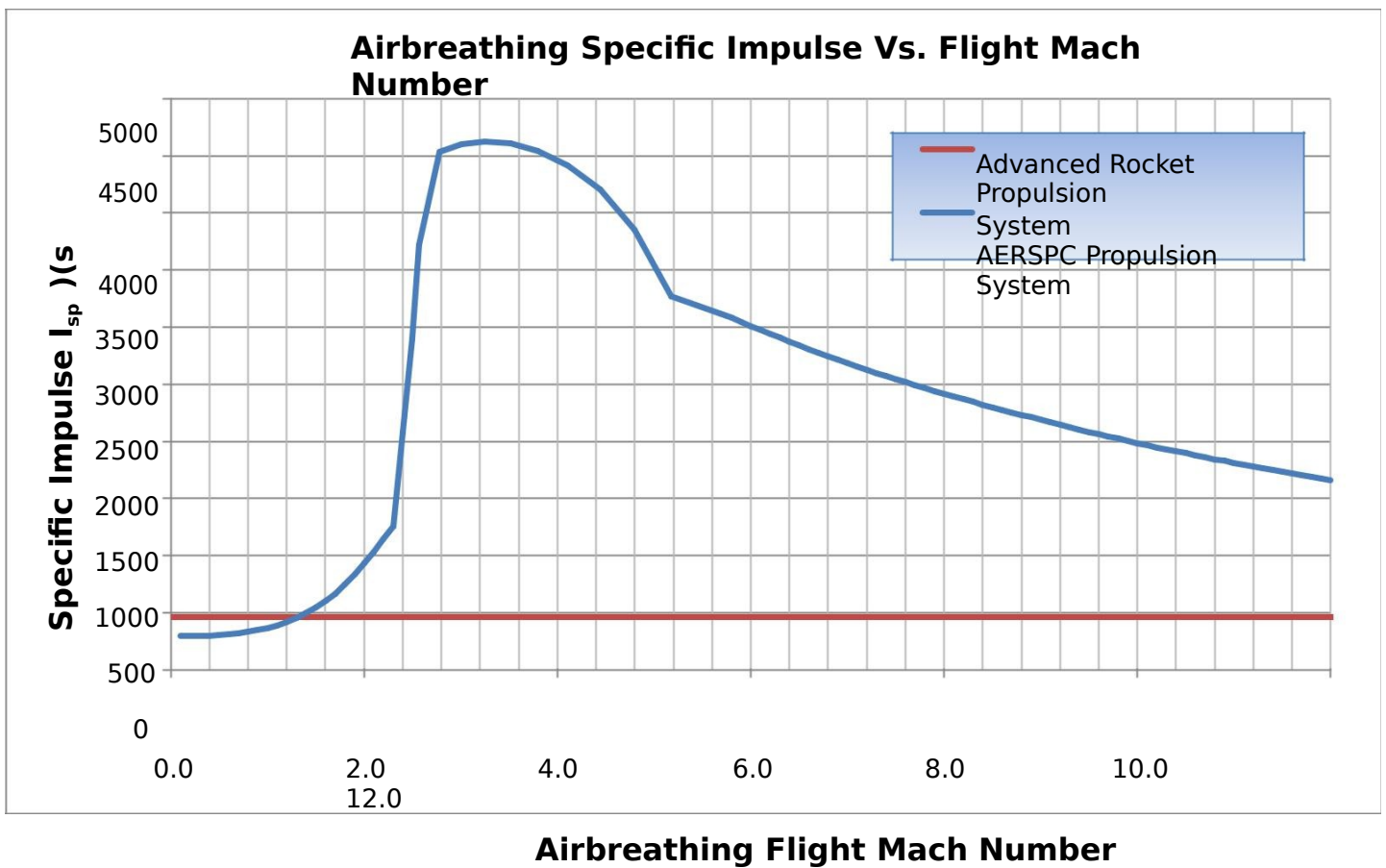


Figure 8.1: AERSPC specific impulse as a function of airbreathing flight Mach number.

Using LOX/LH₂ with a constant specific impulse of 460 s is depicted in this graph for comparison. It is quite apparent that a RBCC vehicle utilizing the same propulsion systems as the AERSPC, as defined in this project, has the potential to achieve significant improvements in the overall specific impulse. It was calculated that the I_{sp} of the

propulsion system over the entire range of airbreathing Mach numbers (Mach 0 to 12) is 2065 s while the overall I_{sp} over the entire flight regime (Mach 0 to 25) is 1293 s. Compared to the I_{sp} of a conventional all-rocket propulsion system (350s), this is quite a large improvement. This ultimately translates to a lower required propellant mass fraction and thus more mass available to allocate to vehicle structural improvements and robustness as well as payload improvements.

Other common propulsion system performance parameters are depicted in Figures 8.2, 8.3, and 8.4. They are the specific thrust, thrust-specific fuel consumption, and the overall propulsion system efficiency.

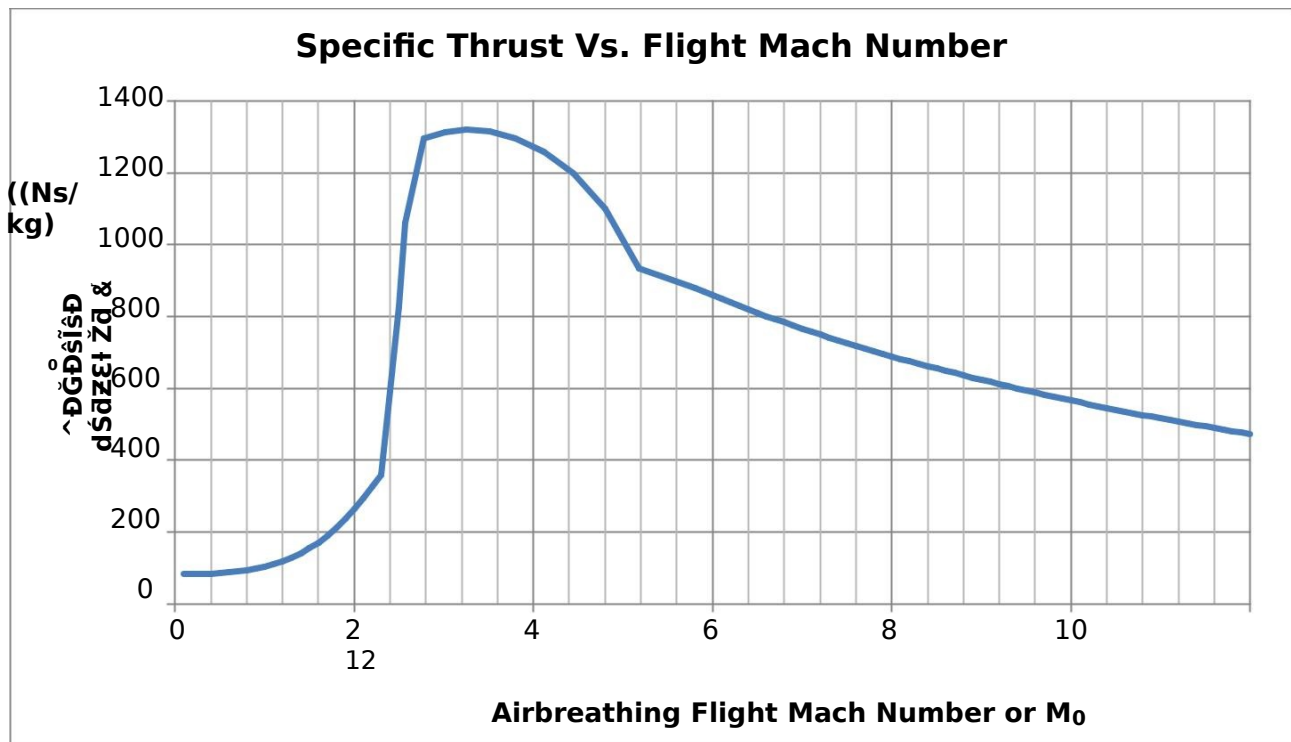


Figure 8.2: AERSPC specific thrust as a function of flight Mach number.

The specific thrust curve is nearly identical to the specific impulse curve except for the scale factor of $1/fg_0$ between them. If a constant fuel to oxidizer ratio and acceleration due gravity are assumed, then this is how the specific thrust varies throughout the flight regime. As predicted, the higher the performance of the engine, the less fuel needed to produce a given thrust. For example, for the ramjet portion of the trajectory, the highest thrust is produced for the least fuel consumed. On a similar note, the thrust specific fuel consumption is essentially the

inverse of the specific thrust as it measures the amount of fuel consumed in grams to produce one kN worth of thrust for one second.

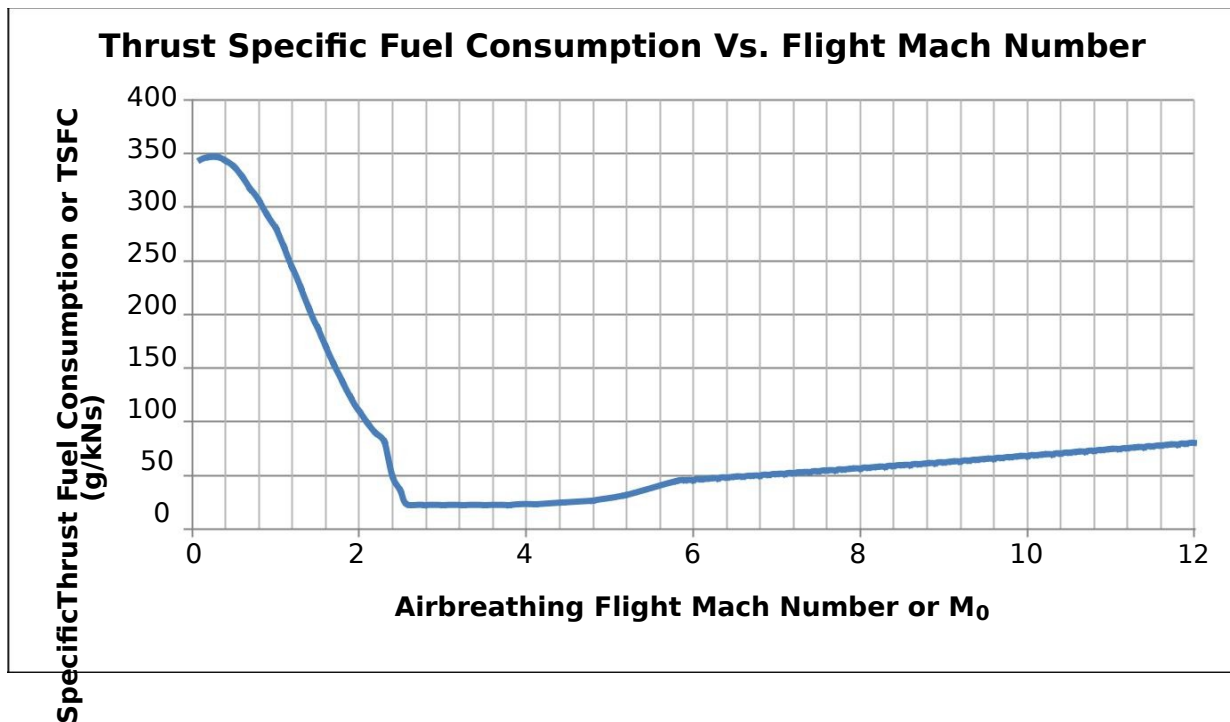


Figure 8.3: AERSP thrust specific fuel consumption as a function of airbreathing flight Mach number.

Another important propulsive parameter is the overall efficiency of the propulsion system, shown below in Figure 8.4. This value is typically calculated as a combination of the thermal and propulsive efficiencies for ideal propulsion systems. For real propulsion systems, a great deal more realistic efficiencies have to be taken into consideration. As can be seen here, the

SURSXOVLQRQV\VWHPLVWKHPRVWHIILFLHQWLQWKHUDPMHWDQGVFUDPMHWPRGHVZKHQLW¶\VFDSWXULQJWKH PRVWDLUDQGEXUQLQJWKHOHDVWIXHO7KHUHIRUH

¶ LW¶\VGHVLUDEOHWRH[WHQGWKHRSHUDWLQJUDQJHRIWKH airbreathing modes so that the benefit of this efficiency can be extended a wider range of Mach numbers.

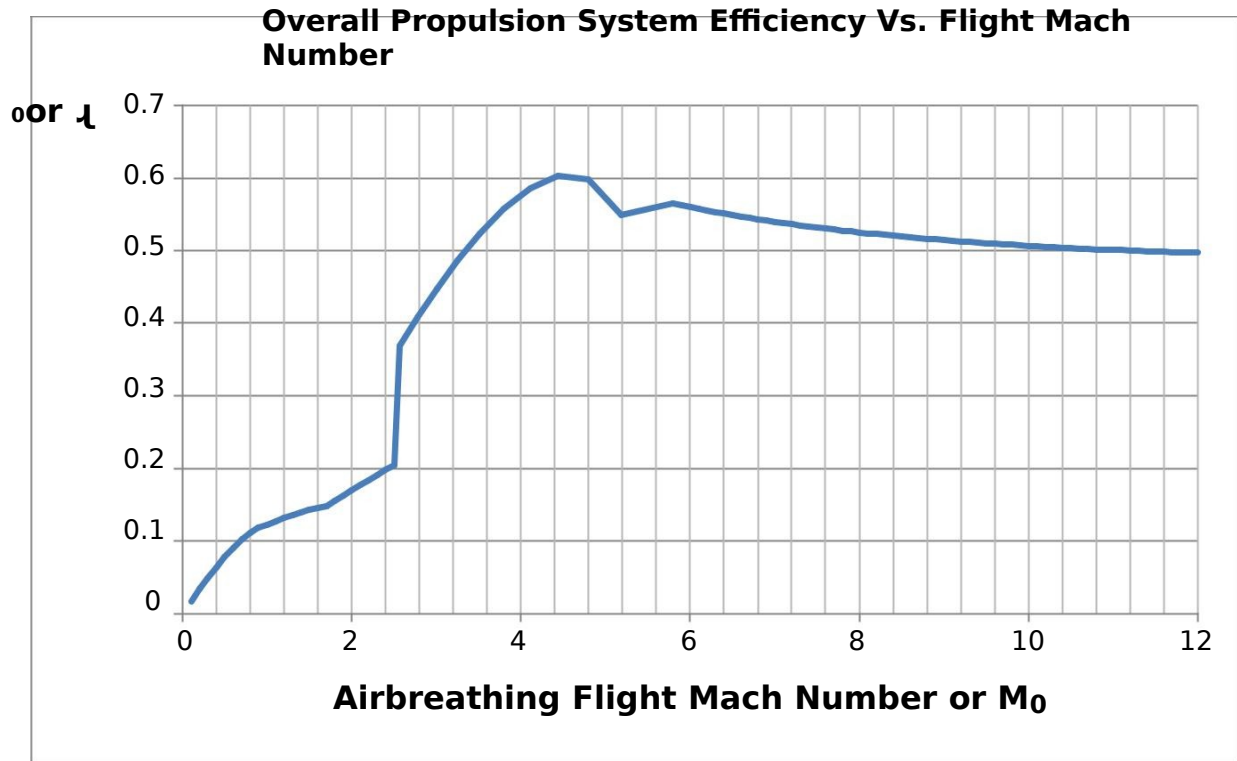


Figure 8.4: AERSPC overall propulsive efficiency as a function of airbreathing flight Mach number.

9. Conclusion

These propulsion performance parameters listed so far are useful, but it must also be noted that these were all calculated with a great deal of assumptions and also without considering the effects of the overall losses due to drag and gravity. Such a large portion of the trajectory is spent in the atmosphere that the losses due to the drag of hypersonic flight cannot be ignored. Therefore, it is imperative to be able to measure the aerodynamics of the vehicle at every point in

W_{KHWUDMHFWRU}\WR³FRUUHFW

W_{KHRYHUDOOYDOXHIRUWKHVSHFLILFLPSXOVH} and to calculate the equivalent effective specific impulse I^* , which takes into account all of the positive propulsive forces minus the losses. This is the specific impulse value that would be used in the traditional rocket equation to determine the possible payload mass fraction capability.

The next step in designing a RBCC propulsion system then would be to determine a vehicle/propulsion system combination through the use of CAD systems. Design considerations mentioned herein would weigh into the vehicle design and ultimately dictate the geometry, the propulsion system/vehicle integration, the engine operating cycles (and associated flight Mach numbers), and the take-off/landing scheme. In addition, a trajectory has been determined for a constant dynamic pressure. To carry out the design to a detailed rather than conceptual level, this trajectory would be used with an appropriate CFD package to calculate the lift and drag on selected vehicle geometry and thus allow for a realistic calculation for the vehicle performance.

In addition CFD could be used to determine the efficiencies of every component of the propulsion system to alter the 1-D equations with more realistic values. This level of detailed design could have been carried out if a combustion modeling CFD package capable of simulating real gases with dissociation had been acquired early on in the design process. Nevertheless, the 1-D finite volume approach used herein is sufficiently useful for examining the influence of component efficiencies and varying propulsion system parameters on the overall efficiency of a RBCC propulsion system.

References

- Anderson, J. D. (2007). *Fundamentals of Aerodynamics* (4th Edition ed.). New York: McGraw-Hill.
- Anderson, J. D. (2006). *Hypersonic and High-Temperature Gas Dynamics*. (J. A. Schetz, Ed.) Reston: American Institute of Aeronautics and Astronautics.
- Anderson, J. D. (2004). *Modern Compressible Flow* (3rd Edition ed.). New York: McGraw-Hill.
- Bartolotta, P.A., McNellis, N.B., Shafer, D.G. (2003). High Speed Turbines: Development of a Turbine Accelerator (RTA) for Space Access. *12th AIAA International Space Planes and Hypersonic Systems and Technologies*. AIAA 2003- 6943.
- Biblarz, O. & Sutton, G. P. (2001). *Rocket Propulsion Elements* (7th Edition ed.). Danvers: Wiley-Interscience.
- Biblarz, O. & Zucker, R.D. (2002). *Fundamentals of Gas Dynamics*. John Wiley and Sons.
- Billig, F.S. (1996). The Low Speed Operation of an Integrated Rocket-Ram-Scramjet for a Transatmospheric Accelerator. *Progress in Astronautics and Aeronautics*. Vol. 165. AIAA, Inc.
- Cengel, Y. A., & Boles, M. A. (2008). *Thermodynamics: An Engineering Approach* (6th Edition ed.). New York: McGraw-Hill.
- Curran, E. (1990). The Potential and Practicality of High Speed Combined Cycle Engines. *Advisory Group for Aerospace Research & Development Conference Proceedings*. Vol. 479, pp. K1 - K7.
- DeBonis, J., Trefny, C., Steffen, C. J. (1999). *Inlet Development for a Rocket Based Combined Cycle, Single Stage to Orbit Vehicle Using Computational Fluid Dynamics*. *35th Joint Propulsion Conference & Exhibit*. Los Angeles: National Aeronautics and Space Administration.
- Dissel, A., Kothari, A., & Lewis, M. (2006). *Stage-to-Orbit Air-Breathing*. *Journal of Spacecraft and Rockets*, AIAA. Vol. 43, No. 3. May-June 2006, pp. 568-574.
- Dykstra, F., Caporicci, M., Immich, H. (1997). *Development of a Turbine Accelerator (RTA) for Space Access*. AIAA 2003- 6943.
- Escher, W.J. & Flornes, B.J. (1967). *Development of a Turbine Accelerator (RTA) for Space Access*. AIAA 2003- 6943.
- The Marquardt Corporation Report No. 25,194.

Escher, W.J., Foster, R., Robinson, J. (1989). ³Air Augmented Rocket Propulsion Concepts'.
Madison: Astronautics Corporation of American.

Escher, W.J., Foster, R., 5RELQVRQ □-□

□

of an Extensively Axisymmetric Rocket Based Combined Cycle (RBCC) Engine
Power

Escher, W.J., Hyde, E.H., Anderson, D.M. (1995).

Assessments of All-Rocket and Rocket-
Based CCPs for Advanced Earth-to-Orbit Space
-2474.

Falempin, F. (2001). Scramjet Developments in France. Vol. 189 of Progress in Astronautics
and Aeronautics. American Institute of Aeronautics and Astronautics.

Foust, Jeff. Reducing launch costs: a lower limit? 27 September 2004. 26 October 2010.
<http://www.thespacereview.com/article/233/1>.

Gyorgy, Nagy Isptvan. (1977). "Albert Fono: A Pioneer of Jet Propulsion". International
Astronautical Congress, 1977. IAF/IAA.

Heiser, W. H., Pratt, D. T. (1994). *Hypersonic Airbreathing Propulsion*. AIAA
Education Series, American Institute of Aeronautics and Astronautics, Inc.

Heppenheimer, T. A. (2006). *Facing the Heat Barrier: A History of Hypersonics*. NASA
History Series, National Aeronautics and Space Administration.

Kirkpatrick, D., Klungle, D. (1999). *Space Mission Analysis and Design: Third Edition*. El
Segundo: Microcosm Press.

Kors, D. L. (1990). Considerations for Combined Air Breathing-Rocket Propulsion
Proceedings. Hypersonic Combined Cycle Propulsion. Vol. 479, pp. 12.1-12.13.

Lockheed Martin Space Systems Company. (2007, April). *Advanced Development
Programs*. Retrieved November 5, 2010, from Lockheed Martin Web site:
<http://www.lockheedmartin.com/data/assets/12742.pdf>.

Mattingly, J. D. (2006). *Elements of Propulsion: Gas Turbines and Rockets*. Reston:
American Institute of Aeronautics and Astronautics, Inc.

Peat, C. *ISS - Orbit Data*. Retrieved October 23, 2010, from heavens-above:
<http://www.heavens-above.com/orbit.aspx?satid=25544>.

Sabel'nikov, V. A., Penzin, V. I. (2001). Scramjet Research and Development in Russia.
Vol. 189 of Progress in Astronautics and Aeronautics. AIAA.

- Segal, C. (2004). "Propulsion Systems for Hypersonic Flight." University of Florida, Gainesville.
- Siebenhaar, A., M. J. Bulman. (1995). "The Strutjet Engine: The Overlooked Option For Space Launch." 31st AIAA/ASME/SAE/ASEE Joint Propulsion Conference and Exhibit. San Diego: Aerojet.
- Space Shuttle. 1 September 2010. <http://www.braeunig.us/space/specs/shuttle.htm>.
- Sutton, G. P., Biblarz, O. (2001). *Rocket Propulsion Elements* (7th Edition ed.). Danvers: Wiley-Interscience.
- Thomas, S. R., Palac, D. T., Trefny, C. J., Roche, J. M. (2001). *Performance Evaluation of the NASA GTX RBCC Flowpath*. Cleveland: National Aeronautics and Space Administration, Glenn Research Center.
- Trefny, Charles J. (1999). "An Air-Breathing Launch Vehicle Concept for Single-Stage-to-Orbit." *35th Joint Propulsion Conference and Exhibit*. Cleveland: Glenn Research Center.
- Trefny, C. J. (2003, June 25). *Air-Breathing Launch Vehicle Technology Being Developed*. Retrieved November 2010, from NASA Web site: <http://www.grc.nasa.gov/WWW/RT/RT2002/5000/5880trefny.html>
- Woodrow, W. Jr., Blech, R.A., Blankson, I.M. (2000). "Innovative Airbreathing Propulsion Concepts for Access to Space." *Novel Aero Propulsion Systems International Symposium*. Cleveland: Glenn Research Center.

Appendix A : RB C C V Studied in N ASA Contract (N AS7-377)

RB C C V6WXGLHGLQWKH³&ODVV
HVLJQRI³\$6WXG\RI&RPSRVLWH3URSXOVLQRQ6\VWHPVIRU
\$GYDQFHG/DXQFK9HKLFOH\$SSOLFDWLRQV'E\
(VFKHU)ORUQHV

4. Hyperjet
5. Hyperjet \pm Scramjet
6. Basic LACE
7. Recycled Basic LACE
8. Basic Air Augmented Rocket
9. Basic Air Augmented Rocket - Ramjet
10. Basic Air Augmented Rocket \pm Convertible Ramjet
11. Basic Air Augmented Rocket \pm SCRAMJET
12. Ejector Ramjet
13. Ejector SCRAMJET
14. Supercharged Ejector Ramjet
15. Supercharged Ejector SCRAMJET
16. Supercharged Basic Air Augmented Rocket
17. Supercharged Basic Air Augmented Rocket \pm Ramjet
18. Supercharged Basic Air Augmented Rocket - Convertible Ramjet
19. Supercharged Basic Air Augmented Rocket \pm SCRAMJET
20. Air Augmented LACE \pm Ramjet
21. Air Augmented LACE \pm Convertible Ramjet
22. Recycled Air Augmented LACE \pm Ramjet
23. Recycled Air Augmented LACE \pm Convertible Ramjet
24. RamLACE
25. ScramLACE
26. Recycled RamLACE
27. Recycled ScramLACE
28. Supercharged Air Augmented LACE \pm Ramjet
29. Supercharged Air Augmented LACE \pm Convertible Ramjet
30. Recycled Supercharged Air Augmented LACE \pm Ramjet
31. Recycled Supercharged Air Augmented LACE \pm Convertible Ramjet
32. Supercharged RamLACE
33. Supercharged ScramLACE
34. Recycled Supercharged RamLACE
35. Recycled Supercharged ScramLACE
36. Augmenter LACE
37. Recycled Augmenter LACE
38. Air Augmented Regenerative Monofuel Rocket \pm Ramjet
39. Air Augmented Regenerative Monofuel Rocket \pm Convertible Ramjet

Appendix B: U.S. Standard Atmosphere 1976 Properties

Altitude (km)	Pressure (N/m ² or Pa)	Temperature (K)	'HQLW\ (kg/m3)	Speed of Sound (m/s)
0	101300	288.200	1.22500000	340.300
1	89853.1	281.687	1.11168750	336.455
2	79479.98	275.202	1.00658250	332.541
3	70099.6	268.718	0.90931750	328.594
4	61641.05	262.204	0.81940250	324.578
5	54033.42	255.720	0.73647000	320.563
6	47205.8	249.235	0.66015250	316.445
7	41097.41	242.751	0.59008250	312.327
8	35647.47	236.266	0.52577000	308.108
9	30795.2	229.782	0.46709250	303.854
10	26489.95	223.297	0.41356000	299.532
11	22691.2	216.813	0.36480500	295.142
12	19398.95	216.698	0.31188500	295.074
13	16572.68	216.698	0.26656000	295.074
14	14171.87	216.698	0.22785000	295.074
15	12105.35	216.698	0.19477500	295.074
16	10352.86	216.698	0.16647750	295.074
17	8847.542	216.698	0.14234500	295.074
18	7563.058	216.698	0.12164250	295.074
19	6465.979	216.698	0.10399025	295.074
20	5527.941	216.698	0.08891050	295.074
21	4727.671	217.620	0.07571725	295.721
22	4046.935	218.600	0.06450850	296.367
23	3466.486	219.608	0.05500250	297.048
24	2971.129	220.588	0.04694200	297.732
25	2548.708	221.597	0.04008200	298.409
26	2188.08	222.577	0.03426325	299.056
27	1879.115	223.586	0.02930200	299.736
28	1615.735	224.565	0.02507575	300.383
29	1389.836	225.545	0.02147425	301.063
30	1196.353	226.554	0.01841175	301.710
31	1031.234	227.534	0.01579025	302.357
32	888.8062	228.543	0.01356075	303.037
33	767.1449	231.021	0.01157258	304.671
34	663.2111	233.788	0.00988698	306.508
35	574.4723	236.555	0.00846353	308.312
36	498.396	239.321	0.00725813	310.115
37	433.1588	242.088	0.00623525	311.885
38	377.0386	244.855	0.00536673	313.655
39	328.7185	247.593	0.00462683	315.424
40	287.0842	250.388	0.00399595	317.194
41	251.0214	253.155	0.00345695	318.929
42	219.9223	255.922	0.00299513	320.665
43	192.8752	258.688	0.00259945	322.400
44	169.4749	261.455	0.00225890	324.136
45	149.1136	264.222	0.00196613	325.837

46	131.2848	266.960	0.00171378	327.539
47	115.7859	269.726	0.00149695	329.206
48	102.313	270.706	0.00131688	329.819
49	90.31908	270.706	0.00116277	329.819
50	79.76362	270.706	0.00102692	329.819
55	42.51561	260.821	0.00056816	323.727
60	21.95171	247.074	0.00030968	315.084
65	10.93027	233.327	0.00016317	306.202
70	5.219989	219.637	0.00008283	297.082
75	2.387641	208.426	0.00003992	289.391
80	1.052507	198.685	0.00001846	282.551
85	0.36342	186.946	0.00000700	274.096
90	0.1644	187.000	0.00000317	234.075
100	0.0289	210.000	0.00000058	248.052

Appendix C : Ejector-Ramjet Mode Performance Calculation Tabulated Results

Mode I: Ejector Ramjet Performance																				Key													
																				Constant (no user input)													
																				Requires user input													
																				Iterated Value													
																				Calculated Value													
																				Based on Trajectory													
Primary Flow (Constant):				Secondary Flow (Select M ₀):				Exhaust Flow (Constant):				Isentropic Flow Calculated Values						Conservation Of Energy and Mass		Test selected	Thrust Augmentation Propulsion Performance Measures					Speed of Sound		System Performance Parameters					
P _{tp} /P ₀	T _{tp} /T ₀	A/A _p *	ε	M ₀	P _{ts} /P ₀	T _{ts} /T ₀	ε	P ₁₀ /P ₀	T ₁₀ /T ₀	ε	P _i /P ₀	M _{pi}	A _{pi} /A _p *	A _{pi} /A	A _{si} /A	M _{si}	η	T _e /T _{tp}	P _e /P ₀	Iterate	P _{te} /P ₀	M _{p0}	V ₀ /V _{p0}	M ₁₀	V ₁₀ /V _{p0}	r _p	a (m/s)	f	F ₀	S (g/kN*s)	I _{sp}	Δ ₀	
Validation	15.000	10.000	12.000	1.350	0.500	1.1804	1.040	1.350	1.000	1.000	1.350	0.910	2.470	2.700	0.225	0.775	0.630	1.957	0.347	1.266	1.000	2.359	2.412	0.093	1.193	0.629	1.677	340.3	0.029	86.12886	337.8658313	301.7079	0.004175
Solved	15.000	10.000	12.000	1.350	0.000	1.0000	1.000	1.350	1.000	1.000	1.350	0.717	2.618	3.135	0.269	0.737	0.717	1.725	0.366	1.199	1.000	2.234	2.412	0.000	1.151	0.611	1.664	340.3	0.029	0	0	0	0
Solved	15.000	10.000	12.000	1.350	0.100	1.0072	1.000	1.350	1.000	1.000	1.350	0.725	2.611	3.112	0.259	0.741	0.712	1.734	0.365	1.202	1.000	2.239	2.412	0.019	1.152	0.611	1.639	340.3	0.025	84.52405	344.2807219	296.0863	0.000819
Solved	15.000	10.000	12.000	1.350	0.200	1.0277	1.000	1.350	1.000	1.000	1.350	0.750	2.590	3.046	0.254	0.746	0.697	1.759	0.363	1.209	1.000	2.253	2.412	0.037	1.157	0.614	1.627	340.3	0.029	83.8901	346.8823907	293.8656	0.001627
Solved	15.000	10.000	12.000	1.350	0.300	1.0626	1.010	1.350	1.000	1.000	1.350	0.790	2.558	2.950	0.244	0.756	0.677	1.803	0.359	1.222	1.000	2.277	2.412	0.056	1.166	0.617	1.629	340.3	0.029	83.932605	346.7067805	294.0144	0.002441
Solved	15.000	10.000	12.000	1.350	0.400	1.1128	1.020	1.350	1.000	1.000	1.350	0.843	2.518	2.832	0.236	0.764	0.652	1.868	0.354	1.241	1.000	2.311	2.412	0.075	1.177	0.622	1.645	340.3	0.029	84.66221	343.7188935	296.5703	0.003283
Solved	15.000	10.000	12.000	1.350	0.500	1.1804	1.040	1.350	1.000	1.000	1.350	0.911	2.470	2.699	0.225	0.775	0.630	1.957	0.347	1.266	1.000	2.358	2.412	0.093	1.193	0.629	1.676	340.3	0.029	86.12886	337.8658313	301.7079	0.004175
Solved	15.000	10.000	12.000	1.350	0.600	1.2663	1.060	1.350	1.000	1.000	1.350	0.992	2.417	2.560	0.213	0.787	0.610	2.072	0.338	1.299	1.000	2.420	2.412	0.112	1.213	0.637	1.726	340.3	0.029	88.47911	328.8911785	309.9408	0.005147
Solved	15.000	10.000	12.000	1.350	0.700	1.3736	1.080	1.350	1.000	1.000	1.350	1.091	2.358	2.416	0.201	0.793	0.593	2.221	0.328	1.342	1.000	2.499	2.412	0.130	1.238	0.647	1.796	340.3	0.029	91.75968	317.1327659	321.4326	0.006227
Solved	15.000	10.000	12.000	1.350	0.800	1.5062	1.110	1.350	1.000	1.000	1.350	1.208	2.295	2.272	0.189	0.811	0.580	2.408	0.317	1.395	1.000	2.598	2.412	0.149	1.267	0.659	1.888	336.45	0.029	95.03311	306.2090806	332.8993	0.007287
Solved	15.000	10.000	12.000	1.350	0.900	1.6672	1.140	1.350	1.000	1.000	1.350	1.347	2.227	2.129	0.177	0.823	0.572	2.640	0.304	1.461	1.000	2.721	2.412	0.168	1.301	0.673	2.009	332.54	0.029	99.40598	292.7389203	348.2174	0.008476
Solved	15.000	10.000	12.000	1.350	1.000	1.8635	1.170	1.350	1.000	1.000	1.350	1.511	2.155	1.990	0.166	0.834	0.564	2.930	0.291	1.542	1.000	2.873	2.412	0.186	1.341	0.689	2.162	324.59	0.029	103.7532	280.4733353	363.4456	0.009595
Solved	15.000	10.000	12.000	1.350	1.100	2.0982	1.210	1.350	1.000	1.000	1.350	1.704	2.080	1.857	0.155	0.845	0.562	3.286	0.278	1.643	1.000	3.060	2.412	0.205	1.386	0.706	2.354	320.56	0.029	110.7023	262.8672549	387.7881	0.011121

Solved	15.00 0	10.00 0	12.00 0	1.35 0	1.200	2.3792	1.25 0	1.35 0	1.000	1.000	1.35 0	1.931	2.002	1.731	0.14 4	0.85 6	0.56 4	3.71 8	0.264	1.765	1.000	3.287	2.41 2	0.224	1.43 7	0.725	2.592	316.45	0.02 9	119.127 3	244.27651 3	417.300 9	0.01288 8
Solved	15.00 0	10.00 0	12.00 0	1.35 0	1.300	2.7176	1.29 0	1.35 0	1.000	1.000	1.35 0	2.196	1.921	1.613	0.13 4	0.86 6	0.56 9	4.24 7	0.251	1.914	1.000	3.565	2.41 2	0.242	1.49 4	0.746	2.886	312.33	0.02 9	129.355 9	224.96073 19	453.131 5	0.01496 4
Solved	15.00 0	10.00 0	12.00 0	1.35 0	1.400	3.1191	1.34 0	1.35 0	1.000	1.000	1.35 0	2.506	1.837	1.504	0.12 5	0.87 5	0.57 7	4.88 5	0.239	2.095	1.000	3.902	2.41 2	0.261	1.55 5	0.768	3.245	308.11	0.02 9	141.361 1	205.85580 54	495.185 4	0.01737 2
Solved	15.00 0	10.00 0	12.00 0	1.35 0	1.500	3.5991	1.39 0	1.35 0	1.000	1.000	1.35 0	2.868	1.750	1.404	0.11 7	0.88 3	0.58 9	5.65 2	0.229	2.314	1.000	4.311	2.41 2	0.279	1.62 2	0.791	3.680	303.85	0.02 9	155.336 4	187.33531 11	544.140 9	0.02017 1
Solved	15.00 0	10.00 0	12.00 0	1.35 0	1.600	4.1701	1.44 0	1.35 0	1.000	1.000	1.35 0	3.288	1.660	1.314	0.10 9	0.89 1	0.60 2	6.57 2	0.219	2.580	1.000	4.805	2.41 2	0.298	1.69 4	0.814	4.206	299.53	0.02 9	171.339 4	169.83833 16	600.199 7	0.02339 4
Solved	15.00 0	10.00 0	12.00 0	1.35 0	1.700	4.8491	1.50 0	1.35 0	1.000	1.000	1.35 0	3.779	1.567	1.233	0.10 3	0.89 7	0.61 7	7.66 2	0.212	2.898	1.000	5.399	2.41 2	0.317	1.77 0	0.838	4.831	295.14	0.02 9	189.210 8	153.79669 08	662.802 3	0.02704 7
Solved	15.00 0	10.00 0	12.00 0	1.35 0	1.800	5.6557	1.56 0	1.35 0	1.000	1.000	1.35 0	4.349	1.471	1.162	0.09 7	0.90 3	0.63 4	8.95 3	0.205	3.282	1.000	6.113	2.41 2	0.335	1.85 0	0.862	5.576	295	0.02 9	212.074 4	137.21602 11	742.892 8	0.03208 3
Solved	15.00 0	10.00 0	12.00 0	1.35 0	1.900	6.6112	1.63 0	1.35 0	1.000	1.000	1.35 0	5.008	1.371	1.103	0.09 2	0.90 8	0.65 3	10.47 7	0.201	3.742	1.000	6.971	2.41 2	0.354	1.93 4	0.885	6.455	295	0.02 9	237.540 2	122.50556 92	832.099 3	0.03793 2
Solved	15.00 0	10.00 0	12.00 0	1.35 0	2.000	7.7421	1.70 0	1.35 0	1.000	1.000	1.35 0	5.775	1.267	1.054	0.08 8	0.91 2	0.67 2	12.25 6	0.198	4.290	1.000	7.992	2.41 2	0.373	2.02 0	0.909	7.481	295	0.02 9	265.157 1	109.74626 58	928.840 7	0.04457 1
Solved	15.00 0	10.00 0	12.00 0	1.35 0	2.100	9.0812	1.77 0	1.35 0	1.000	1.000	1.35 0	6.656	1.157	1.020	0.08 5	0.91 5	0.69 2	14.33 5	0.196	4.944	1.000	9.210	2.41 2	0.391	2.10 9	0.931	8.677	295	0.02 9	294.830 3	98.700843 14	1032.78 5	0.05203 6
Solved	15.00 0	10.00 0	12.00 0	1.35 0	2.200	10.661	1.84 17	1.35 0	1.000	1.000	1.35 0	7.668	1.042	1.001	0.08 3	0.91 7	0.71 4	16.75 0	0.196	5.720	1.000	10.65	2.41 5	0.410	2.20 0	0.953	10.05	295	0.02 9	326.082 7	89.241173 74	1142.26 2	0.06029 3
Solved	15.00 0	10.00 0	12.00 0	1.35 0	2.300	12.521	1.92 46	1.35 0	1.000	1.000	1.35 0	8.824	0.918	1.006	0.08 4	0.91 6	0.73 7	19.53 0	0.197	6.634	1.000	12.35	2.41 8	0.428	2.29 2	0.974	11.63	295	0.02 9	358.267 9	81.224334 08	1255.00 3	0.06925 5
Solved	15.00 0	10.00 0	12.00 0	1.35 0	2.400	14.712	2.00 68	1.35 0	1.000	1.000	1.35 0	10.09	0.786	1.045	0.08 7	0.91 3	0.76 6	22.73 4	0.200	7.712	1.000	14.36	2.41 6	0.447	2.38 5	0.994	13.44	295	0.02 9	592.408 4	49.121517 56	2075.19 6	0.11949 4
Solved	15.00 0	10.00 0	12.00 0	1.35 0	2.500	17.292	2.09 24	1.35 0	1.000	1.000	1.35 0	11.41	0.647	1.140	0.09 5	0.90 5	0.80 6	26.39 6	0.203	8.973	1.000	16.71	2.41 5	0.466	2.47 9	1.013	15.47	295	0.02 9	826.549 8	35.206590 23	2895.39 9	0.17367

Appendix D: Ramjet Propulsion Performance Calculations Using PAR A

Inputs															Results					
M_o	h (km)	T_o (K)	P_o (KPa)	ρ_o (kg/m ³)	$C_{p,c}$ (kJ/kg)	$C_{p,t}$ (kJ/kg)	Max T_{t4} (K)	h_{PR} (kJ/kg)/K	P_o/P_g	τ_c	τ_b	τ_e	P_{t9}/P_g	f	\dot{m} (N*s/kg)	S (g/kN*s)	τ_T	τ_P	τ_o	I_{sp}
2.57	167	216.6	10.355	0.153	1.09	1.23	1777.8	119954	19	0.9	0.9	0.9	11.97	0.0140	1060.69118	22.96	0.502	0.735	0.369	7679.2
2.78	177	216.6	8.85	0.131	1.09	1.23	1777.8	119954	19	0.9	0.9	0.9	16.05	0.0136	1294.83257	22.47	0.541	0.753	0.407	9683.8
3.01	187	216.6	7.565	0.112	1.09	1.23	1777.8	119954	19	0.9	0.9	0.9	21.95	0.0130	1312.95465	22.16	0.578	0.774	0.447	10224.5
3.25	197	216.6	6.471	0.0959	1.09	1.23	1777.8	119954	19	0.9	0.9	0.9	30.08	0.0124	1319.23883	22.05	0.610	0.795	0.486	10766.9
3.51	207	216.6	5.531	0.0891	1.09	1.23	1777.8	119954	19	0.9	0.9	0.9	41.75	0.0117	1314.68760	22.13	0.638	0.819	0.523	11376.5
3.8	217	216.6	4.73	0.0701	1.09	1.23	1777.8	119954	19	0.9	0.9	0.9	59.04	0.0109	1296.13851	22.45	0.659	0.845	0.558	12099.3
4.11	227	216.6	4.041	0.05989	1.09	1.23	1777.8	119954	19	0.9	0.9	0.9	83.61	0.0099	1259.49371	23.1036	0.671	0.874	0.586	12929.4
4.44	237	216.6	3.457	0.05122	1.09	1.23	1777.8	119954	19	0.9	0.9	0.9	117.9	0.0087	1199.55894	24.26	0.667	0.903	0.603	13911.2
4.8	247	216.6	2.957	0.04382	1.09	1.23	1777.8	119954	19	0.9	0.9	0.9	166.0	0.0074	1100.46044	26.435	0.639	0.936	0.598	15057.4
5.18	258	216.6	2.526	0.0374	1.09	1.23	1777.8	119954	19	0.9	0.9	0.9	229.4	0.0059	933.992027	31.1342	0.564	0.972	0.548	16082.5

Appendix E: Scramjet Mode Propulsion Performance Using Stream Thrust Analysis

Mode II: Dual Mode Ramjet Performance Analysis																	Key					
																	Constant (no user input)					
																	Requires user input					
																	Iterated Value					
																	Calculated Value					
																	Based on Trajectory					
Inputs (Constant here)																						
C	4c	4b	4e	f _{PR} (J/kg)	f	R (m/s) ² /K	C _{pc} (J/kg)/K	C _{pb} (J/kg)/K	C _{pe} (J/kg)/K	α _c	α _b	α _e	h _f	V _{rx} /V ₃	T ⁰ (K)	V _f /V ₃	C _f *A _w /A ₃	p10/p0				
7	0.9	0.9	0.9	3510000	0.0291	289.3	1090	1510	1510	1.362	1.238	1.238	0	0.5	222	0.5	0.1	1.4				
Input	Trajectory Based (from Mach number)				Compression Component				Combustion Component (Constant Area)				Expansion Component			Propulsion Performance Parameters						
M ₀	P ₀ (Pa)	a ₀ (m/s)	V ₀ (m/s)	T ₀ (K)	Sa ₀ (N*s/kg)	T ₃ (K)	V ₃ (m/s)	Sa ₃ (N*s/kg)	p ₃ /p ₀	A ₃ /A ₀	V ₄ (m/s)	T ₄ (K)	A ₄ /A ₃	Sa ₄ (N*s/kg)	T ₁₀ (K)	V ₁₀ (m/s)	Sa ₁₀ (N*s/kg)	A ₁₀ /A ₀	ξ ₀ (Ns/kg)	S (g/kN*s)	I _{sp} (s)	t ₀
5.8	2108.601	299.120	1734.896	222.730	1772.037	1559.108	310.739	1762.279	260.030	0.150	291.248	3557.408	2.505	3824.855	1532.477	2490.000	2668.050	3.524	879.915	33.071	3082.326	0.565
5.9	2037.729	299.290	1765.811	222.983	1802.343	1560.881	448.855	1454.888	260.030	0.106	420.701	3562.609	2.506	2870.573	1534.720	2510.222	2687.096	3.559	869.464	33.469	3045.719	0.563
6	1970.370	299.460	1796.760	223.236	1832.704	1562.655	555.351	1369.388	260.030	0.087	520.517	3567.884	2.507	2503.525	1536.992	2530.658	2706.364	3.593	859.203	33.869	3009.773	0.560
6.1	1906.298	299.630	1827.743	223.490	1863.118	1564.429	646.062	1346.598	260.030	0.076	605.538	3573.228	2.508	2312.673	1539.295	2551.305	2725.850	3.627	849.126	34.271	2974.474	0.558
6.2	1845.300	299.800	1858.763	223.744	1893.584	1566.205	726.927	1350.240	260.030	0.069	681.330	3578.642	2.509	2200.859	1541.627	2572.158	2745.550	3.660	839.230	34.675	2939.809	0.556
6.3	1787.184	299.970	1889.811	223.997	1924.101	1567.982	800.937	1367.295	260.030	0.064	750.628	3584.128	2.510	2131.929	1543.988	2593.214	2765.462	3.692	829.511	35.081	2905.763	0.553
6.4	1731.771	300.130	1920.832	224.236	1954.605	1569.655	869.818	1391.883	260.030	0.059	815.259	3589.579	2.511	2089.042	1546.335	2614.426	2785.536	3.724	819.985	35.488	2872.393	0.551
6.5	1678.895	300.301	1951.955	224.492	1985.227	1571.442	934.761	1421.108	260.030	0.056	876.128	3595.202	2.512	2063.274	1548.760	2635.878	2805.862	3.755	810.607	35.899	2839.542	0.549
6.6	1628.405	300.468	1983.089	224.742	2015.875	1573.193	996.503	1453.225	260.030	0.054	933.998	3600.863	2.513	2049.343	1551.199	2657.506	2826.372	3.786	801.402	36.311	2807.296	0.547
6.7	1580.159	300.468	2013.136	224.742	2045.433	1573.193	1055.032	1486.417	260.030	0.051	988.856	3604.851	2.516	2043.492	1552.917	2678.559	2846.283	3.817	792.684	36.711	2776.760	0.545
6.8	1534.025	300.635	2044.319	224.992	2076.159	1574.944	1111.911	1521.684	260.030	0.049	1042.167	3610.646	2.517	2044.463	1555.414	2700.540	2867.166	3.847	783.799	37.127	2745.633	0.543
6.9	1489.883	300.802	2075.535	225.242	2106.931	1576.694	1166.911	1557.804	260.030	0.048	1093.710	3616.510	2.518	2050.323	1557.940	2722.701	2888.239	3.876	775.069	37.545	2715.054	0.542
7	1447.619	300.969	2106.784	225.492	2137.748	1578.445	1220.288	1594.498	260.030	0.046	1143.746	3622.446	2.520	2060.010	1560.496	2745.039	2909.499	3.904	766.491	37.965	2685.006	0.540
7.1	1407.128	300.969	2136.881	225.492	2167.409	1578.445	1271.544	1630.670	260.030	0.045	1191.798	3626.688	2.523	2072.146	1562.323	2766.718	2930.082	3.934	758.382	38.371	2656.600	0.538
7.2	1368.313	301.136	2168.179	225.742	2198.300	1580.196	1322.231	1667.973	260.030	0.044	1239.297	3632.754	2.524	2087.322	1564.937	2789.383	2951.690	3.961	750.097	38.795	2627.577	0.537
7.3	1331.082	301.303	2199.510	225.992	2229.235	1581.946	1371.811	1705.427	260.030	0.043	1285.766	3638.895	2.526	2104.524	1567.581	2812.214	2973.475	3.988	741.955	39.221	2599.050	0.535
7.4	1295.349	301.303	2229.641	225.992	2258.964	1581.946	1419.619	1741.999	260.030	0.042	1330.577	3643.324	2.529	2122.724	1569.491	2834.326	2994.524	4.016	734.267	39.631	2572.124	0.534
7.5	1261.037	301.469	2261.021	226.242	2289.969	1583.697	1467.299	1779.548	260.030	0.041	1375.263	3649.593	2.530	2142.991	1572.193	2857.465	3016.640	4.042	726.398	40.061	2544.561	0.532
7.6	1228.070	301.636	2292.434	226.493	2321.017	1585.448	1514.177	1817.094	260.030	0.041	1419.201	3655.941	2.532	2164.454	1574.926	2880.763	3038.925	4.067	718.663	40.492	2517.464	0.531
7.7	1196.379	301.803	2323.880	226.743	2352.107	1587.199	1560.328	1854.610	260.030	0.040	1462.455	3662.355	2.533	2186.936	1577.689	2904.216	3061.376	4.093	711.058	40.925	2490.825	0.529
7.8	1165.900	301.803	2354.060	226.743	2381.925	1587.199	1604.931	1891.035	260.030	0.039	1504.263	3667.043	2.537	2209.509	1579.709	2926.868	3083.011	4.119	703.891	41.342	2465.716	0.528
7.9	1136.570	301.969	2385.555	226.993	2413.083	1588.949	1649.790	1928.421	260.030	0.039	1546.303	3673.597	2.538	2233.603	1582.531	2950.606	3105.770	4.143	696.537	41.778	2439.956	0.527
8	1108.333	302.135	2417.082	227.243	2444.281	1590.700	1694.093	1965.736	260.030	0.038	1587.833	3680.211	2.540	2258.360	1585.383	2974.492	3128.687	4.167	689.305	42.216	2414.624	0.525
8.1	1081.136	302.135	2447.296	227.243	2474.159	1590.700	1736.928	2001.873	260.030	0.038	1627.980	3685.098	2.544	2282.840	1587.486	2997.517	3150.730	4.193	682.498	42.638	2390.777	0.524
8.2	1054.928	302.301	2478.872	227.493	2505.422	1592.451	1780.225	2039.010	260.030	0.037	1668.566	3691.851	2.545	2308.666	1590.398	3021.672	3173.939	4.216	675.501	43.079	2366.269	0.523
8.3	1029.661	302.301	2509.101	227.493	2535.332	1592.451	1822.083	2074.923	260.030	0.037	1707.793	3696.866	2.549	2334.042	1592.555	3044.926	3196.235	4.240	668.920	43.503	2343.216	0.522
8.4	1005.291	302.468	2540.728	227.743	2566.660	1594.201	1864.516	2111.874	260.030	0.037	1747.568	3703.765	2.551	2360.703	1595.527	3069.341	3219.727	4.263	662.148	43.948	2319.495	0.521
8.5	981.776	302.634	2572.386	227.993	2598.027	1595.952	1906.573	2148.740	260.030	0.036	1786.983	3710.734	2.553	2387.725	1598.529	3093.891	3243.364	4.285	655.487	44.395	2296.158	0.520
8.6	959.077	302.634	2602.649	227.993	2627.992	1595.952	1947.212	2184.325	260.030	0.036	1825.073	3715.933	2.556	2414.101	1600.770	3117.481	3266.031	4.309	649.228	44.822	2274.235	0.519
8.7	937.156	302.800	2634.357	228.243	2659.422	1597.703	1988.570	2221.007	260.030	0.036	1863.833	3723.048	2.559	2441.718	1603.332	3142.277	3289.937	4.330	642.777	45.272	2251.636	0.518
8.8	915.978	302.800	2664.636	228.243	2689.417	1597.703	2028.513	2256.372	260.030	0.035	1901.275	3728.377	2.562	2468.588	1606.127	3166.073	3312.833	4.353	636.721	45.703	2230.423	0.517
8.9	895.510	302.965	2696.393	228.493	2720.908	1599.454	2069.261	2292.878	260.030	0.035	1939.463	3735.617	2.564	2496.689	1609.249	3191.107	3336.998	4.374	630.472	46.156	2208.532	0.516
9	875.720	303.131	2728.181	228.743	2752.437	1601.204	2109.741	2329.307	260.030	0.035	1977.403	3742.938	2.567	2525.010	1612.403	3216.264	3361.299	4.395	624.321	46.611	2186.985	0.515
9.1	856.579	303.131	2758.494	228.743	2782.484	1601.204	2148.796	2364.372	260.030	0.035	2014.011	3748.466	2.570	2552.456	1614.782	3240.364	3384.532	4.417	618.554	47.045	2166.785	0.514

9.2	838.059	303.595	2793.07 3	229.444	2816.838	1606.106	2190.920	2402.999	260.030	0.034	2053.49 5	3759.29 6	2.570	2583.112	1619.4 50	3267.901	3411.268	4.434	612.078	47.543	2144.10 0	0.513
9.3	820.133	303.595	2823.43 2	229.444	2846.942	1606.106	2229.495	2437.903	260.030	0.034	2089.65 0	3764.96 0	2.574	2610.887	1621.8 90	3292.220	3434.741	4.456	606.496	47.981	2124.54 6	0.512
9.4	802.777	304.058	2858.14 4	230.144	2881.439	1611.008	2271.277	2476.477	260.030	0.034	2128.81 2	3775.96 9	2.573	2641.956	1626.6 32	3320.066	3461.806	4.473	600.212	48.483	2102.53 2	0.511
9.5	785.965	304.520	2892.94 1	230.844	2916.026	1615.910	2312.934	2515.050	260.030	0.034	2167.85 6	3787.07 5	2.573	2673.240	1631.4 17	3348.087	3489.054	4.489	594.024	48.988	2080.85 6	0.510
9.6	769.676	304.520	2923.39 3	230.844	2946.237	1615.910	2350.911	2549.762	260.030	0.033	2203.45 0	3792.95 8	2.577	2701.443	1633.9 51	3372.743	3512.897	4.510	588.706	49.430	2062.22 8	0.510
9.7	753.888	304.982	2958.32 2	231.545	2980.965	1620.812	2392.293	2588.297	260.030	0.033	2242.23 7	3804.24 1	2.577	2733.071	1638.8 11	3401.062	3540.462	4.525	582.699	49.940	2041.18 4	0.509
9.8	738.581	304.982	2988.82 0	231.545	3011.232	1620.812	2429.905	2622.876	260.030	0.033	2277.49 0	3810.26 5	2.581	2761.492	1641.4 07	3425.918	3564.526	4.546	577.547	50.385	2023.13 8	0.508
9.9	723.736	305.442	3023.88 3	232.245	3046.100	1625.714	2471.050	2661.382	260.030	0.033	2316.05 4	3821.72 6	2.581	2793.429	1646.3 44	3454.528	3592.401	4.561	571.713	50.900	2002.70 1	0.507
10	709.333	305.903	3059.02 6	232.945	3081.056	1630.616	2512.114	2699.899	260.030	0.033	2354.54 3	3833.28 6	2.581	2825.534	1651.3 24	3483.303	3620.451	4.576	565.966	51.417	1982.57 0	0.507
10.1	695.357	305.903	3089.61 3	232.945	3111.428	1630.616	2549.276	2734.323	260.030	0.033	2389.37 3	3839.53 4	2.585	2854.255	1654.0 15	3508.471	3644.857	4.596	561.053	51.867	1965.35 8	0.506
10.2	681.789	306.362	3124.89 3	233.645	3146.524	1635.518	2590.150	2772.824	260.030	0.032	2427.68 3	3851.27 3	2.585	2886.628	1659.0 73	3537.527	3673.206	4.611	555.469	52.388	1945.79 9	0.505
10.3	668.615	306.362	3155.52 9	233.645	3176.950	1635.518	2627.029	2807.140	260.030	0.032	2462.25 0	3857.66 5	2.590	2915.503	1661.8 26	3562.879	3697.817	4.631	550.705	52.841	1929.11 0	0.505
10.4	655.819	306.821	3190.93 7	234.346	3212.183	1640.420	2667.740	2845.633	260.030	0.032	2500.40 5	3869.58 8	2.590	2948.122	1666.9 62	3592.209	3726.458	4.645	545.278	53.367	1910.10 1	0.504
10.5	643.386	306.821	3221.61 9	234.346	3242.663	1640.420	2704.364	2879.849	260.030	0.032	2534.73 4	3876.12 3	2.594	2977.132	1669.7 77	3617.740	3751.267	4.664	540.658	53.823	1893.91 4	0.504
10.6	631.304	307.279	3257.15 7	235.046	3278.033	1645.322	2744.935	2918.342	260.030	0.032	2572.76 0	3888.22 9	2.595	3009.981	1674.9 92	3647.337	3780.194	4.678	535.382	54.354	1875.43 3	0.503
10.7	619.559	307.279	3287.88 5	235.046	3308.566	1645.322	2781.328	2952.466	260.030	0.032	2606.87 0	3894.90 9	2.599	3039.111	1677.8 70	3673.041	3805.195	4.697	530.899	54.813	1859.72 9	0.503
10.8	608.139	307.736	3323.55 2	235.746	3344.073	1650.224	2821.779	2990.967	260.030	0.032	2644.78 4	3907.20 1	2.600	3072.174	1683.1 65	3702.900	3834.403	4.711	525.768	55.348	1841.75 5	0.502
10.9	597.032	307.736	3354.32 6	235.746	3374.658	1650.224	2857.961	3025.007	260.030	0.032	2678.69 6	3914.02 6	2.604	3101.412	1686.1 05	3728.771	3859.589	4.729	521.417	55.809	1826.51 4	0.502
11	586.226	308.193	3390.12 4	236.447	3410.301	1655.126	2898.313	3063.522	260.030	0.031	2716.51 7	3926.50 5	2.605	3134.677	1691.4 81	3758.888	3889.071	4.743	516.425	56.349	1809.02 9	0.501
11.1	575.711	308.193	3420.94 3	236.447	3440.939	1655.126	2934.302	3097.485	260.030	0.031	2750.24 9	3933.47 7	2.609	3164.013	1694.4 84	3784.921	3914.439	4.761	512.201	56.814	1794.23 1	0.501
11.2	565.476	308.649	3456.87 0	237.147	3476.717	1660.028	2974.571	3136.021	260.030	0.031	2787.99 1	3946.14 3	2.610	3197.469	1699.9 41	3815.289	3944.189	4.774	507.344	57.358	1777.21 7	0.500
11.3	555.512	308.649	3487.73 5	237.147	3507.406	1660.028	3010.384	3169.914	260.030	0.031	2821.55 9	3953.26 2	2.615	3226.895	1703.0 08	3841.479	3969.732	4.793	503.241	57.825	1762.84 6	0.500
11.4	545.809	309.104	3523.79 1	237.847	3543.318	1664.930	3050.584	3208.477	260.030	0.031	2859.23 7	3966.11 8	2.616	3260.532	1708.5 46	3872.093	3999.746	4.805	498.513	58.374	1746.28 4	0.500
11.5	536.358	309.104	3554.70 2	237.847	3574.059	1664.930	3086.238	3242.306	260.030	0.031	2892.65 4	3973.38 6	2.620	3290.040	1711.6 77	3898.437	4025.459	4.824	494.528	58.844	1732.32 3	0.499
11.6	527.150	309.559	3590.88 7	238.547	3610.105	1669.832	3126.382	3280.900	260.030	0.031	2930.28 1	3986.43 3	2.621	3323.852	1717.2 97	3929.292	4055.731	4.836	489.924	59.397	1716.19 6	0.499
11.7	518.178	309.559	3621.84 3	238.547	3640.897	1669.832	3161.889	3314.672	260.030	0.031	2963.56 1	3993.84 9	2.626	3353.436	1720.4 92	3955.784	4081.610	4.854	486.051	59.870	1702.62 9	0.498
11.8	509.432	310.013	3658.15 6	239.248	3677.077	1674.734	3201.991	3353.303	260.030	0.031	3001.14 7	4007.08 9	2.627	3387.416	1726.1 95	3986.876	4112.134	4.866	481.567	60.428	1686.92 3	0.498
11.9	500.906	310.013	3689.15 8	239.248	3707.919	1674.734	3237.364	3387.023	260.030	0.031	3034.30 1	4014.65 8	2.632	3417.071	1729.4 54	4013.513	4138.175	4.884	477.803	60.904	1673.73 4	0.498
12	492.593	310.467	3725.60 0	239.948	3744.232	1679.636	3277.434	3425.696	260.030	0.031	3071.85 8	4028.08 8	2.633	3451.213	1735.2 41	4044.837	4168.947	4.896	473.434	61.466	1658.43 1	0.497
Test Case			3048.00 0	222.000	3069.071	1554.000	2527.161	2705.057	260.030	0.032	2368.64 6	3761.35 5	2.658	2828.048	1620.3 37	3475.105	3609.997	4.706	567.893	51.242	1989.32 0	0.493